EXCESS MOLAR ENTHALPIES OF CARBON DIOXIDE WITH POLAR SOLVENTS IN THE VICINITY OF THE CRITICAL POINT

JIAN PING ZHAO

THE VIRTUE OF THE CRITICAL VOICE

By

Der-Ping Zhou

A thesis

presented to the School of Graduate Studies

in partial fulfillment of the requirements

for the degree of Master of Science

Department of Chemistry

Memorial University of Newfoundland

July 1995

St. John's   Newfoundland

EXCESS MOLAR ENTHALPIES OF CARBON DIOXIDE WITH POLAR SOLVENTS

IN

THE VICINITY OF THE CRITICAL POINT

by

Jian Ping Zhao

A thesis

submitted to the School of Graduate Studies

in partial fulfilment of the requirements

for the degree of Master of Science

Department of Chemistry

Memorial University of Newfoundland

Fall 1995

St. John's   Newfoundland

TABLE OF CONTENTS

III

TO MY PARENTS

IV

ABSTRACT

The excess molar enthalpies, H^E, of the binary mixtures (carbon dioxide + propylene carbonate), (carbon dioxide + N-methyl-ϵ-caprolactam), (carbon dioxide + 1-formyl piperidine), (carbon dioxide + ethanol), (carbon dioxide + ethylene glycol dimethyl ether), (carbon dioxide + 2-methoxyethyl ether), and the ternary mixture (carbon dioxide + [x_2 sulfolane + ($1-x_2$) water]), $x_2 = 0.8085$, were measured at the temperatures 298.15 K and 308.15 K and pressures of 7.5 MPa, 10.0 MPa and 12.5 MPa.

The H^E values for a reference system (ethanol + water) at 298.15 K and 0.4 MPa, 5.0 MPa, and 10.0 MPa are in agreement with similar measurements made by Ott *et al.* to within ± 1 percent. The excess molar enthalpies for (carbon dioxide + ethanol) at the lower temperature and higher pressures demonstrate S-shaped excess molar enthalpy curves, with minima in the solvent-rich region and maxima in the CO_2-rich region. For other mixtures, the experimental results exhibit negative H^E values over the entire composition range. In general, the H^E values become progressively more negative as the temperature increases and the pressure decreases. Large changes in the values of H^E were observed near the critical temperature ($T_c = 304.2$ K) and pressure ($p_c = 7.38$ MPa) of CO_2. At all temperatures and pressures

studied, the H^E curves for (CO_2 + propylene carbonate) and (CO_2 + sulfolan⌄ + water) display linear sections which apparently correspond to two-phase regions. The magnitude of the linear region increases with increasing temperature and decreasing pressure, consistent with this assumption. For the other mixtures, no linear sections are present at the lower temperature and higher pressures, but linearity was observed at 308.15 K and 7.5 MPa. Vapour-liquid phase boundaries were determined from regions of linear behaviour in the H^E data.

The Peng-Robinson equation of state with a composition-dependent interaction parameter was used to model the behaviour of H^E. The composition-dependent model gave much better agreement with experimental data over the full range of pressures and temperatures than that obtained by using the traditional one-fluid mixing rule for all mixtures studied. This was especially true for highly polar solvents. The interaction coefficients show no temperature and pressure dependence for any of the systems studied. All of these results suggest that the model is a useful semi-quantitative tool for identifying the relative importance of near-critical effects and intermolecular interaction in highly polar systems.

Significant deviations between the model and the experimental H^Es were always observed in the two-phase regions, wherein the model overpredicted the miscibility of the solvent and CO_2. For the binary mixture (carbon dioxide +

VI

propylene carbonate) and the ternary mixture {carbon dioxide + [x_2 sulfolane + (1-x_2) water]}, $x_2 = 0.8085$, the predicted H^E values in the CO_2-rich region were more negative than the experimental results. The fits to the mixing curves of the other solutions were somewhat better, but show similar discrepancies at $T = 308.15$ K and $p = 7.5$ MPa. These may be explained by the limitations in the Peng-Robinson equation of state and/or in the Panagiotopoulos-Reid mixing rule. It is not clear whether the large deviations may be reduced by introducing vapour-liquid equilibrium values in the fit. Propylene carbonate, sulfolane and ethanol are highly polar solvents, and it is unreasonable to expect that strong directional, intermolecular interactions can be modelled quantitatively by a linear mixing rule over the full range of compositions.

LIST OF TABLES

LIST OF FIGURES

NOMENCLATURE

a parameter in the Peng-Robinson and the van der Waals equations of state, $Pa \cdot m^6 \cdot mol^{-2}$

b parameter in the Peng-Robinson and the van der Waals equations of state, $m^3 \cdot mol^{-1}$

c heat capacity in equation (14)

f volumetric flow rate, $cm^3 \cdot s^{-1}$

g characteristic constant for power-compensated calorimeter defined in equation (15)

k interaction parameter defined by equation (43)

n number of moles

p pressure, MPa

q heat of reaction, J

t time, s

w pV work defined in equation (1), J

x mole fraction

A_n	parameter in equation (22)
A	Helmholtz free energy, J
B_n	parameter in equation (24)
D_n	parameter in equation (22)
C_p	constant pressure heat capacity, $J \cdot mol^{-1} \cdot K^{-1}$
E	calibration constant for the heat of mixing cell, $J \cdot volt^{-1}$
F	molar flow rate, $mol \cdot s^{-1}$
H	enthalpy, $J \cdot mol^{-1}$
M	molar mass, $g \cdot mol^{-1}$
R	gas constant, $J \cdot mol^{-1} \cdot K^{-1}$
SCF	standard cubic foot
T	temperature, K
U	internal energy of a system, J
V	molar volume, $cm^3 \cdot mol^{-1}$
W	the power of the calibration heater defined by equation (16), watts
Z	compressibility factor

Greek Letters

α	dimensionless function defined by equations (33) and (34)

ρ	density, $g \cdot cm^{-3}$
σ	standard deviation
δ	composition-dependent parameter defined by equations (53) and (54)
Δ	difference
ϵ	parameter defined by equation (35)
η	parameter defined by equation (36)
κ	Peng-Robinson constant defined by equation (34)
ν	molar volume, $m^3 \cdot mol^{-1}$
ω	acentric factor

Subscripts

a	"after" symbol used in equation (17)
b	"before" symbol used in equation (17)
c	critical property
f	"final" symbol used in equation (20)
h	"heater" symbol used in equation (17)
i	component i
id	ideal state
j	component j

m	mixing
s	surroundings
std	standard
L	saturation liquid
p	constant pressure
R	reduced property
T	constant temperature

Superscripts

n	index of parameters in equation (22)
E	excess molar property
R	reduced property

ACKNOWLEDGMENTS

1. INTRODUCTION

The properties of binary mixtures in the vicinity of the critical point of one of the components have attracted considerable attention in recent years. Many processes involving high temperature and pressure are designed specifically to take advantage of the unique phase behaviour and thermodynamic properties in the critical region.

In the manufacture of hydrogen, ammonia, and synthetic natural gas, and in the treatment of natural gas, very large quantities of CO_2 must be removed from gas streams at high pressure. Absorption is probably the most important acidic gas removal technique. It involves the transfer of CO_2 from the gaseous to the liquid phase through the phase boundary. The absorbed gas may dissolve physically in the liquid or react chemically with it. The efficiency of CO_2 removal depends strongly on the absorbent chosen. "Chemical solvents", like the aqueous alkanolamines or $CaCO_3$, are characterized by liquid phase reactions between the acidic gas and the soluble base. The so-called "physical solvents" are some polar organic liquids with a high capacity for dissolving CO_2 and/or H_2S. In general, chemical solvents have
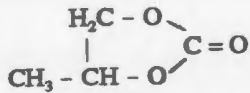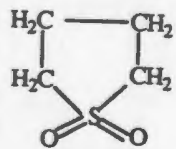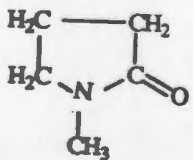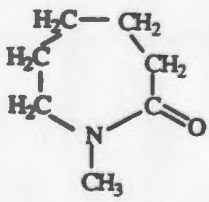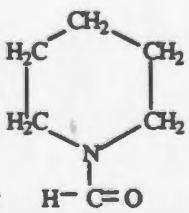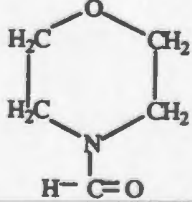
advantages when a high degree of removal is required at low partial pressures of the acidic gas. However, the disadvantages of chemical solvents, such as high cost, large enthalpy of absorption, corrosion of carbon steel, side reactions, and possible environmental problems, suggest that methods based on physical absorption may increase in importance in the future.[1-4]

Although many organic solvents appear to be suitable for use in physical absorption processes, their actual number is limited by the criteria required for economic operation. In order to be practical, the solvents must have an equilibrium capacity for acidic gases several times that of water, coupled with a low capacity for the primary constituents of the gas stream, *e.g.*, hydrocarbons and hydrogen. In addition, they must have an extremely low vapour pressure, permitting operation at essentially ambient temperatures without excessive losses through vaporization. They must have low viscosity and low or moderate hygroscopicity. They must also be noncorrosive to common metals as well as nonreactive with all components in the gas. Finally, they must be available commercially at a reasonable cost.[2] Some of the commonly used physical solvents are listed in table 1.

There have been several commercial processes[3] using organic solvents, such as the Fluor, Purisol, Selexol, Estasolvan, and Sulfinol solvent processes. The operation of a typical solvent process is illustrated in the schematic flow diagram

Table 1.   Summary of solvents used in acidic gas removal.

Solvent	Skeletal formula	
propylene carbonate	H_2C-O, CH_3-CH-O $C=O$	
dimethyl ether of polyethylene glycol ("Selexol")	$(CH_3-O-CH_2-CH_2-)_n-O-CH_3$	(n = 1 to 7)
ethanol	CH_3-CH_2-O-H	
sulfolane + 3% water		
N-methyl pyrrolidone		
N-methyl-ϵ-caprolactam		
1-formyl piperidine		
N-formyl morpholine		

shown in figure 1. The raw gas enters the bottom of the absorber, and is washed by a descending stream of regenerated solvent at low temperature and high pressure. Treated gas leaves from the top of absorber. The gas-rich solvent leaving the bottom of the absorber is regenerated by pressure reduction, usually at two or three different pressure levels, the last of which may be atmospheric or subatmospheric. The depleted solvent leaving the lowest pressure unit is directly recycled to the top of the absorber. Complete removal of the last remaining acidic gas is effected by heat regeneration and reboiling the solvent. The acidic gas is then separated from the solvent, and is collected or vented to the atmosphere.

The acidic gas removal process requires a knowledge of several physical-chemical parameters. Information about phase equilibria (including vapour-liquid and liquid-liquid equilibria), absorption enthalpy (heat of absorption), solubility, density, heat capacity and viscosity of both the pure components and their mixtures at different steps are all important in process design and operation. In order to achieve an efficient removal of acidic gas, many studies on the thermodynamic properties of mixtures of CO_2 with physical solvents have been carried out. [1,4,5] Xu et al.[1] measured the solubility of CO_2 in propylene carbonate and other physical solvents in the range from 298.15 K to 343.15 K. Murrieta-Guevara and coworkers[6] measured the solubilities of CO_2 in propylene carbonate, sulfolane and N-methyl
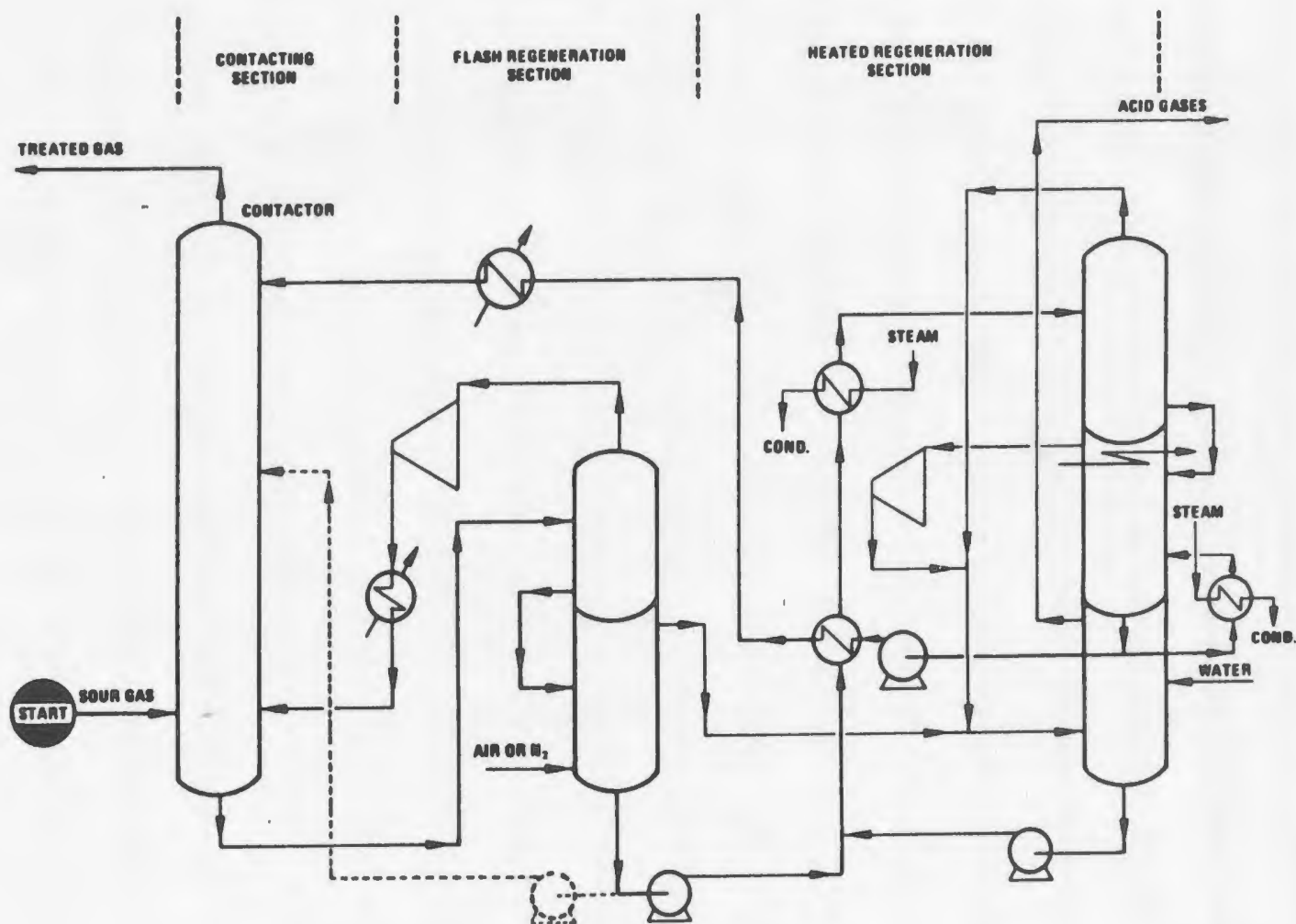
Figure 1. Typical flow diagram of acid-gas removal with a physical organic solvent.[2]

pyrrolidone at temperatures ranging from 298 K to 373 K and pressures from 51 kPa to 2330 kPa. Mather *et al.*[5] measured solubilities of CO_2 and other acidic gases in sulfolane at elevated pressures. The measurements were typically carried out at temperatures from 298.15 K to 303.15 K and pressures up to 7.5 MPa. Figure 2 shows a plot of the solubility of several acidic gases in Selexol solvent (the dimethyl ether of polyethylene glycol). It is clear that the higher the partial pressure of acidic gases, the higher the solubility of the gases in the solvent. Since these physical solvent processes are most efficient when operated at the highest possible pressure, carbon dioxide removal from the gas stream is usually carried out after compression of the gas at ambient temperature to the ultimate pressure required in gas-treating processes.

An important element in the design of gas-treating processes for CO_2 removal is the estimation of heat effects associated with gas absorption or desorption. Studies on mixtures containing CO_2 indicate that large exothermic effects are to be expected as the critical locus is approached. CO_2 has a low critical temperature, T_c = 304.19 K, and a moderately high critical pressure, p_c = 7.38 MPa. The critical loci of mixtures extend to much higher pressures and temperatures. Therefore, a knowledge of the thermodynamic properties of these mixtures under conditions that include the critical temperature and pressure of CO_2 is required for process design and operation.
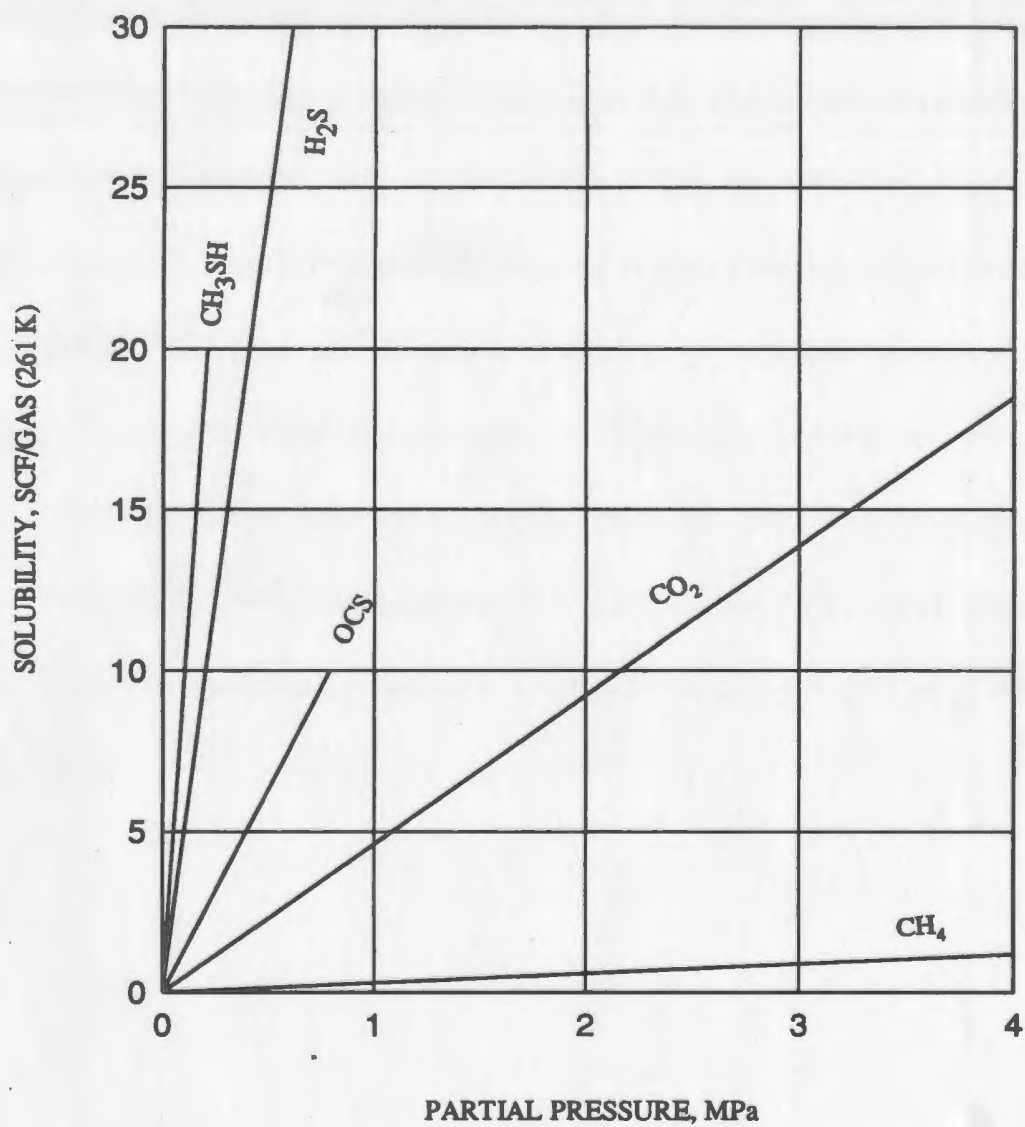
Figure 2. Solubility of gases in selexol solvent.

The purpose of this work was to systematically measure the excess molar enthalpies of mixtures of CO_2 with some physical solvents used in acidic gas removal processes in the vicinity of the critical point of CO_2. The solvents studied here are propylene carbonate, N-methyl-ϵ-caprolactam, 1-formyl piperidine, ethylene glycol dimethyl ether, 2-methoxyethyl ether, ethanol and a sulfolane-water mixture (0.1915 mole fraction water). Excess molar enthalpies were measured at temperatures T = 298.15 K and 308.15 K, and pressures p = 7.5 MPa, p = 10.0 MPa, and p = 12.5 MPa. Further, the experimental results were interpreted by means of the Peng-Robinson equation of state combined with a composition-dependent interaction parameter. The experimental and correlated results, as well as limitations in the model, are discussed in terms of reduced temperature, $T_R = T / T_c$ and reduced pressure, $p_R = p / p_c$.

2.   ENTHALPY

Thermodynamics is a phenomenological treatment of the thermal properties of matter that describes the relationships between work, heat and temperature. The importance of thermodynamics is a consequence of the fact that these properties are involved in every material macroscopic process. Enthalpy is a thermodynamic function of state used to quantify constant pressure processes.

2.1   Definition

For a constant pressure process where only pV work is involved

$$w = -\int_{V_1}^{V_2} p \, dV = -p(V_2 - V_1) \tag{1}$$

the heat of a process is expressed in terms of the first law of thermodynamics as follows:

$$q_p = \Delta U - w = (U_2 + pV_2) - (U_1 + pV_1) \tag{2}$$

Since U, p and V are thermodynamic properties, $(U_i + pV_i)$ is also a thermodynamic property which depends only on the state of a system. This function is defined as enthalpy and identified with the symbol H,

$$q_p = H_2 - H_1 = \Delta H \tag{3}$$

Equation (3) indicates that the quantity of heat transferred to or from a system at constant pressure is equal to the change in its enthalpy. At constant pressure, processes in which heat is absorbed by the system are known as endothermic processes and ΔH is positive. Conversely, processes in which heat is evolved are known as exothermic processes and ΔH is negative. A knowledge of the enthalpies at the initial and final states leads to a straightforward evaluation of the heat necessary to bring about the required change of state.

For a binary mixture, the change in molar enthalpy, ΔH, is expressed by the equation

$$\Delta H = H_m - x_1 H_1 - x_2 H_2 \tag{4}$$

where H_1 and H_2 are the molar enthalpies of the pure components and H_m is the enthalpy of the mixture at the temperature and pressure of the experiment. Since there is no interaction between molecules in an ideal mixture, no heat is absorbed from or released to the system, and the heat of mixing of an ideal mixture, ΔH_{id}, is

zero.

For a real mixture, the change in molar enthalpy ΔH is unlikely to be zero due to various interactions between unlike molecules. In order to express the difference between a real mixture and an ideal mixture, excess molar enthalpy is defined as follows:

$$H^E = \Delta H - \Delta H_{id} = H_m - \sum_i x_i H_i \tag{5}$$

Since ΔH_{id} is zero, H^E is actually equal to ΔH. It expresses the quantity of heat transferred to or from a binary mixture during the constant pressure mixing process.

2.2   Factors Affecting H^E

The excess molar enthalpy is a measure of molecular interactions. The enthalpy for a system may be expressed as a function of temperature and pressure:

$$H = H(T,p) \qquad (n_i \; constant) \tag{6}$$

and the total differential equation is:

$$dH = (\partial H/\partial T)_p \, dT + (\partial H/\partial p)_T \, dp \qquad (n_i \; constant) \tag{7}$$

The temperature derivative is the heat capacity, C_p, and the pressure derivative is found from the Gibbs equation for dH:

$$dH = T \, dS + V \, dp \tag{8}$$

Therefore,

$$(\partial H/\partial p)_T = -T(\partial V/\partial T)_p + V \qquad (9)$$

The change in enthalpy for an arbitrary process (including a phase transformation) is given by the equation:

$$H_f - H_i = \int_{T_i,P_1}^{T_f,P_1} C_p dT + \int_{T_f,P_1}^{T_f,P_f} [V - T(\partial V/\partial T)_p] dp + \sum \Delta H_{trans} \qquad (10)$$

It is clear that the effect of temperature and pressure on the excess molar enthalpy depends on the properties C_p and V (*i.e.* density) for the system. A detailed discussion about the effects of the properties of pure components (CO_2 and solvent) on experimental excess molar enthalpies will be given in Chapter 6.

2.3 H^E for CO_2 Mixtures in the Vicinity of the Critical Region

Many of the interesting phenomena that occur in the vicinity of the critical locus of binary mixtures have been recognized for a long time. But very few enthalpies of mixing have been obtained in this region due to the difficulties of designing calorimeters capable of operating under near - critical conditions.[7-11] Those that have been obtained indicate that large exothermic effects are to be expected as the critical locus is approached. In recent years, the development of high-pressure flow calorimeters has made it possible to measure the excess molar enthalpies of binary mixtures containing dissolved gases. Quite a lot of work has

been done on CO_2 because of the potential use of supercritical CO_2 as a solvent in oil-well flooding, for the extraction of volatile components from coal, oil shale, and tar sands,[1, 12] and for the extraction of oils from vegetable products[12] as well as the gas-processing applications of interest here.[3, 4] Christensen *et al.*[13-18] and Wormald *et al.*[19-21] have reported excess molar enthalpies for a number of binary mixtures of CO_2 with saturated and unsaturated hydrocarbons in the vicinity of the critical point of CO_2. However, few experimental H^E values for the binary mixtures used in gas-treating processes have been reported. Hauser[22] has measured the excess molar enthalpies of CO_2 with several polar physical solvents at $T = 298.15$ K and $T = 308.15$ K, and pressures from 7.5 MPa to 12.6 MPa. These include N-methyl pyrrolidone, propylene carbonate, selexol (dimethyl ether of polyethylene glycol), methanol, methyl cyanoacetate, and N-formyl morpholine.

In this thesis project, the excess enthalpies of mixtures of carbon dioxide with seven physical solvents commonly used in acidic gas removal processes were measured. The measurements include new values for (carbon dioxide + propylene carbonate) at $T = 298.15$ and $T = 308.15$ K, and pressures from 7.5 MPa to 12.5 MPa, and data for six other solvents that have not previously been studied. The H^E values show the expected large exothermic change in magnitude near the critical point of CO_2.

3.   FLOW CALORIMETERS

3.1   General Aspects of Calorimeters

Means for the accurate measurement of mass and heat were prerequisites for the development of modern chemistry and chemical engineering.   Nevertheless, the somewhat elusive nature of heat, so difficult to collect and to measure quantitatively, was a continuing challenge to scientists. A number of calorimeters have now been devised to measure the heat evolved in mixing experiments.

Calorimeters can be described by the principle used to monitor the evolution of heat: (1) adiabatic calorimeter, (2) isoperibol calorimeter, (3) isothermal calorimeter. An adiabatic calorimeter is a well insulated calorimeter where provision is made for minimizing the heat flow between the calorimetric vessel and the surrounding shield. Isoperibol calorimeters are insulated calorimeters in which there is no temperature control between the calorimetric vessel and the shield, but in which the surrounding shield is maintained at a constant temperature. Although most of the heat evolved in an isoperibol calorimeter is accumulated in the calorimetric vessel,

some is exchanged with the surrounding shield. Isothermal calorimeters measure heats of mixing by monitoring the energy required to maintain a reaction vessel at the temperature of its surroundings. Many modern batch calorimeters have been designed with a twin-cell differential assembly to eliminate stray heat losses found in single-cell calorimeters.[23,24]

Isothermal calorimeters are among the most widely used calorimeters for measurements of heats of mixing. They are particularly suitable for flow experiments of the kind required for this work. A detailed discussion of modern isothermal calorimeter systems is given in the next section.

3.2   Isothermal Flow Calorimeters

Isothermal calorimeters are designed to measure the energy required to maintain a reaction vessel at exactly the same temperature as a surrounding constant-temperature bath, *i.e.*

$$T_{surrounding} = T_{vessel} = constant \tag{11}$$

One advantage of the design is that the heat leaks are minimized, so that slow reactions can be studied. Because of the experimental difficulties in maintaining truly isothermal conditions between a measuring unit and its surroundings, flow calorimeters are also designed as twin-cell devices in which two symmetrical flow

cells, one containing a reference fluid, are arranged together to cancel most of the thermal effects not related to the mixing.

Most of the research involving microcalorimetric measurements in the literature has been carried out with cell-type instruments.[25-28] However, for thermodynamic measurements on fluid systems that reach chemical equilibrium in a relatively short time, the advantages of flow calorimeters are considerable.[29,30] The flow technique eliminates time-consuming cell filling and weighing procedures, and significantly reduces the time required for thermal equilibrium prior to measurement. It also eliminates the thermal effects of the mixing operation in cell-type instruments, *e.g.* membrane puncturing[31] or mercury seal displacement,[28,32] and is ideal for studying liquids at elevated temperature.

The general principle of differential flow calorimeters is illustrated in figure 3. The reactant fluids, A and B, at a known temperature are allowed to mix thoroughly in a mixing chamber, and the heat evolved is measured by some means that preserves isothermal conditions. At a constant flow rate of A and B, the system will reach a steady state after a period of time. A duplicate flow system in which the AB mixture is circulated is used as a reference. This differential measurement is designed to cancel most of the thermal effects not related to the mixing of the two fluids.
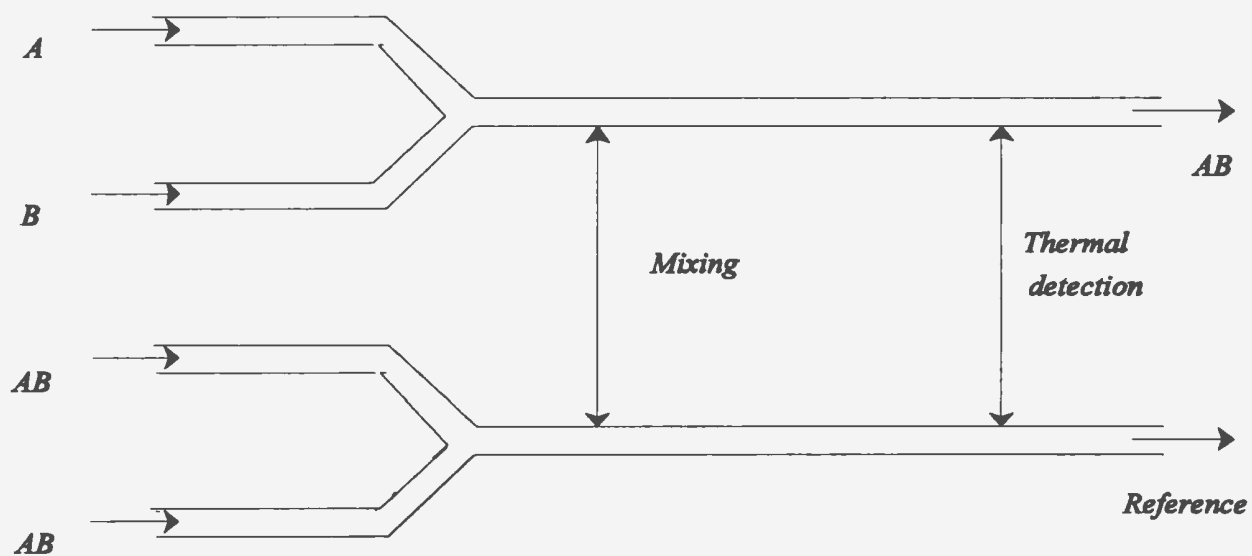
Figure 3. Schematic diagram of a differential flow calorimeter.

Heat of mixing measurements under isothermal conditions may be achieved by various methods. The two most widely used designs are "heat-flow" calorimeters, in which the reaction vessel is in contact with a large constant-temperature heat sink and "power-compensated isothermal calorimeters", in which the vessel temperature is actively controlled by regulating an assembly of heaters and coolers. The heat of mixing is measured in heat-flow calorimeters by a thermopile or some other device that monitors the flow of heat between the vessel and the heat sink. In power-compensated isothermal calorimeters, the heat of mixing is determined by measuring the power required by the heater and cooler to maintain the vessel at the temperature of the isothermal surroundings.

3.2.1 Heat Flow Calorimeters

A schematic diagram of a typical heat flow calorimeter is illustrated in figure 4. The heat released or consumed in the reaction vessel initially causes a change of temperature relative to the surroundings. This causes a relaxation process in which the heat flows to or from the sink until isothermal conditions are re-established. In a suitably designed instrument the heat flow towards the surrounding heat sink can be monitored by measuring the voltage of a network of thermopile junctions with a defined thermal resistance between the vessel and sink. The thermopile senses a very
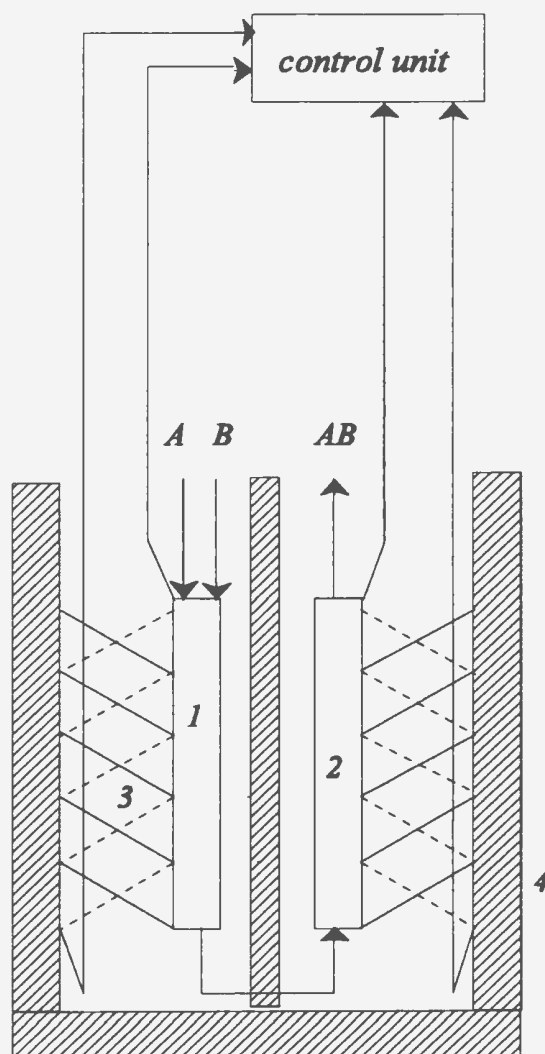
Figure 4. Schematic diagram of a heat - flow calorimeter

1. reaction vessel   2. reference vessel 3. thermopiles   4. surroundings

small time-dependent temperature difference between the vessel wall and the surrounding heat sink. A record of the time dependence of this local temperature difference provides a means for the measurement of heat flow according to the relationship:

$$q = 1/R \int_{t_i}^{t_f} \Delta T(t) \tag{12}$$

where R is the thermal resistance.

Another class of heat flow calorimeters includes instruments which measure the temperature drop through a known thermal resistance across the material surrounding the calorimetric vessel.[33,34] For example, the Picker isothermal flow microcalorimeter[34] is a differential design. The heat produced in the reaction coil is completely transferred to a countercurrent auxiliary liquid through an efficient heat exchanger. Usually, the auxiliary liquid is water. The heat is determined by measuring the temperature difference of the auxiliary liquid between the reaction and reference coils.

3.2.2 Power-Compensated Isothermal Calorimeters

In this type of calorimeter, isothermal operation between the measuring system

and its surroundings is achieved by power compensation. This is to say, the heat evolved or absorbed in the reaction vessel is cancelled by means of the negative heat flux provided by a Peltier cooler and the positive heat flux provided by a controlled heater. A typical device is shown schematically in figure 5. In a reaction run, the temperature of the reaction vessel is forced to follow that of the surrounding shield, so that at any time, the temperature difference is maintained at a value of zero. In terms of design principles there are three possibilities:

(1) The temperature difference between calorimetric vessel and shield is virtually cancelled and the shield is kept at constant temperature[35,36]. If we assume that $P_1(t)$ is the power generated by the process studied and $P_2(t)$ is the compensating heater power, the relevant equation is:

$$P_1(t) + P_2(t) = 0 \qquad (13)$$

(2) ΔT is cancelled but the shield is temperature programmed[37,38], so that the power compensation maintains the calorimetric vessel at the time dependent temperature of the shield,

$$c\,dT_1(t)/dt = P_1(t) + P_2(t) \neq 0 \qquad (14)$$

where c is the heat capacity of the calorimetric vessel and its contents.

(3) ΔT is not cancelled but maintained at a constant value. Generally, the shield temperature is set several degrees (K) lower than that of the calorimetric vessel
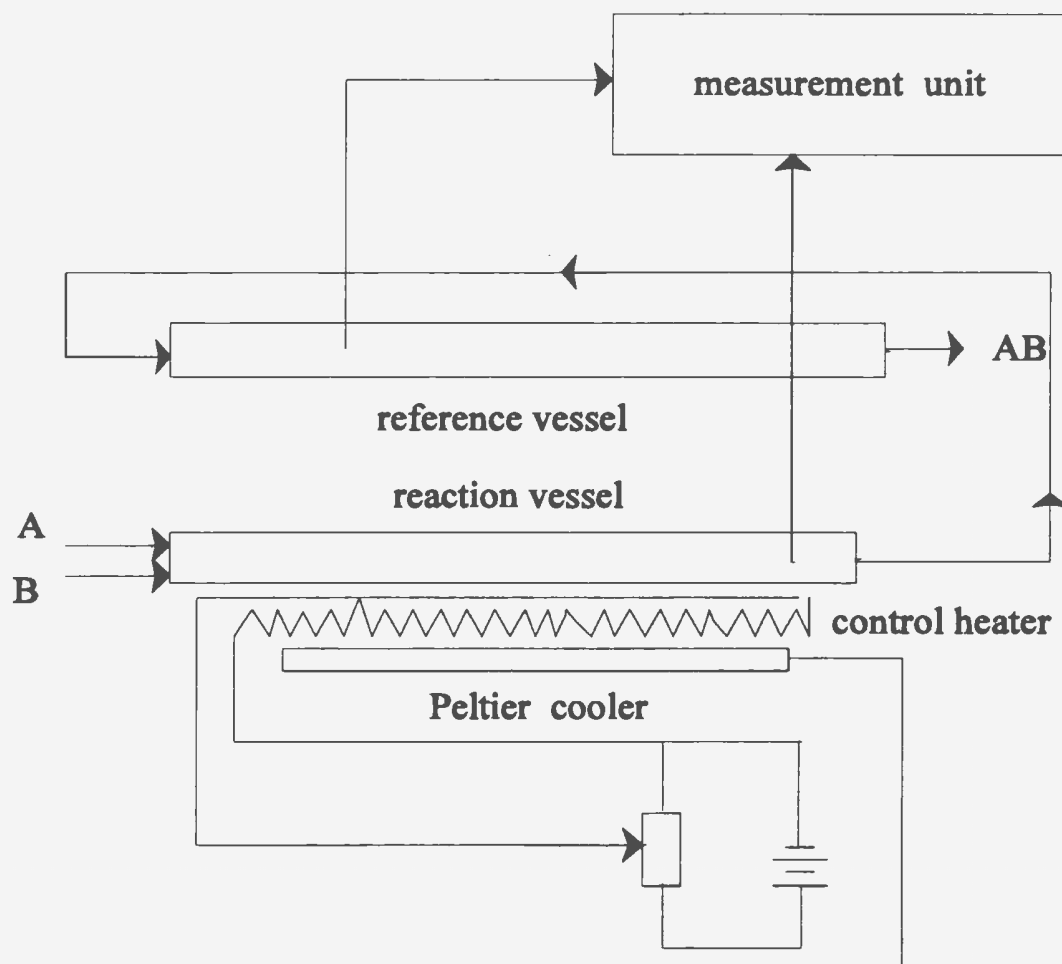
Figure 5. Schematic diagram of a power - compensated isothermal calorimeter.

so that the heat flow between the calorimetric vessel and surrounding shield allows the study of either endothermal or exothermal effects. The appropriate equation here is :

$$g\Delta T = P_1(t) + P_2(t) = constant \tag{15}$$

where g is a constant characteristic of the calorimeter. These instruments measure the energy required to maintain the reaction zone at a constant temperature difference relative to the shield. This condition is achieved by adjusting the energy output of a controlled heater to balance the energy arising from the reaction plus the energy removed by a constant heat leak path. This kind of calorimeter is usually designed for measurements under high temperature conditions.[39]

4.   EXPERIMENTAL APPARATUS

The experimental apparatus used throughout this work was a Tronac Model 1640 isothermal flow calorimeter with a high-pressure isothermal flow cell. The calorimeter belongs to the category of power-compensated calorimeters. The main components of the calorimeter are the reaction vessel, the water bath, the flow system which injects the sample fluids under high pressure, and two electronic consoles. The Model 450 console contains a Wheatstone bridge for monitoring the temperature difference between the reaction vessel and the bath. The Model 550 console controls a heater and a Peltier cooler in the vessel itself. A block diagram showing the main components of the entire system is given in figure 6. A more detailed schematic diagram of the calorimeter is presented in figure 7.

4.1   Principle of Operation

A reaction is initiated by starting the pumps and letting the reactants from inlets A and B flow at a constant rate through the cell. The reaction cell is maintained at a constant temperature, very close to that of the water bath, by means of the control heater and the Peltier cooler. Heat is removed from the reaction vessel through
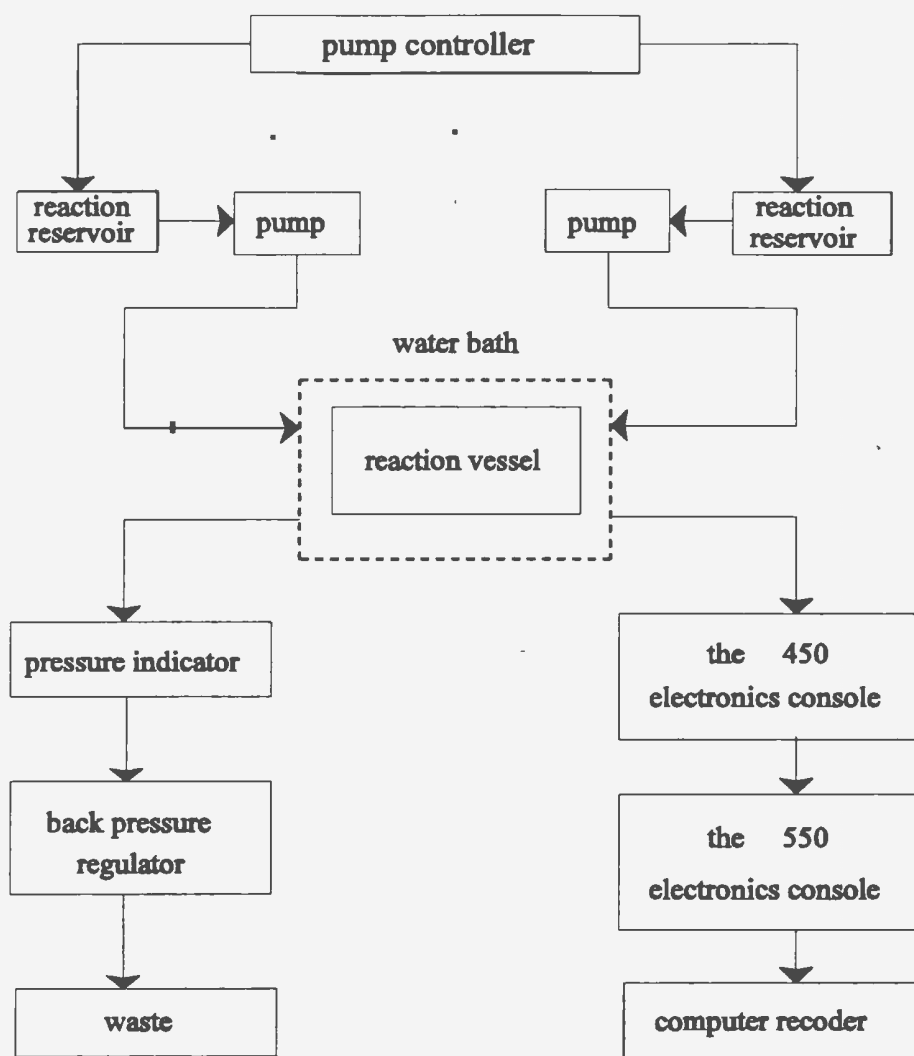
Figure 6. Block diagram of the main components of the calorimeter.
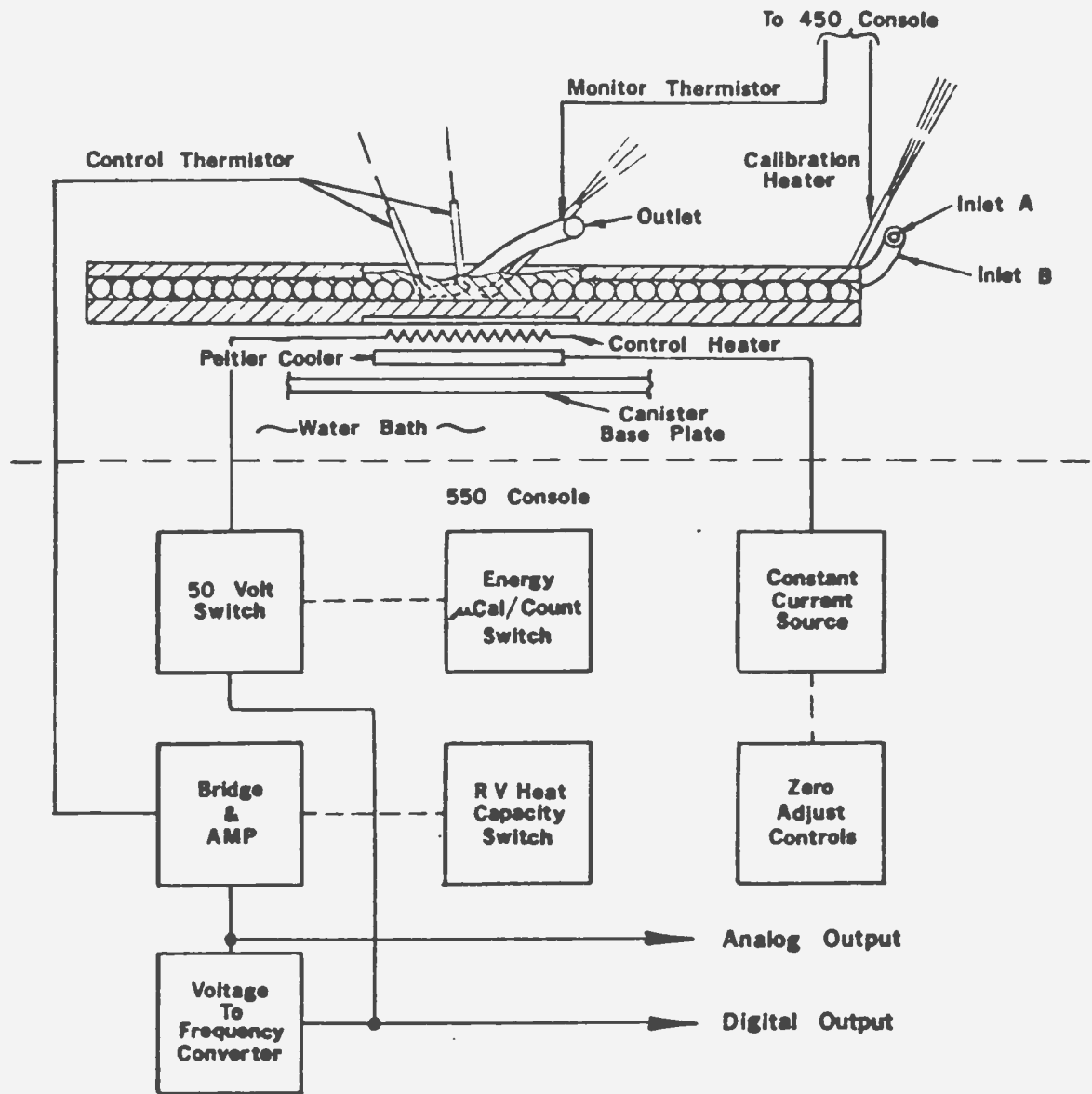
Figure 7.   Schematic diagram of the calorimeter.

the Peltier cooler to the bath at a constant rate. Compensating heat is introduced to the reaction cell by sending fixed energy pulses through the control heater, the rate of which is controlled by the electronics to keep the internal temperature constant. Reactants flowing into the reaction cell mix in an exothermic or endothermic manner, causing a change in the balance between the cooling and heating power. To maintain a constant temperature, the 550 electronics console changes the rate of the heater pulses. The heat of mixing is measured by monitoring the rate at which the control heater is pulsed. A calibration heater is built into the reaction cell assembly.

In operation, the Peltier cooler is adjusted manually to a cooling power which can be balanced by a convenient heater pulse rate (about 12,000 pulses per second). During a mixing run, the Peltier cooler is maintained at constant power. The heater frequency is adjusted automatically to compensate the energy liberated or absorbed by the reaction and maintains the reaction cell and support plate at a constant temperature. The differences in the rates of energy supplied by the heater before, during, and after the experiment are a direct measure of the heat of mixing.

4.2   Reaction Vessel

The reaction vessel (see figure 8) consists of a water-tight, stainless steel container containing the isothermal plate and inlet tubing, coiled into a configuration
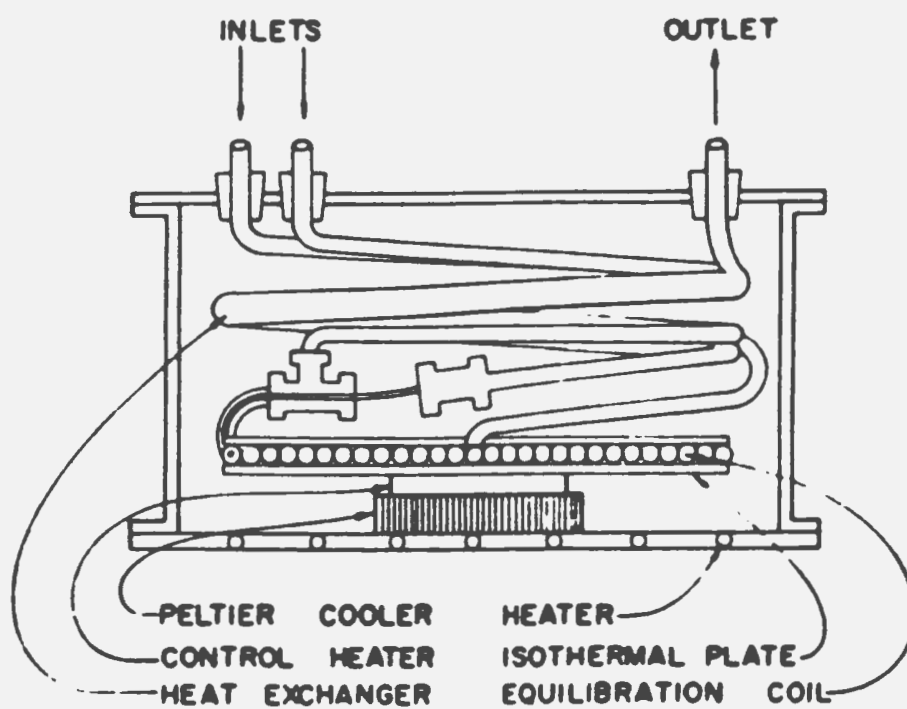
Figure 8.   The reaction vessel and its contents

that ensures thermal equilibrium with the plate. Under the plate are a 100-Ω wafer control heater and a Peltier thermoelectric cooler. They are located adjacent to each other to eliminate heat flow from the heater to the cooler inside the reaction vessel. The cooler is in contact with the bottom of the stainless steel container to facilitate the transfer of heat from the cooler to the water. The unit is suspended 25 cm below a mount situated on the top of the water bath by four stainless steel rods. The isothermal plate consists of a triangular aluminum plate with the equilibration coil attached to the top. The equilibration coil is constructed of 1.83 mm of 0.159 cm o.d., thin wall (0.13mm), stainless steel inlet tubing coiled in a flat helical shape. After entering the reaction vessel and before entering the coil, the reactants are equilibrated with the mixed solution in the outlet tubing by a countercurrent heat exchanger. This exchanger consists of 0.30 m lengths of the inlet and exit tubing which are soldered together, so that the two inlet streams run countercurrent to the exit stream. The two tubes containing the reactants are brought together in the equilibration coil. The thermistors are used to continuously monitor the reaction vessel temperature so that the plate can be maintained at a constant temperature.

4.3 Flow System

A schematic diagram of the flow system is shown in figure 9. Two Isco model
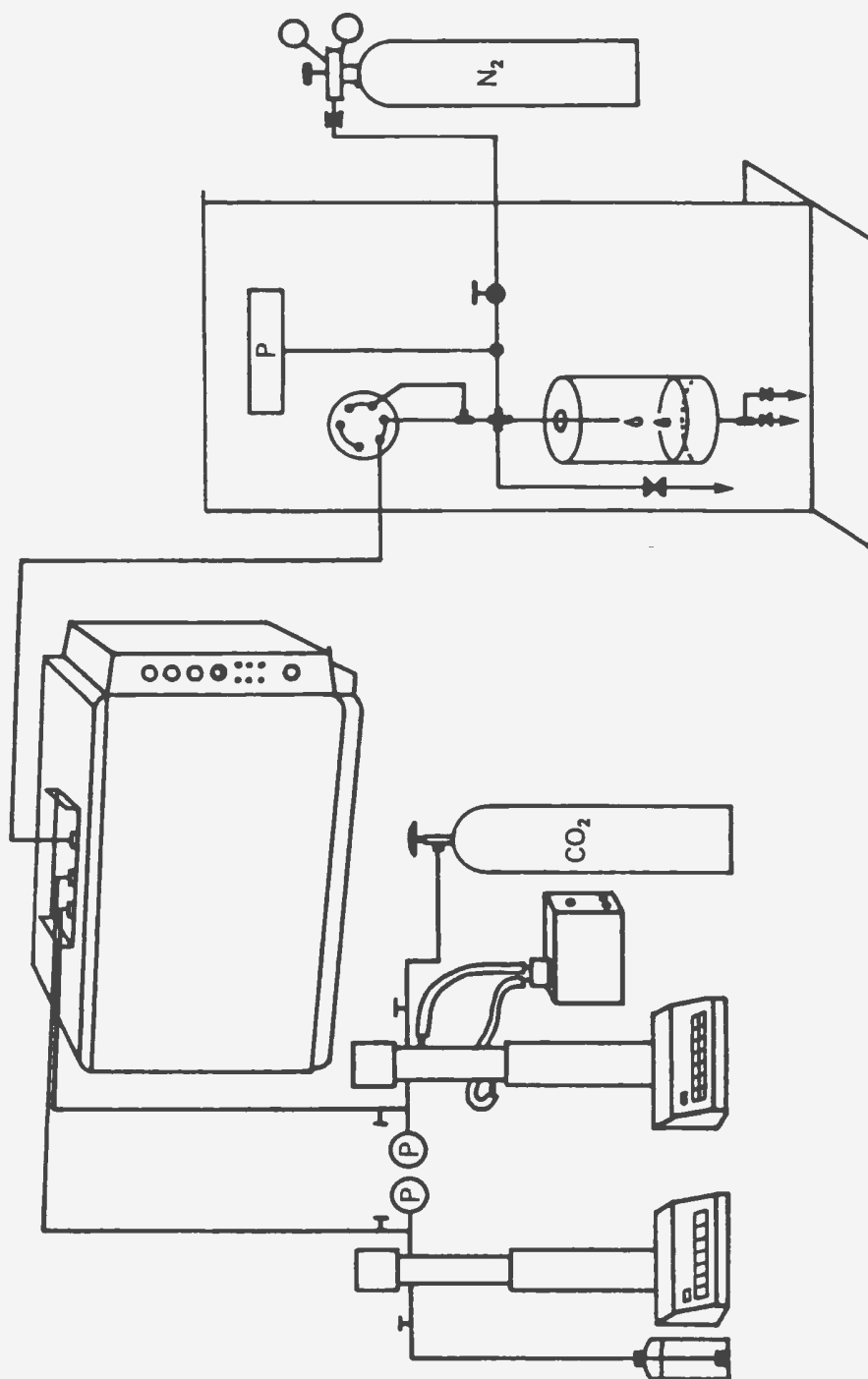
Figure 9.   Arrangement of the flow system.

260D syringe pumps were used to deliver the reactants. The pumps have a pressure capability from 0.07 to 70 MPa, and a flow delivery range from $0.01\mu L/min$ to 25mL/min. Fluids studied here were injected into the flow cell by means of the two pumps operated in a steady-state (fixed-composition) mode. The total flow rate was 0.4 to 0.6 mL/min depending on the magnitude of the measured signal. Extensive calibration of the pumps with respect to flow rate (0.015-0.6 mL/min) was carried out by determining the mass flow rate of Nanopure water. The results are given in Tables A.2.1. and A.2.2. A correction factor of 0.997 ± 0.001 was found for both pumps. Since the high thermal expansivity of liquid CO_2 at room temperature causes uncertainties in the mass flow rate delivered by the pump at room temperature, the density of CO_2 in the Isco pump was controlled by circulating coolant from a HAAKE temperature bath around the barrel of the pump to maintain a constant temperature of (279 ± 0.2) K. The pressure in the whole system was fixed by passing fluids from the exit tubing into a 1-L vessel containing pressurized $N_2(g)$ controlled by a Tescom 26-3200 series back pressure regulator (0 to 24 MPa). The pressure in the flow system was monitored with an Omega PX951 pressure transducer (accuracy, 0.15 percent) connected to an Omega DP41-E high performance process indicator with an internal shunt calibration function. The pressure could be maintained with a precision of ± 30 kPa over a 12-h period. Figure 10 shows a detailed arrangement of the flow system.
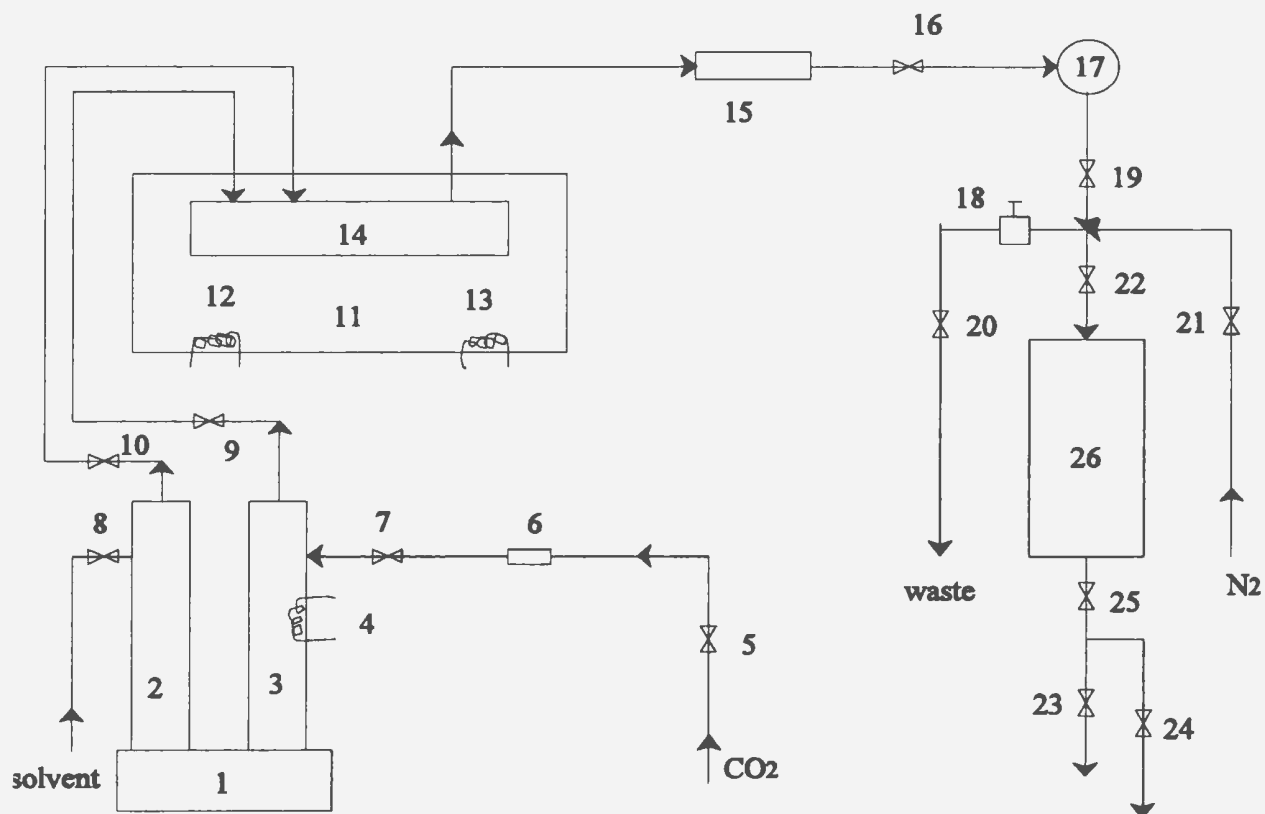
Figure 10. Schematic Diagram of the Flow System.

1. pump controller   2. pump for solvent   3. pump for CO_2 4. cooling for CO_2 pump   5. shut-off valve   6. filter   7-10. shut-off valves   11. water bath 12. heat input for water bath   13. cooling for water bath   14. reaction vessel 15. pressure indicator   16. shut-off valve   17. two-way valve   18. back pressure regulator   19-24. shut-off valves   25. Pressure relief valve   26. solvent collection vessel

The water bath, the 450 and 550 electronics consoles, and the calorimeter operating procedure are described in Appendix I.

4.4   Calculation Procedure

The procedure for calculating the excess molar enthalpies from the raw experimental values is given as follows. Electrical calibration makes use of the relationship:

$$W/(J \cdot s^{-1}) = (V_{heater} \cdot V_{std})/R_{std} \tag{16}$$

where W is the power of the calibration heater. V_{heater} is the voltage reading across the heater. V_{std} is the voltage reading across a standard resistor in series with the calibration heater and R_{std} is the resistance of the heater in ohms. The electrical calibration constant, E , is given as a function of the frequency of heater pulses by the equation:

$$E/(J \cdot volt^{-1} \cdot s^{-1}) = W/\{(V_b + V_a)/2 - V_h\} \tag{17}$$

where V_b and V_a are the analog heater frequency output voltage before and after the heater is turned on, respectively. V_h is the voltage while the heater is on. The molar flow rates F_{CO2} and $F_{solvent}$ for both CO_2 and solvent are given by:

$$F_{CO_2}/(mol \cdot s^{-1}) = 0.9975 \, (f_{CO_2} \cdot \rho_{CO_2}/60 \cdot M_{CO_2}) \tag{18}$$

and

$$F_{solvent}/(mol \cdot s^{-1}) = 0.9975 \left[(f_{total} - f_{CO_2}) \cdot \rho_{solvent}/60 \cdot M_{solvent} \right] \quad \textbf{(19)}$$

where f_{total} is the selected total volumetric flow rate in $cm^3 \cdot min^{-1}$ and ρ_{CO2} and $\rho_{solvent}$ are densities at the temperature and pressure studied. M_{CO2} and $M_{solvent}$ are the molar masses of CO_2 and solvent, and the term 0.9975 is the correction factor for both pumps (given in Appendix II). The heat flux, dQ/dt, generated by the mixing reaction in the calorimeter is calculated from the equation:

$$(dq/dt)/(J \cdot s^{-1}) = [V_{exp.} - (V_a - V_f)/2] \cdot E \quad \textbf{(20)}$$

where V_f is voltage of the final baseline (obtained when only the second component of the mixture is running through the reaction vessel), and V_{exp} is the average voltage at the point where the enthalpy of mixing is to be measured. Thus the excess molar enthalpy of the mixture is obtained by dividing the heat of the reaction by the total molar flow rate:

$$H^E/(J \cdot mol^{-1}) = (dq/dt)/(F_{CO2} + F_{solvent}) \quad \textbf{(21)}$$

The computer programs employed for data acquisition are given in Appendix VI. A sample calculation is given in Appendix III.

5. H^E OF CO_2 WITH PHYSICAL SOLVENTS

5.1 Introduction

The liquids studied in this work, N-methyl-ϵ-caprolactam, 1-formyl piperidine, propylene carbonate, sulfolane, ethanol and polyethylene glycols are among the most common physical solvents used in gas-treating processes. Although the pVT properties of the solvents and their mixtures with CO_2 are well known[2-3], only a few laboratories are equipped to measure the excess molar enthalpies of mixtures containing CO_2 at high pressure. With the exception of Hauser's study[22], no measurements on polar solvents related to CO_2 removal processes have been reported. In this work, the excess molar enthalpies of CO_2 with the physical solvents mentioned above have been systematically measured at the temperatures T = 298.15 K and T = 308.15 K, and pressures from p = 7.5 MPa to p = 12.5 MPa. In this chapter, the results are presented and compared with the limited literature values available. The effects of the proximity to the critical point of CO_2 are analyzed in detail in Chapter 6.

5.2   Experimental

The Tronac Model 1640 isothermal flow calorimeter with a high-pressure isothermal flow reaction vessel was used to measure the excess molar enthalpies. Details of the equipment, the flow system, the operating procedures and data processing have been described in Chapter 4 and Appendices I and III.

The combined uncertainties in volumetric flow rates, pressure determination and calorimeter measurements are usually considered to limit the reproducibility of results to about 1 to 2 percent.[36-39, 40] Fairly large volumes of solvent are required and it has generally been assumed that impurities below one mole-percent do not affect the enthalpy measurements significantly in the mole fraction range of interest.[17, 41,42] All the organic solvents used here were from Aldrich Chemical Co. The ethanol (mass fraction 0.99) was distilled over strips of magnesium at a reflux ratio of approximately 50 and the purity is estimated to be greater than mass fraction 0.995. Fresh Nanopure water was used as the second component of the reference system. The propylene carbonate (mass fraction 0.99) was distilled according to the method described by Riddick and Bunger.[43] Its purity was estimated to be greater than mole fraction 0.995.[43]   The N-methyl-ε-caprolactam(mass fraction 0.99), 1-formyl piperidine (mass fraction 0.99), ethylene glycol dimethyl ether (mass fraction 0.99), and 2-methoxyethyl ether (mass fraction 0.99) were used as received. All solvents

were stored in tightly sealed bottles and transferred to the syringe pumps in a closed system to minimize contamination by atmospheric water.

Pure sulfolane (mass fraction 0.99) is a solid at room temperature. NMR measurements showed no evidence of water in the sample and it was used as received. In acidic gas removal processes, sulfolane is usually used as an aqueous solution (mass fraction 0.97) or mixed with an aqueous solution of mono-ethanolamine. For our experiments, Nanopure H_2O was added to the sulfolane by mass to form a mixture containing mole fraction 0.1915 water, $i.e.$ {x_2 sulfolane + $(1-x_2)$water, x_2=0.8085}. The CO_2 (mass fraction 0.999) was supplied by Matheson Gas Products Canada and used without further purification.

The densities of the solvents at $T = 298.15$ K were measured with a Sodev vibrating tube densimeter[44] to a precision of ± 0.0003 g·cm^{-3}. The refractive indices of the solvents were measured with an Abbe refractometer at 293.15 K and 298.15 K. Tables 2 and 3 show a comparison of the physical properties of the solvents with literature or supplier values. The densities of liquid CO_2 at the pump temperature ($T = 279.15$ K) and pressures studied here were interpolated from values in the thermodynamic tables[45].

The excess molar enthalpies, H^E, for mixtures of (ethanol + water) at 298.15 K and pressures of 0.4 MPa, 5.0 MPa and 10.0 MPa, (CO_2 + ethanol) at 308.15 K and

Table 2. Molar masses and refractive indices of solvents used.

Name and formula	Mol. mass	n_D[*]	
		measured[*]	Reference
ethanol	46.07	1.3613^{20}	1.3611^{20} (43)
C_2H_5OH		1.3593^{25}	1.35941^{25} (46)
propylene carbonate	102.09	1.4212^{20}	1.4189^{20} (43)
			1.4215^{20} (46)
$C_4H_6O_3$		1.4196^{25}	1.4199^{25} (47)
1-formyl piperidine	113.16	1.4836^{20}	1.4700^{20} (46)
			1.4840^{20} (47)
$C_6H_{11}NO$		1.4822^{25}	-----
N-methyl-ε-caprolactam	127.19	1.4834^{20}	1.4840^{20} (47)
		1.4815^{25}	-----
$C_7H_{13}NO$			
sulfolane	120.17	1.4779^{20}	1.4840^{20} (46)
		1.4764^{25}	-----
$C_4H_8SO_2$			
ethyl glycol dimethyl ether	90.12	1.3775^{20}	1.3790^{20} (47)
		1.3753^{25}	
$C_4H_{10}O_2$			
2-methoxyethyl ether	134.18	1.4063^{20}	1.4080^{20} (47)
		1.4049^{25}	
$C_6H_{14}O_3$			

[*]   The refractive indices were measured at 20 and 25°C.

Table 3. Normal boiling temperatures and densities* of physical solvents used.

Name and formula	bp / K	p / MPa	ρ / g·cm^{-3}	
			measured	reference
carbon dioxide		7.5		0.923 (45)
		10.0		0.941 (45)
CO_2		12.5		0.954 (45)
ethanol	351	0.1	0.7854	0.785 (43)
C_2H_5OH				
propylene carbonate	513	0.1	1.1896	1.189 (46)
$C_4H_6O_3$				
1-formyl piperidine	495	0.1	1.0198	1.019 (46)
$C_6H_{11}NO$				
N-methyl-ϵ-caprolactam	380	0.1	0.9916	0.991 (47)
$C_7H_{13}NO$				
sulfolane	558	0.1		1.27 (48)
$C_4H_8SO_2$				
ethyl glycol dimethyl ether	358	0.1	0.8596	0.867 (47)
$C_4H_{10}O_2$				
2-methoxyethyl ether	435	0.1	0.9289	0.937 (47)
$C_6H_{14}O_3$				

* Densities of CO_2 at the pump temperature (T = 279.15 K) were interpolated from the thermodynamic tables[45]; the densities of the solvents were measured at 293.15 K.

7.5 MPa and 12.5 MPa and (CO_2 + propylene carbonate) at 298.15 K and 7.5, 10.6 and 12.6 MPa have been measured by Ott *et al.*[49], Cordray *et al.*[50] and Hauser[22] with similar isothermal flow calorimeters, respectively. Comparisons between our results and these literature values are presented in the following sections.

5.3   Comparisons with Literature Data

The Ethanol - Water System

The Tronac isothermal flow calorimeter was commissioned by measuring the H^E values of {x ethanol + (1-x) water} at T = 298.15 K, and p = 0.4, 5.0 and 10.0 MPa. The binary mixture has been recommended by Ott *et al.*[49,50] as a standard reference system. The calorimeter baseline obtained by flowing ethanol through the reaction vessel was displaced from the water baseline by no more than 15 $J \cdot mol^{-1}$, and the baseline was independent of flow rate or pressure. The H^E results were calculated by linear interpolation of the baselines for the pure components. The experimental values for {x ethanol + (1-x) water} at T = 298.15 K and p = (0.4, 5.0 and 10.0) MPa are presented in table A.3.1. The excess molar enthalpies are essentially independent of pressure at the temperatures studied here.

Figure 11 shows comparisons of the experimental results of Ott *et al.*[49] with those from this work. The average deviation is less than $2 \cdot 10^{-2} \cdot H^E$ over most of the
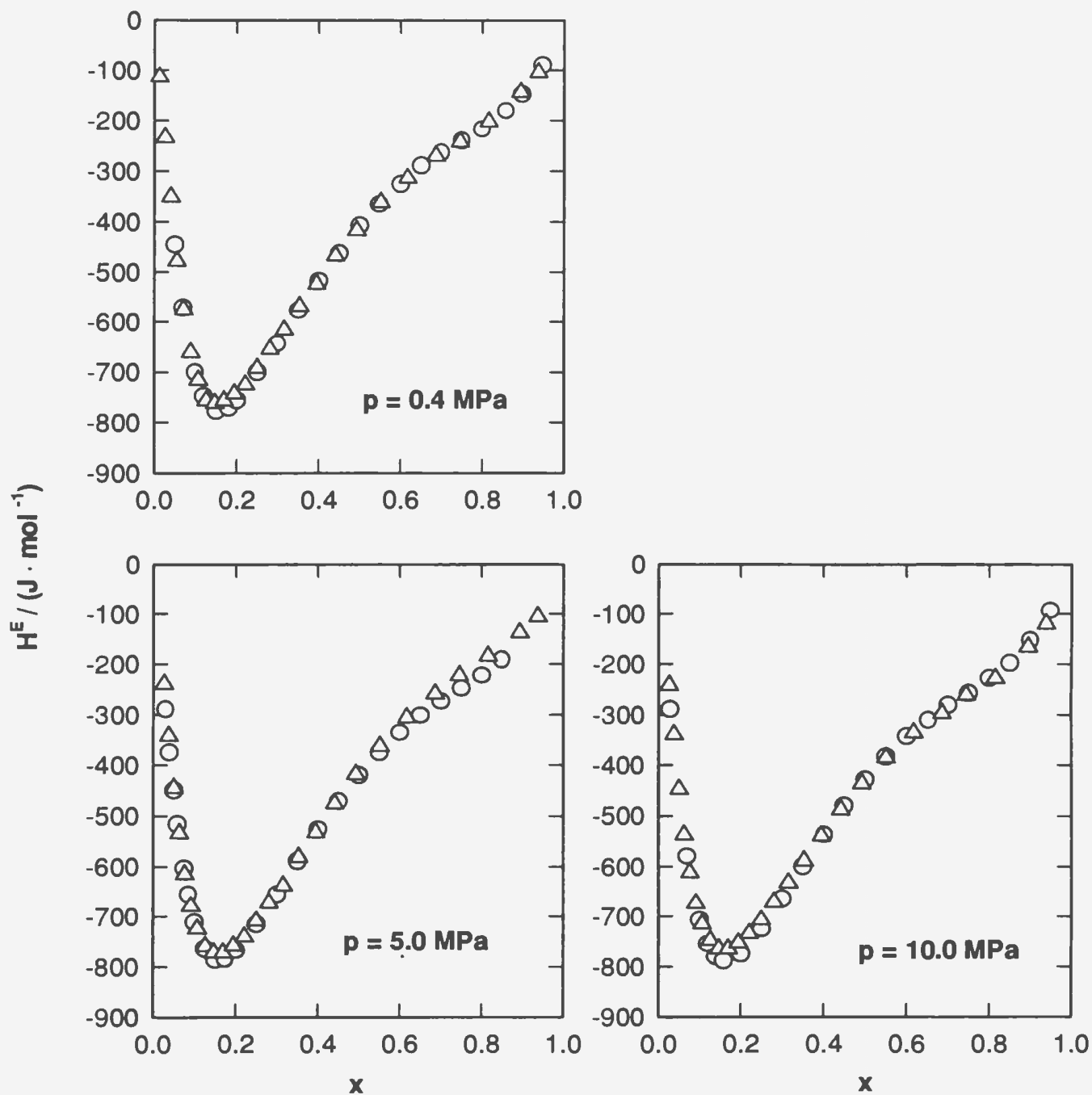
Figure 11. Comparison of the experimental results with literature values for {x Ethanol + (1-x) Water} at T = 298.15 K. ○ , Ott et al.[49]; △ , this work.

mole fraction range ($0.2 \leq x \leq 0.8$). The experimental results from the present investigation agreed with those of Ott *et al.*[49] to within 1 to 2 percent.

The CO_2 - Ethanol System

Excess molar enthalpies for the mixtures of {x CO_2 + (1-x) ethanol} are tabulated in table A.4.2 and plotted in figure 12. At temperature $T = 308.15$ K and pressure $p = 12.5$ MPa, the plot of H^E against x is an S-shaped curve, with a minimum in the range $0.15 \leq x \leq 0.25$ and a maximum at $0.85 \leq x \leq 0.95$. At $T = 308.15$ K and $p = 7.5$ MPa, the H^E values are negative over the entire composition range with a minimum at $x = 0.9$. These values have been also measured by Cordray *et al.*[51] The results from our work were 2 to 5 percent lower than Cordray's data. The deviations are more pronounced in the low mole fraction region. The H^E values for {xCO_2 + (1-x) ethanol} at 298.15 K from 7.5 MPa to 12.5 MPa, and at 308.15 K and 10.0 MPa are new.

The CO_2 - Propylene Carbonate System

The mixtures (xCO_2 + (1-x) propylene carbonate) at 298.15 K and at $p = (7.5, 10.6$ and 12.6) MPa were previously studied by Hauser,[22] who used our calorimeter with less precise pressure and flow rate control. Data from our work were
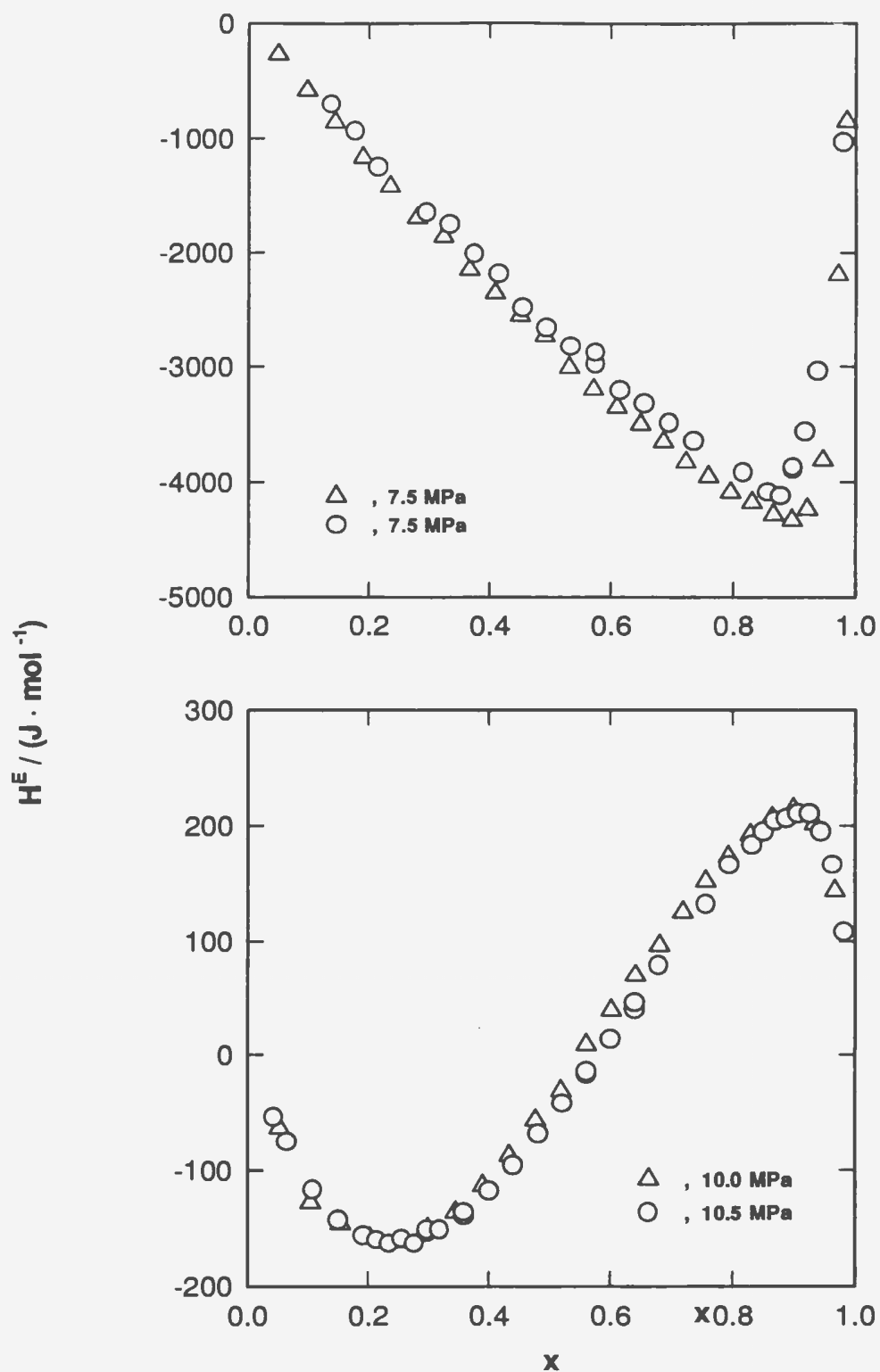
Figure 12. Comparison of the experimental results with literature values for {x CO$_2$ + (1-x) ethanol} at T = 308.15 K. △ ,This work; O ,Cordray et al.[51]

2 to 5 percent more negative than Hauser's results at x = 0.5. The deviations in the solvent-rich region are more marked than those in the CO_2-rich region. This may be caused by the relatively larger effects of fluctuations in the low flow rate of CO_2 required to obtain l ow mole fractions of CO_2. The comparisons are shown in figure 13. Excess molar enthalpies for the system at other temperatures and pressures have not been reported before.

5.4   Experimental Results

The experimental results for {xCO_2 + (1-x) N-methyl-ϵ-caprolactam}, {xCO_2 + (1-x) propylene carbonate}, {xCO_2 + (1-x) 1-formyl piperidine}, {xCO_2 + (1-x) ethylene glycol dimethyl ether}, {xCO_2 + (1-x) 2-methoxyethyl ether} and {x_1CO_2 + (1-x_1)[x_2 sulfolane + (1-x_2) water]} at temperatures T = 298.15 K and T = 308.15 K, and at pressures p = (7.5, 10.0 and 12.5) MPa are summarized in tables from A.4.3 to A.4.8. The equation

$$H^E / (J \cdot mol^{-1}) = [x(1-x) / \{1 + \sum_{n=1}^{i} D_n (1-2x)^n\}] \cdot \sum_{n=0}^{i} A_n (1-2x)^n \quad (22)$$

was fitted to the experimental results at each pressure and temperature by a non-linear least squares routine. This equation was suggested by Christensen et al.[13-18] as a general expression for fitting enthalpy of mixing data. The adjustable coefficients D_n and A_n were optimized independently for each isobaric curve. The deviations
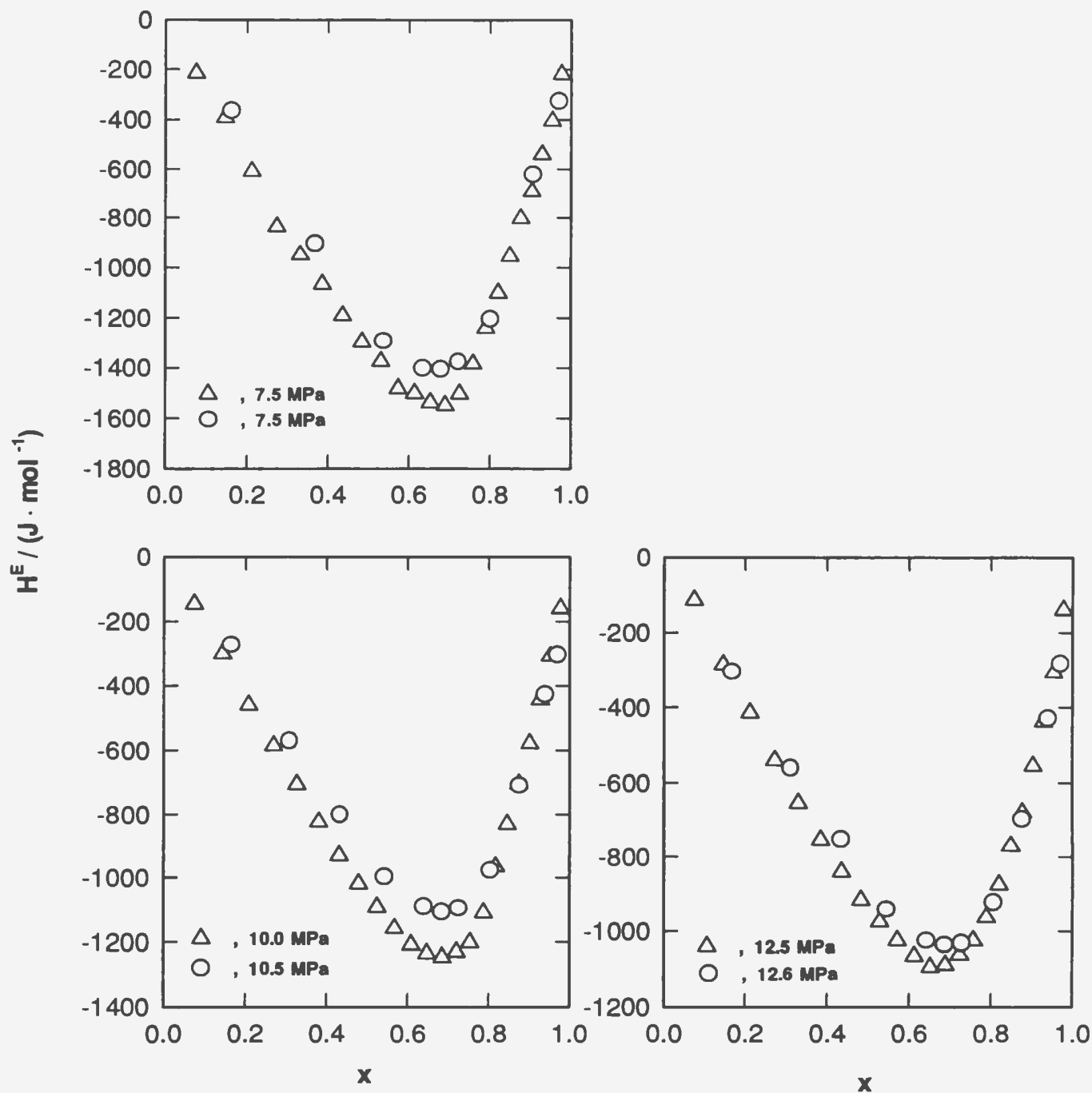
Figure 13. Comparisons of the experimental results with literature values for {x CO$_2$ + (1-x) propylene carbonate} at T = 298.15 K. $\triangle$, this work; $\bigcirc$,Hauser[22].

between equation (22) and the experimental values were calculated by the equation:

$$s = [\sum (H^E_{exp} - H^E_{cal})^2 / (n - f)]^{0.5}$$ (23)

where, n is the number of experimental points and f is the number of fitted coefficients. Figure 14 summarizes the deviations, $s(H^E)$, of H^E {x ethanol + (1-x) water} at T = 298.15 K and p = (0.4, 5.0 and 10.0) MPa. The deviations are within 1 per cent (broken line in figure 14) at all except the highest or lowest values of x. The calculated H^E values for all the mixtures studied are also summarized in tables A.4.1 to A.4.8. The values of the parameters A_n and D_n are given in table A.4.9 together with their standard deviations s. In the CO_2-rich region of some of the mixing curves, the H^E values vary linearly with x. These linear regions were assumed to reflect (vapour+liquid) phase separation[13-16] and described by the equation:

$$H^E / (J \cdot mol^{-1}) = B_0 + B_1 x$$ (24)

The parameters, B_0 and B_1, the standard deviations, s, and the intervals of x for the linear sections of the mixing curves for all mixtures of CO_2-physical solvents are given in table A.4.10.

The H^E values for mixtures of CO_2 with ethanol, propylene carbonate, N-methyl-ϵ-caprolactam, 1-formyl piperidine, ethylene glycol dimethyl ether, 2-methoxyethyl ether and the sulfolane-water mixture against mole fraction x_{CO_2} at the
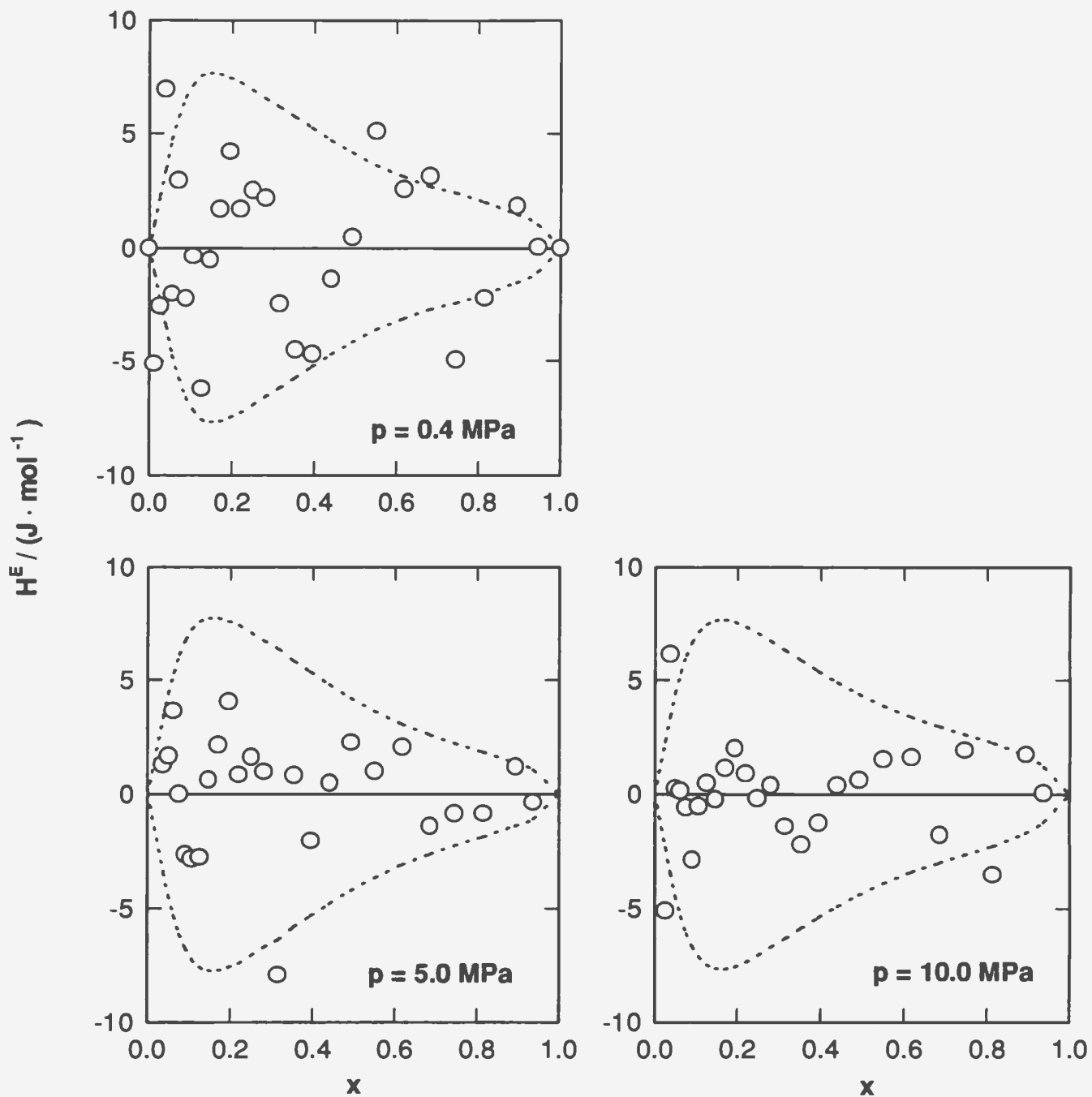
Figure 14. Deviation of the experimantal results from equation (23) for {x ethanol + (1-x) water} at 298.15 K with parameters given in table A.4.10. The dashed lines are the 1 per cent error bounds.

two temperatures and three pressures studied are presented in figures 15 to 21. The symbols are experimental values and the solid curves are calculated from equations (22) or (24). The black symbols are experimental values in the linear sections.

Except for the experimental results for mixtures of $\{xCO_2 + (1-x)ethanol\}$ at $T = 298.15$ K and the higher pressures, the H^E values of all the mixtures studied here are negative over the entire composition range with minima in the vicinity of $x = 0.15$ for $\{x$ ethanol $+ (1-x)$ water$\}$; in the range $(0.6 \leq x \leq 0.7)$ for $\{xCO_2 + (1-x)$propylene carbonate$\}$; at $x = 0.7$ for $\{xCO_2 + (1-x)N$-methyl-ε-caprolactam$\}$, $\{xCO_2 + (1-x)1-$formyl piperidine$\}$, and $x = 0.6$ for $\{xCO_2 + (1-x)$ ethylene glycol dimethyl ether$\}$ and $\{xCO_2 + (1-x)$ 2-methoxyethyl ether$\}$. The minima shift toward the CO_2-rich region with increasing pressure or decreasing temperature.

In general, the H^E values become progressively more negative as temperature increases and pressure decreases. The sharp decrease in H^E at $p = 7.5$ MPa and $T = 308.15$ K reflects the proximity to the critical point of CO_2 (304.15 K and 7.38 MPa). At all temperatures and pressures studied, linear sections of the H^E curves were observed for $\{xCO_2 + $ propylene carbonate$\}$ $(0.79 \leq x \leq 0.95)$ and for $\{x_1CO_2 + (1-x_1)\}\{x_2$ sulfolane $+ (1-x_2)$ water$\}$ $(0.5 \leq x \leq 0.95)$. These linear regions increase with increasing temperature and decrease with increasing pressure consistent with (liquid +vapour) phase separation. Christensen et $al.$[13-16] have confirmed similar behaviour
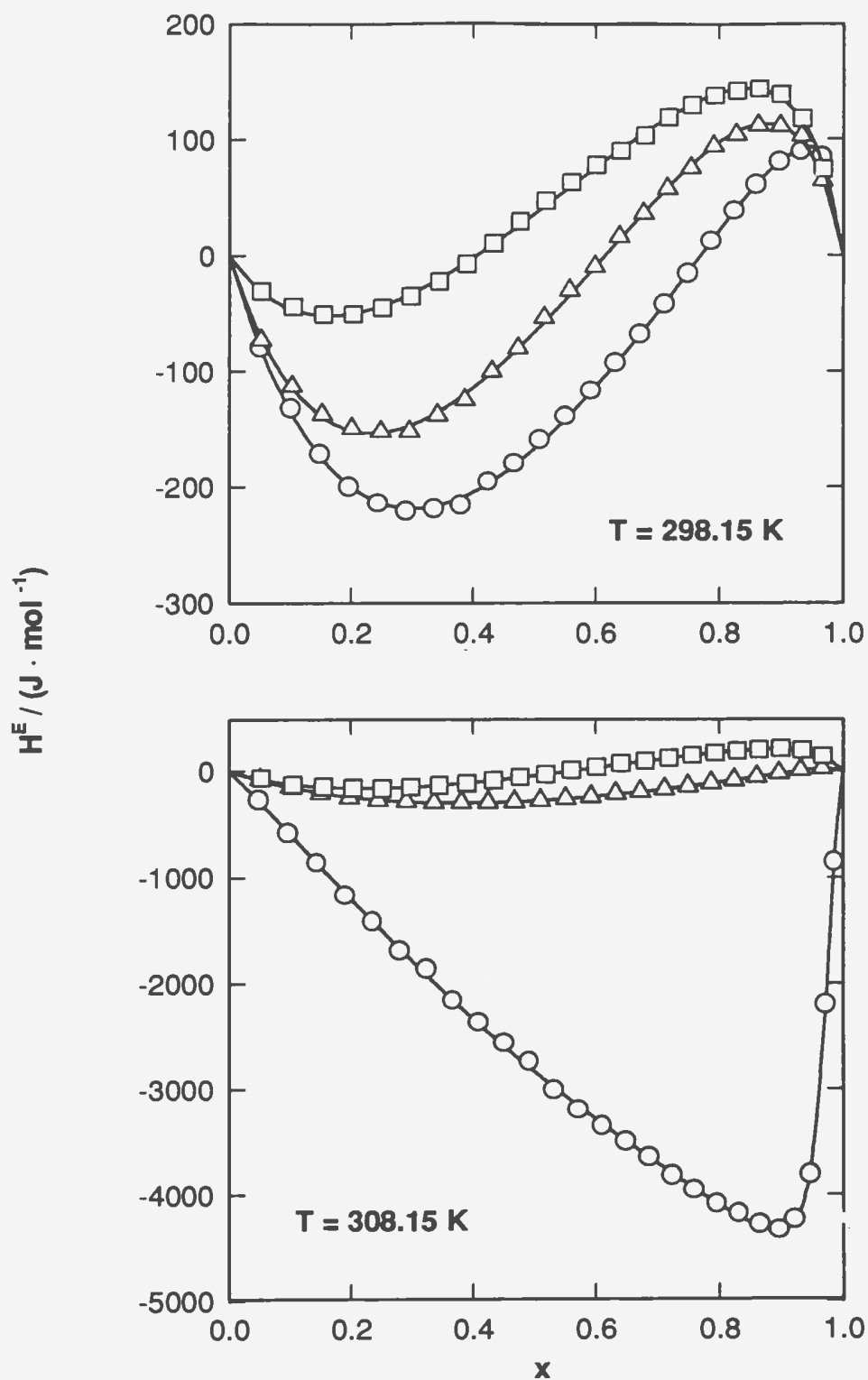
Figure 15. H^E for {x CO_2 + (1-x) ethanol}. ○ , p = 7.5 MPa
△ , p = 10.0 MPa; □ , p = 12.5 MPa.
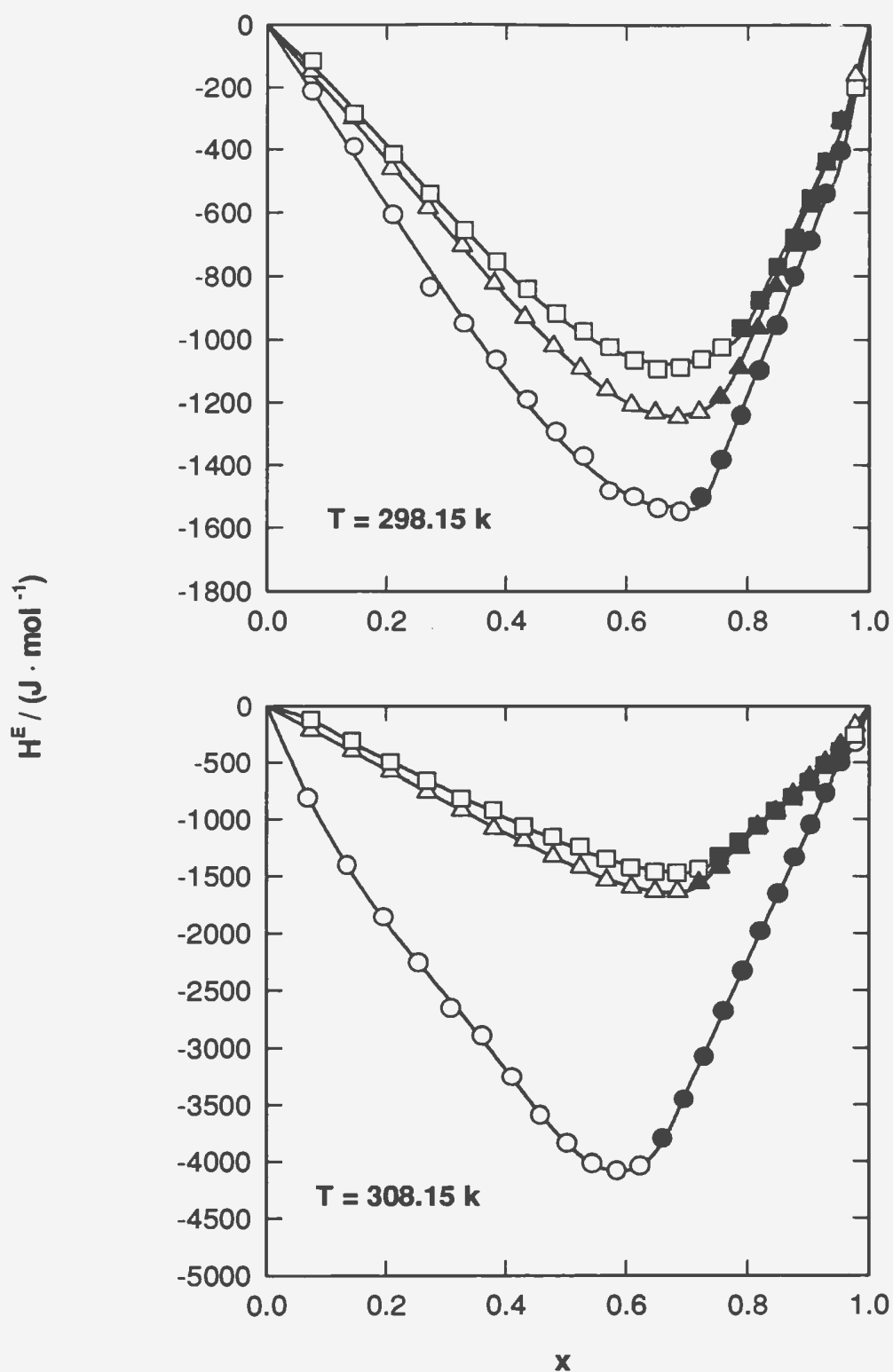
Figure 16. H^E for {x CO_2 + (1-x) propylene carbonate}. ○ , 7.5 MPa; △ , 10.0 MPa; □ , 12.5 MPa.   Black symbols are experimental data in two-phase region.
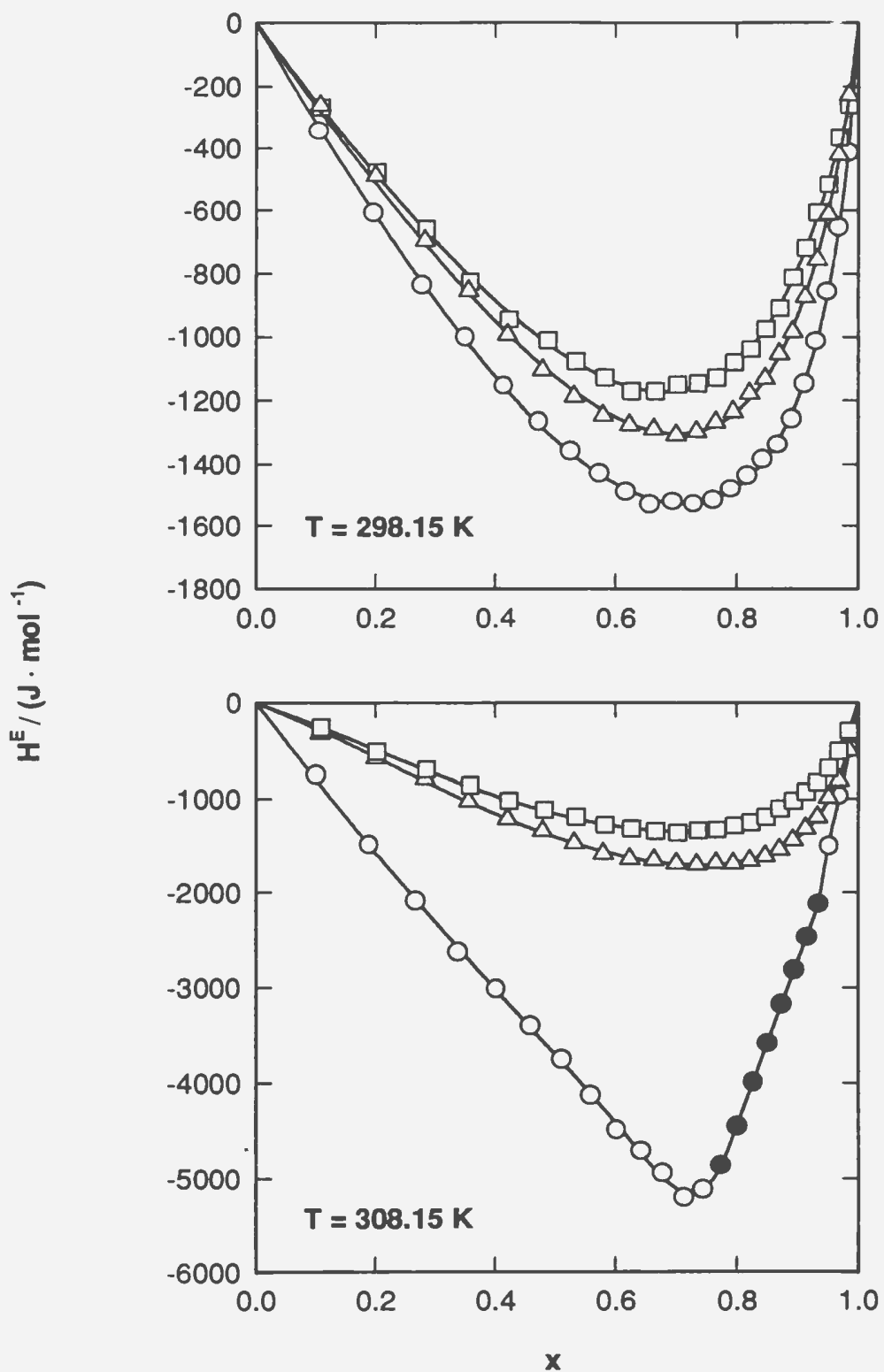
Figure 17. H^E for {x CO$_2$ + (1-x) N-methyl-e-caprolactam}.○ , p = 7.5 MPa △ , p = 10.0 MPa; □ , p = 12.5 MPa. Black symbols are experimental data in the two-phase region.
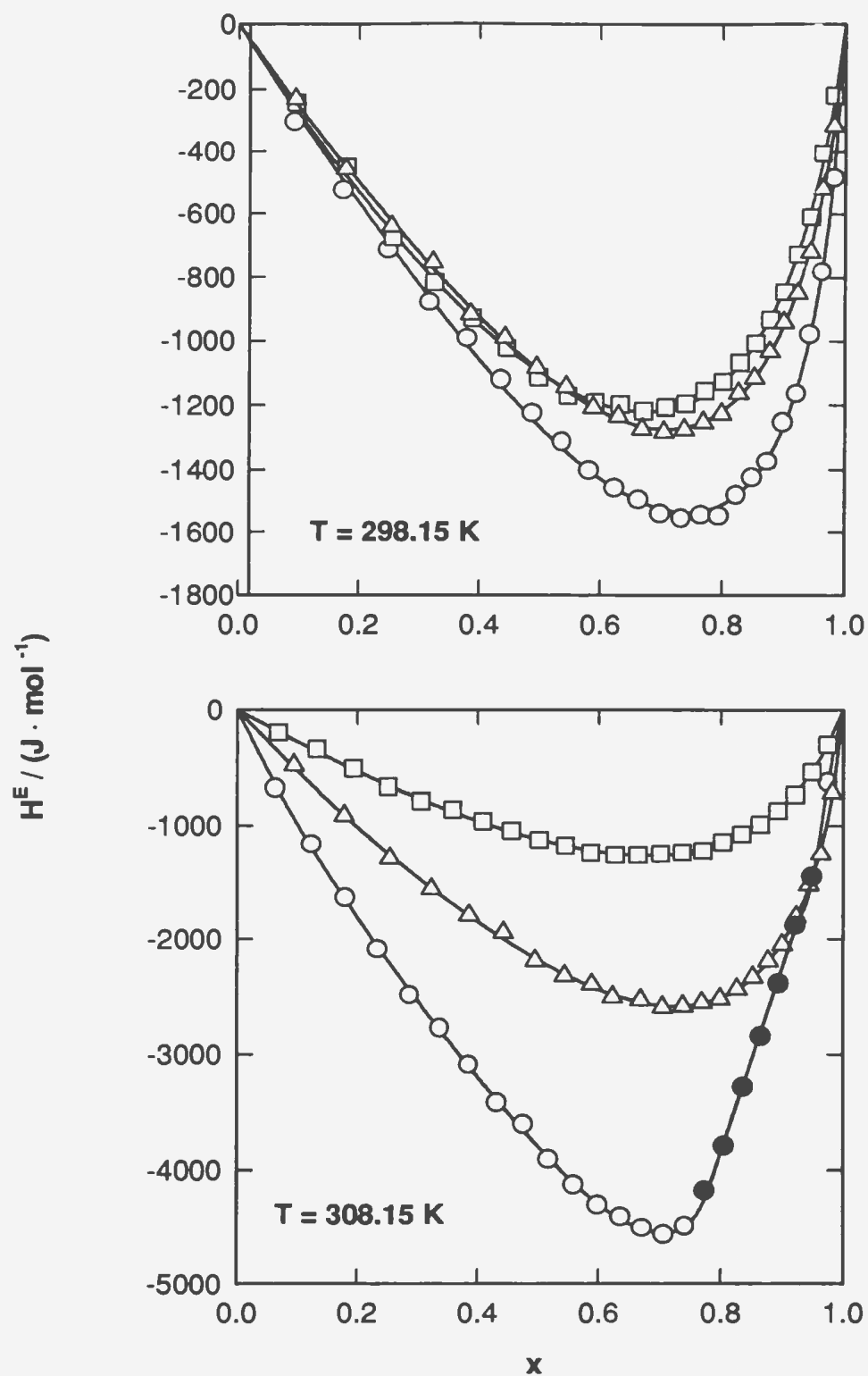
Figure 18. H^E for {x CO_2 + (1-x) 1-formyl piperidine}. $\bigcirc$, p = 7.5 MPa; $\triangle$, p = 10.0 MPa; $\square$, p = 12.5 MPa. Black symbols are experimental data in the two-phase region.
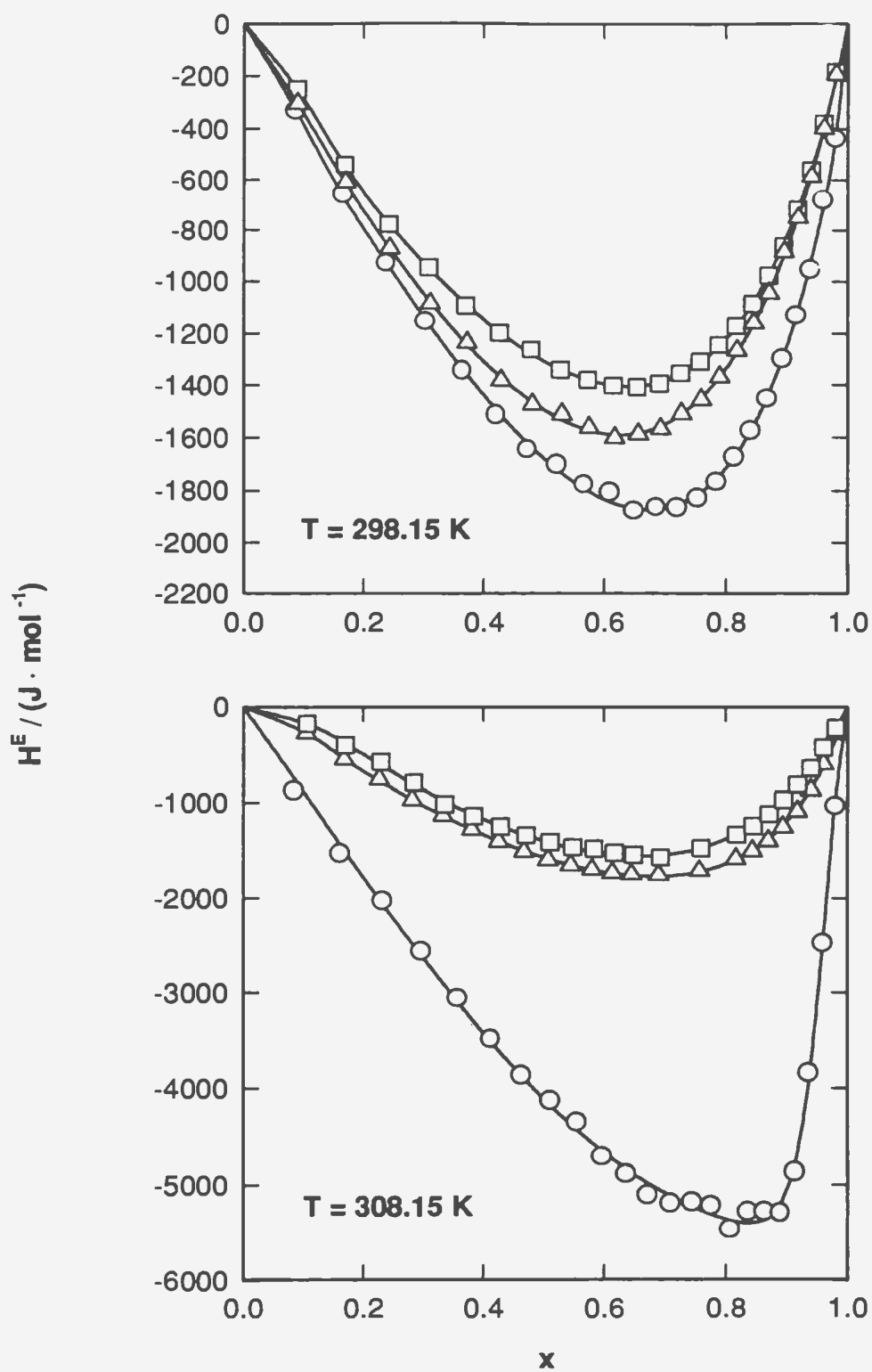
Figure 19. H^E for {x CO_2 + (1-x) ethylene glycol dimethyl ether}.
○ , p = 7.5MPa; △ , p = 10.0 MPa; □ , p = 12.5 MPa.
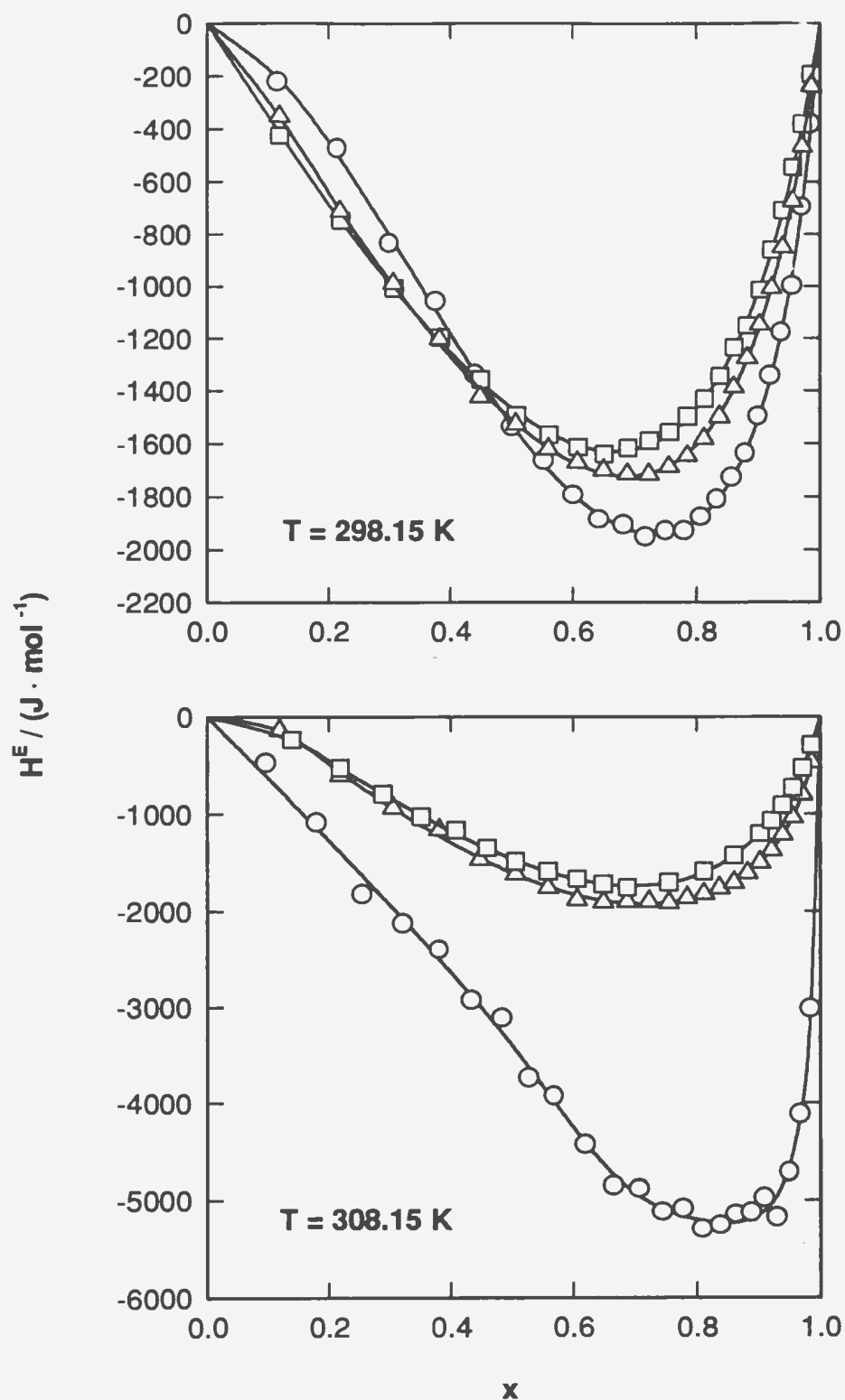
Figure 20. H^E for {x CO_2 + (1-x) 2-methoxyethyl ether}. ○ , p = 7.5 MPa; △ , p = 10.0 MPa; □ , p = 12.5 MPa.
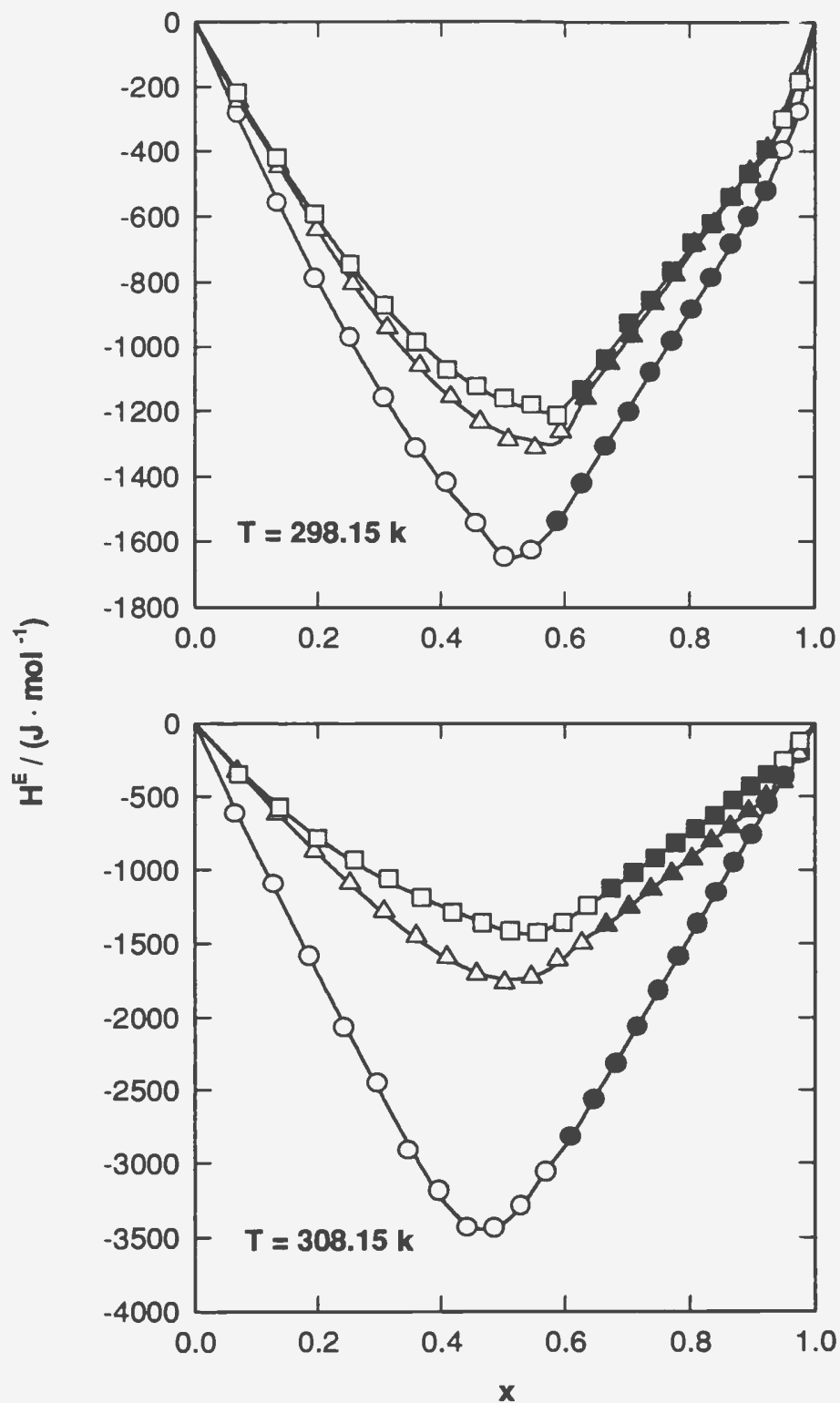
Figure 21. H^E for {x CO_2 + (1-x) sulfolane(3.43% wt. water)}. ○ , p = 7.5 MPa △ , p = 10.0 MPa; □ , p = 12.5 MPa. Black symbols are experimental data in the two-phase region.

in heat of mixing measurements on other (CO_2 + solvent) systems whose phase behaviour is known, and we assume the linear regions in our data do correspond to the (liquid + vapour) phase boundaries. The two-phase regions become most pronounced at 308.15 K and 7.5 MPa. For {xCO_2 + (1-x)N-methyl-ε-caprolactam}, {xCO_2 + (1-x)1-formyl piperidine}, {xCO_2 + (1-x)ethanol}, {xCO_2 + (1-x)ethylene glycol dimethyl ether}, and {xCO_2 + (1-x)2-methoxyethyl ether}, it seems that the linear sections are not present at the lower temperature and the high pressures, but the linearity was observed at T = 308.15 K and p = 7.5 MPa in the range (0.77 $\leq$ x $\leq$ 0.94) for {xCO_2 + (1-x)N-methyl-ε-caprolactam} and (0.77 $\leq$ x $\leq$ 0.93) for {xCO_2 + (1-x)1-formyl piperidine}. For {xCO_2 + (1-x)ethanol}, {xCO_2 + (1-x)ethylene glycol dimethyl ether}, and {xCO_2 + (1-x)2-methoxyethyl ether}, the linear sections only occurred in a very narrow CO_2-rich region. The boundaries for the two-phase mixtures at each temperature and pressure are listed in Table A.4.10.

The experimental plots of H^E vs $x(CO_2)$ for the mixtures {xCO_2 + (1-x) 2-methoxyethyl ether} are similar to the other mixtures studied except that the isobaric H^E curves cross one another in the solvent-rich region. The effect has been observed by Hauser[22] in CO_2-selexol mixtures at 298.15 K. The experimental measurements in this region were characterized by unstable output signals, especially at the highest temperature and lowest pressure.

5.5   Discussion

The excess molar enthalpy data presented above display large variations with temperature and pressure. Clearly both the effects of intermolecular association and the proximity to the critical point of CO_2 play important roles in determining H^E. In the discussion below, three classes of behaviour can be considered: (a) mixtures of two hydrogen bonded solvents (ethanol-water) in which near-critical effects are absent; (b) mixtures of CO_2 with ethanol, a strongly hydrogen bonded solvent; (c) mixtures of CO_2 with highly polar non-hydrogen bonded molecules.

5.5.1   The Ethanol-Water System

Excess molar enthalpies of ethanol-water mixtures have been determined over a wide range of conditions[49,50,52,]. At the temperatures and pressures studied here, both ethanol and water are in the liquid state, and the knowledge that they are strongly self-associated through hydrogen bonding is well established. The shapes of the H^E curves have been interpreted qualitatively by Franks[53] in terms of the molecular interactions in solution. As a solute, ethanol contains a hydroxyl group which can form hydrogen-bonds with water, and an alkyl chain which, by virtue of its large negative entropy of hydration, tends to force the solute out of solution. The negative entropy of hydration is accompanied by more favourable hydrogen bonding in the neighbouring solvent molecules, the so-called "hydrophobic" effect. The excess

molar enthalpy of ethanol-water mixtures is negative throughout the range. It is believed that, in dilute solutions, the ethanol is accommodated in the cavities in the hydrogen-bonded water network and that some of the weakly bonded water forms stronger water-water hydrogen bonds because of the hydrophobic effect. As more ethanol is added, the stabilization of the water structure reaches a maximum when no more solute can be accommodated in the cavities. This point corresponds to the minimum value in the H^E curve ($x \approx 0.15$). Similar behaviour is observed in the excess molar volume curves[53]. At high mole fractions, which correspond to progressively more dilute solutions of water in ethanol, the exothermic behaviour of H^E is due to the energetically favourable solvation of water which is associated with hydrogen bonding effects[53].

The H^E values for the mixtures at 298.15 K were essentially independent of pressure over the entire composition range, probably because of the low isothermal compressibilities of ethanol and water: β_T (ethanol) $= 11 \cdot 10^{-10} \, m^2 \cdot N^{-1}$, and β_T (water) $= 4.6 \cdot 10^{-10} \, m^2 \cdot N^{-1}$.

5.5.2 The CO_2 - Ethanol Mixtures

Excess molar enthalpies and excess volumes of mixtures for (CO_2 + ethanol) and other (CO_2 + alkanol) systems have been reported by Christensen *et al.*[54] and

Cordray *et al.*[51]. The results are very similar to those for (alkane + alkanol) mixtures. These have been analyzed in depth by Ott *et al.*[55] Ethanol is a highly polar molecule which contains one -OH group and thus it can participate in hydrogen bonding to form chain or ring structures. When CO_2 is added to the liquid, small amounts can be accommodated in the cavities in the hydrogen-bonded ethanol network and these stabilize the solution "structure". Figure 15 indicates that H^E curves display a minimum in the range $0.2 < x < 0.3$ (except at 308.15 K and 7.5 MPa), which presumably corresponds to the optimum concentration for stabilization. In the CO_2-rich region, the positive H^E values suggest that the hydrogen bonded networks of ethanol are significantly disrupted.

Alkanols are known to undergo reversible reactions with CO_2 to form hydrogen carbonates and bicarbonates. Experiments to measure formation constants for these equilibria are difficult and no values were found in the literature. However, these species are unstable[56,57] and are not believed to contribute significantly to H^E. If the degree of carbonate formation is similar to that in the (CO_2 + water) system, which undergoes reactions to form H_2CO_3, the effect on H^E for the CO_2-ethanol system would be less than 0.2 percent[58,59]

By definition, the H^E values of a mixture reflect the difference in enthalpy between the solution and the pure components. So, H^E is strongly affected when one of the fluids is near its critical point.[13-18] The large negative H^E values at 308.15 K

and 7.5 MPa are predominately due to this effect, which is discussed in detail below.

5.5.3 Mixtures of CO_2 with Highly Polar Solvents

N-methyl-ϵ-caprolactam, propylene carbonate, sulfolane, and 1-formyl piperidine are large molecules with high dipole moments and no hydrogen bonding between like molecules. The solubility of CO_2 in these solvents is unusually high[1-3], consistent with the excess molar enthalpies which are more negative than those observed for the CO_2-ethanol system at 298.15 K. It is likely that this behaviour arises from a void-filling mechanism (mainly at low mole fractions) and strong dipole-quadrupole interactions between CO_2 and the solvents. It is possible that an additional exothermic effect may arise from reversible rearrangement reactions within the cyclic amide rings of N-formyl piperidine and N-methyl-ϵ-caprolactam at high pressures of CO_2.[56] No spectroscopic measurements have been made on these systems, and the nature of the intermolecular interactions has not been reported in the literature. However, similar enthalpic behaviour is also observed for propylene carbonate, ethylene glycol dimethyl ether and 2-methoxyethyl ether, systems in which no such reactions can take place. This suggests that the chemical effects in the mixtures are very small.

Compared with the (ethanol + water) systems in which the H^E values are independent of pressure over the range studied, the mixtures (CO_2 + physical solvent)

show significant changes in H^E as the pressure is varied. At 308.15 K and 7.5 MPa the changes become striking. These large changes in H^E with temperature and pressure may be explained by classical near-critical effects associated with the fluid properties of CO_2.

As mentioned in Chapter 2, the change in the excess enthalpy with temperature at constant pressure can be expressed by the equation

$$(\partial H^E/\partial T)_p = C_p^E = C_p(mixture) - x C_p(CO_2) - (1-x) C_p(solvent) \quad (25)$$

where C_p^E is the excess molar heat capacity at constant pressure. The change in H^E with pressure at constant temperature is given by the equation

$$(\partial H^E/\partial p)_T = V^E - T(\partial V^E/\partial T)_p \quad (26)$$

where V^E is the excess molar volume. A detailed analysis by Wormald[21] has shown that large changes in the values of C_p^E and V^E may be expected in mixtures at temperatures and pressures near the critical region. Since the critical temperatures of the solvents are far from the temperatures of this study, the large negative values of H^E at 308.15 K and 7.5 MPa in all of the mixtures studied undoubtedly arise from the effect of the near-critical properties of CO_2. In Chapter 6, an attempt is made to estimate the relative magnitude of these effects by modelling the behaviour of H^E for all the systems studied here by a cubic equation of state with a composition-dependent interaction parameter.

5.5.4 Mixtures of CO_2 with Dimethyl Ethers of Polyethylene Glycols

The dimethyl ether of polyethylene glycol $CH_3(OCH_2CH_2)_nOCH_3$ is the solvent used in the "Selexol" gas-treating process. This work examined two of the pure components of selexol as model systems: ethylene glycol dimethyl ether (n = 1) and 2-methoxyethyl ether (n = 2). Although these are also polar physical solvents, no evidence of phase separation was observed in the H^E curves, even at 308.15 K and 7.5 MPa. For the mixture (CO_2 + ethylene glycol dimethyl ether), the experimental plots of H^E vs x are similar to those for the mixtures discussed in the previous section. However, the isobaric H^E curves for (CO_2 + 2-methoxyethyl ether) cross one another in the solvent-rich region, *i.e.* the H^E curves do not follow the usual pressure-dependence H^E (p = 12.5 MPa) > H^E (p = 10.0 MPa) > H^E (p = 7.5 MPa) observed in other mixtures. The experimental measurements in this region were characterized by unstable output signals, especially at the higher temperatures and lower pressures. The phenomenon may be explained by two possibilities: (1) incomplete mixing or heating effects due to difference in viscosity between the two fluids at the temperatures and pressures studied and (2) the formation of a heterogeneous phase on mixing, (*i.e.* a liquid-liquid two-phase region). No evidence of liquid-liquid phase separation has been reported in the literature.

6.   EQUATIONS OF STATE

6.1   General Background

A mathematical relation between pressure, volume, and temperature (pVT properties) is called an equation of state. The use of a single equation of state to reproduce the thermodynamic properties of both pure compounds and mixtures in the vapour or liquid phase has been one of the most elusive research goals of thermodynamics for over a century. In principle, a complete description of the thermodynamic properties of a mixture may be obtained from an equation of state providing the equation is valid at the temperature of interest over the entire composition range from an ideal gas to a liquid state. In 1873, van der Waals[60] proposed an equation of state which was an attempt to extend the ideal-gas equation to real fluids. The van der Waals equation of state has the form:

$$(p + a/V^2) \ (V - b) = RT \tag{27}$$

Equation (27) is a "cubic" equation of state, because it can be rearranged into a cubic form which is straightforward to solve in pratical calculations. To account for the

intrinsic volume occupied by the particles, the molar volume in the ideal-gas equation of state has been replaced by the term (V - b). To allow for the effect of inter-molecular interactions, the pressure was replaced by the term (p + a / V^2). The constant b is the intrinsic, hard-sphere volume of the particles, and the constant a is a measure of the attractive forces. The fit between experiment and this equation is good in the gaseous region for $T_R < 1$; it is also good up to $p_R = 1$ for $T_R > 1$. For higher pressures and in the liquid region, the van der Waals equation is unsatisfactory. Modern equations of state range in complexity from simple cubic expressions containing two or three constants to complicated forms containing more than fifty constants. Although the many-constant equations have been utilized for precise representation of experimental results, they are not generally preferred for calculations involving process applications, partly because they require excessive computer time and partly because it is difficult to obtain generalized forms of these equations suitable for mixture calculations. In many situations, therefore, the use of simple equations of state represents a satisfactory compromise between accuracy and speed of computation. In 1949, Redlich and Kwong[61] proposed a modified van der Waals equation:

$$p = RT/(V - b) - a/T^{0.5}/[V(V + b)] \qquad (28)$$

This cubic equation was used successfully to represent the vapour-liquid equilibrium

(VLE) properties of both pure gases and pure liquids, as well as some mixtures. Since that time, numerous modified Redlich-Kwong (RK) equations have been reported[62-65].

6.2   The Peng-Robinson Equation of State

The Peng-Robinson equation of state is among the most successful cubic equations for vapour-liquid equilibrium and other thermodynamic property calculations. The equation has the following form[61] :

$$p = RT/(V - b) - a(T)/[V(V + b) + b(V - b)] \qquad (29)$$

At the critical point, the constants a and b are defined by the equations:

$$a_c = 0.45724 \ R^2 T_c^2/p_c \qquad (31)$$

$$b_c = 0.07780 \ RT_c/p_c \qquad (30)$$

where a_c and b_c are the constants at the critical point of a pure component. At temperatures other than the critical, $b(T) = b_c$, and $a(T)$ is calculated by the equation:

$$a(T) = a_c \cdot \alpha(T_R, \omega) \qquad (32)$$

Here $\alpha(T_R, \omega)$ is a dimensionless function of reduced temperature and the Pitzer acentric factor[62], and equals unity at T_c. The parameters, α and T_R can be linearized by the following expression:

$$\alpha^{1/2} = 1 + \kappa(1 - T_R^{1/2}) \tag{33}$$

where κ is a constant that has been correlated against the Pitzer acentric factor for simple classes of hydrocarbons.[62] The resulting equation is:

$$\kappa = 0.37464 + 1.54226\,\omega - 0.26992\,\omega^2 \tag{34}$$

As a consequence of equations (29) to (31), the compressibility factor at the critical point, Z_c, is a constant ($Z_c = 0.307$) for all liquids.

6.3   Evaluation of Parameters

The determination of the pure component parameters a and b in the Peng-Robinson equation requires values for the critical properties p_c, T_c and the acentric factor ω of each component involved in the calculation. The parameters a and b for CO_2, C_2H_5OH and H_2O were obtained from equations in the original paper of Peng and Robinson.[62] Critical properties for propylene carbonate, N-methyl-ϵ-caprolactam, 1-formyl piperidine, sulfolane, ethyl glycol dimethyl ether and 2-methoxyethyl ether were not available in the literature. Other alternatives to overcome the problem were sought.

Panagiotopoulos and Kumar[66] proposed a generalized technique for the calculation of the pure component parameters for use in a two-parameter equation of state. In their considerations, two dimensionless parameters ϵ and η were defined as:

$$\varepsilon = bp/RT \tag{35}$$

$$\eta = ap/R^2T^2 \tag{36}$$

Here, ϵ and η are functions of the compressibility factor of the saturated liquid, Z_L, which is defined by the equation:

$$Z_L = p^{vp}V_L/RT \tag{37}$$

where, p^{vp} is the vapour pressure and V_L is the saturated liquid molar volume of a component at a given temperature. The relationships between Z_L, ϵ, η were summarized in tabular form in the paper.[66] For most of the physical solvents studied here, however, the vapour pressures and saturated liquid molar volumes required by the method are also not available.

Dohrn[67] has recently reported an alternative method to obtain pure-component parameters of two-parameter equations of state. The procedure requires only the liquid molar volume of a fluid at $T = 293.15$ K, and the normal boiling temperature. The parameters are defined as follows:

$$b_c = \Omega_b [b^{(1)}V_{L20}T_b + b^{(2)}] \tag{38}$$

$$a_c = \Omega_a a^{(1)}(b_cT_b/\Omega_b)^{a^{(2)}} \tag{39}$$

where Ω_a and Ω_b are constants which have distinct values for each cubic equation of

state. For example, in the Peng-Robinson equation they are 0.45724 and 0.07780, respectively. The parameters $a^{(1)}$, $a^{(2)}$, $b^{(1)}$ and $b^{(2)}$ are constants reported by Dohrn in tabular form. The acentric factor, ω, is estimated from the equation:

$$\omega = -(3/7)\,[\log(101.3\,kPa/p_c)]\,/\,[(T_c/T_b)-1]-1 \qquad (40)$$

The critical parameters and acentric factors for all the polar solvents in this study were estimated from equations (29) to (34) and (38) to (40). The ternary mixture $\{x_1 CO_2 + (1-x_1)[x_2 \text{ sulfolane} + (1-x_2) \text{ water}]\}$ was treated as a pseudo-binary system because the mole ratio of sulfolane/water is fixed. The values T_c, p_c and ω for the sulfolane were estimated by Dohrn's method[67] from the density at 20°C and the boiling point of pure sulfolane.[48] The values for the mixture [x_2 sulfolane + (1-x_2) water] were calculated from the procedures proposed by Li[68], Kreglewski and Kay[69] and Spencer *et al.*[70] as modified by Reid *et al.*[71] The estimated values T_c, p_c and ω of all solvents are summarized in table A.5.1 together with the a and b parameters derived from them.

6.4   Mixing Rules

To extend the application of cubic equations of state from pure fluids to mixtures, a mixing rule is generally used. For simple nonpolar mixtures, the "one-

fluid" mixing rules of van der Waals are most commonly used:

$$a_m = \sum_{i=1}^{nc} \sum_{j=1}^{nc} x_i x_j a_{ij} \tag{41}$$

and

$$b_m = \sum_{i=1}^{nc} \sum_{j=1}^{nc} x_i x_j b_{ij} \tag{42}$$

where a_{ii} and b_{ii} are the pure fluid parameters and a_{ij} and b_{ij} are cross interaction parameters obtained from a set of combining rules. The most commonly used combining rules are:

$$a_{ij} = a_i^{1/2} a_j^{1/2} (1 - k_{ij}) \tag{43}$$

and

$$b_m = \sum_{i=1}^{nc} x_i b_{ii} \tag{44}$$

Here nc is the number of components and the interaction parameter k_{ij} is a correction term which, generally, is considered to be composition-independent. For a mixture of compounds similar in size and chemical nature (*i.e.*, the hydrocarbons and inorganic gases), composition-dependent phase equilibria can be correlated quite well with the one-fluid mixing rules and a single adjustable k_{ij}. However, the predicted

results for mixtures containing molecules dissimilar in size or chemical nature may not be in good agreement with experiment. The agreement becomes worse for mixtures containing strongly polar components.

Several mixing rules for polar systems have been proposed in the literature. Luedecke and Prausnitz[72] proposed density-dependent mixing rules. When used in the Peng-Robinson equation of state, a_m is expressed by the equation:

$$a_m = \sum_{i=1}^{nc} \sum_{j=1}^{nc} x_i x_j (a_{ii} a_{jj})^{1/2} (1 - k_{ij}) + [\frac{\rho}{RT} \sum_{i=j}^{nc} \sum x_i x_j (x_i \bar{c}_{ji} a_{jj}^2 (T_c))] \quad (45)$$

In 1992, Wong and Sandler[73] proposed an alternative composition-dependent mixing rule which is theoretically more rigorous. They assumed that in a liquid solution the molecules are so closely packed that there is no free volume. The limit in an equation of state is :

$$\lim_{p \to \infty} V_i = b_i, \qquad \lim_{p \to \infty} V_m = b_m \quad (46)$$

Therefore, if we equate the excess Helmholtz free energy at infinite pressure from an equation of state to that of a liquid solution model we have:

$$A^E = - a_m/b_m + \sum_i x_i a_i/b_i \quad (47)$$

Equations (45) and (47) define a_m and b_m in terms $A^E(x)$. These equations can be solved to obtain

$$b_m = \frac{\sum_i \sum_j x_i x_j (b - a/RT)_{ij}}{1 + (A^E(x)/RT) - \sum_i x_i (a_i/b_i RT)} \tag{48}$$

and

$$a_m/b_m = \sum_i x_i a_i/b_i - A^E(x) \tag{49}$$

The mixing rule was applied to examine experimental vapour-liquid, liquid-liquid and vapour-liquid-liquid equilibrium data for several binary or ternary systems at both low pressures and high pressures. The results indicated that the mixing rule is very good for both the correlation and prediction of phase behaviour. It has not yet been extended to the calculation of H^E.

Panagiotopoulos and Reid[74] proposed the use of a nonquadratic mixing rule for a_m in phase equilibrium calculations. They used a linear function of mole fraction in the combining rule for a_{ij}:

$$a_{ij} = (a_i a_j)^{1/2} [1 - k_{ij} + (k_{ij} - k_{ji}) x_i] \tag{50}$$

The term $[1 - k_{ij} + (k_{ij} - k_{ji}) x_i]$ is composition-dependent. If $k_{ij} = k_{ji}$, equation (44) is obtained. Panagiotopoulos and Reid successfully applied this mixing rule to highly polar ternary mixtures of carbon dioxide, water and ethanol.

6.5   Prediction of H^E

In this work we seek to model the experimental H^E values of all the mixtures studied using the Peng-Robinson equation of state as a means of correlating pressure and temperature effects. The mixing rules used here are those suggested by Panagiotopoulos and Reid[74]. The mixing rule is given by

$$a_m = \sum_i \sum_j x_i x_j a_{ij} \tag{51}$$

$$b_m = \sum_i x_i b_i \tag{52}$$

where

$$a_{ij} = (1 - \delta_{ij}) \, a_i^{1/2} a_j^{1/2} \tag{53}$$

$$\delta_{ij} = x_i k_{ij} + x_j k_{ji} \tag{54}$$

Here, i and j express the components of a mixture. For binary mixtures, i and j are 1 and 2, respectively. The linear dependence of δ_{ij} on x is used to represent variations in the composition dependence of solute-solvent interactions in highly nonideal mixtures.

The Peng-Robinson equation was fitted to our experimental results by optimizing the adjustable interaction parameters k_{12} and k_{21} to produce the best fit to results at T = 308.15 K and p = 12.5 MPa at low x (CO_2). Since k_{12} and k_{21} are

constants, a comparison with H^E values obtained at other temperatures and pressures provides a test of the model's self consistency. The fitted values of k_{12} and k_{21} for each binary mixture are given in table A.5.2.

6.6   Results

6.6.1 Comparisons with Literature Data

In order to check the generality of the model, first the predicted results were compared with those calculated using the one-fluid mixing rule. Figures 22 to 24 compare the consequence of fitting the Peng-Robinson equation with the Panagiotopoulos-Reid mixing rules (Eqns. 51-54) and the usual van der Waals mixing rules (Eqns. 41-44) to H^E for some typical mixtures. Figures 22 and 23 compare values for the systems $\{xCO_2 + (1-x)n\text{-hexane}\}^{(17)}$, $\{xCO_2 + (1-x)\text{toluene}\}^{(15)}$ and $\{xCO_2 + (1-x)\text{ethanol}\}$ respectively at 308.15 K and 12.5 MPa. Figures 22 and 23 show that the Panagiotopoulos-Reid model results in much better agreement with experimental data for simple hydrocarbons. Figure 24 shows even more striking differences between the models for $\{xCO_2 + (1-x) \text{ethanol}\}$. The van der Waals mixing rule performed poorly and even fails to predict the correct shape of the mixing curve. Figures 25 to 27 present H^E values which were calculated from the Panagiotopoulos-Reid mixing rules for CO_2-decane, CO_2-toluene and CO_2-ethanol
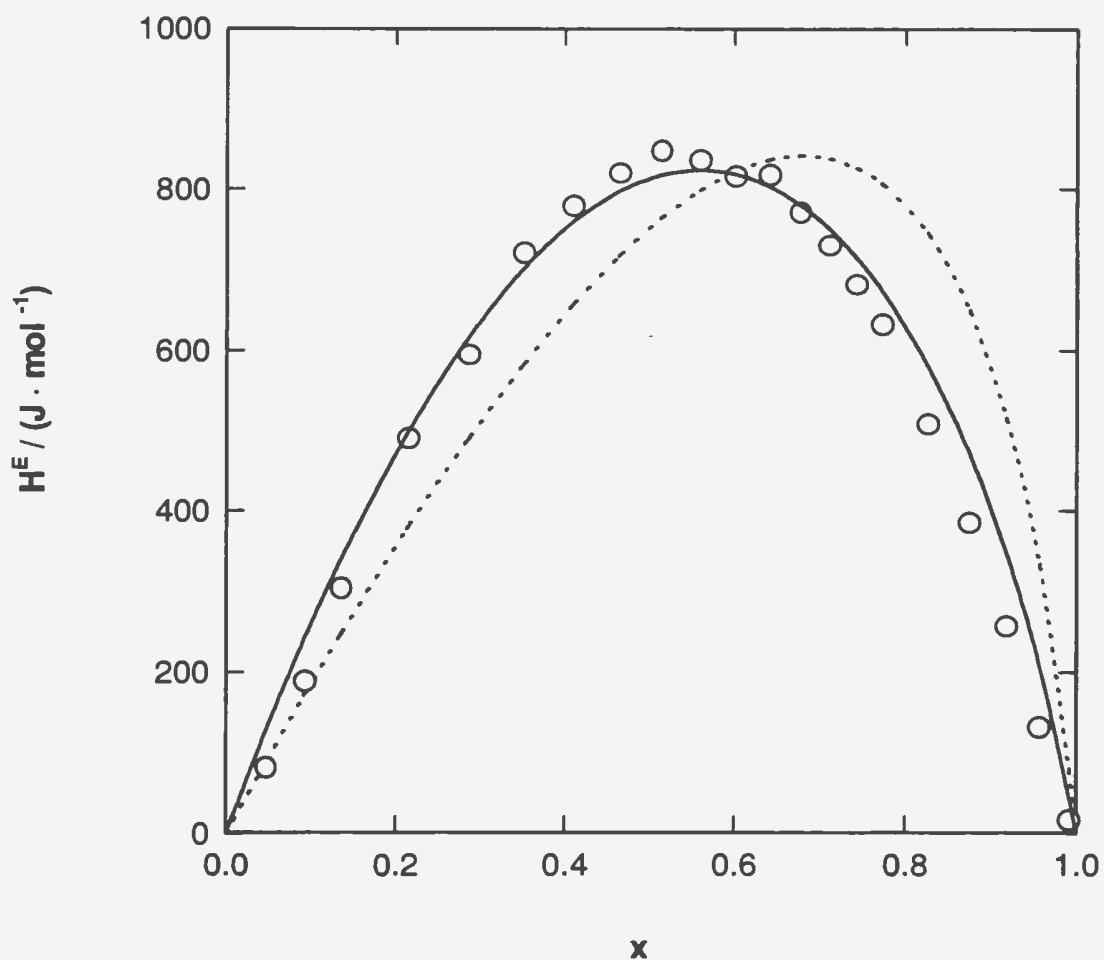
Figure 22. Comparison of results predicted for {x CO$_2$ + (1-x)n-hexane} at 308.15 K and 12.5 MPa by the conventional and the composition-dependent mixing rules, as defined by equations (41- 44)(the dotted line) and equations (51-54) (the solid line). o, the experimental data reported by Christensen et al[17].
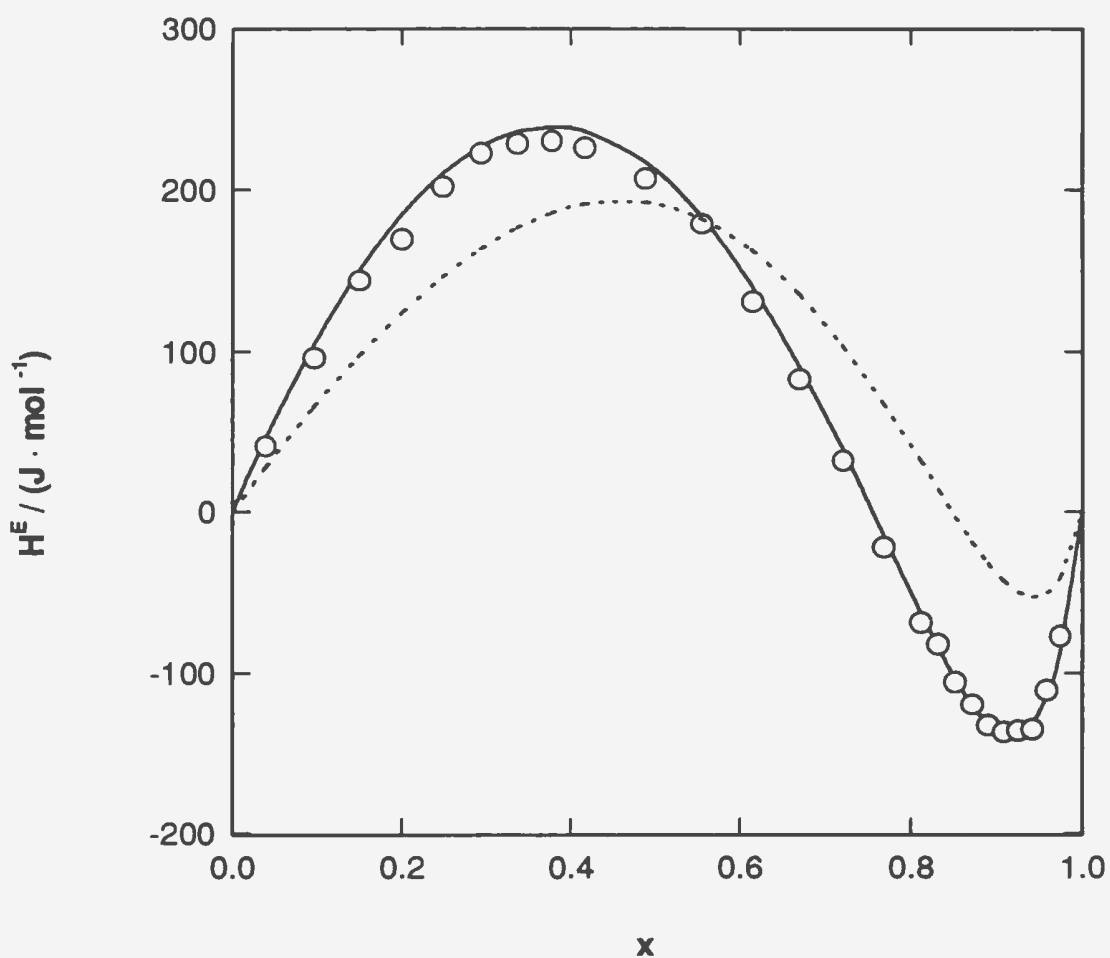
Figure 23. Comparison of results predicted for $\{x\ CO_2 + (1\text{-}x)\ \text{toluene}\}$ at 308.15 K and 12.67 MPa by the conventional and the composition -dependent mixing rules, as defined by equations (41-44) (the dotted line) and equations (51-54) (the solid line). o, the experimental data reported by Christensen et al[16].
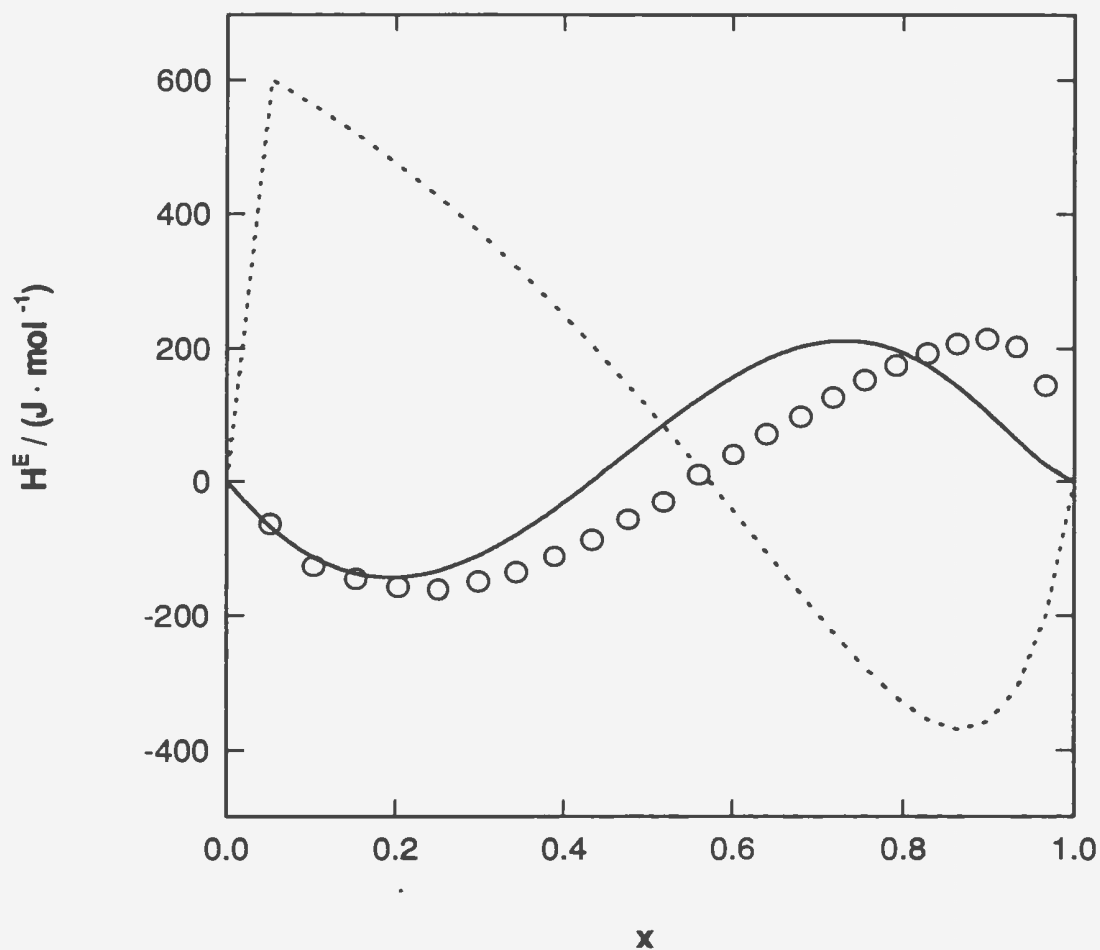
Figure 24. Comparison of results predicted for {xCO$_2$ + (1-x) ethanol}
at 308.15 K and 12.5 MPa by the conventional and the composition-
dependent mixing rules, as defined by equations (41-44) (the dotted
line) and equations (51-54) (the solid line). o, the experimental data
measured in this work.
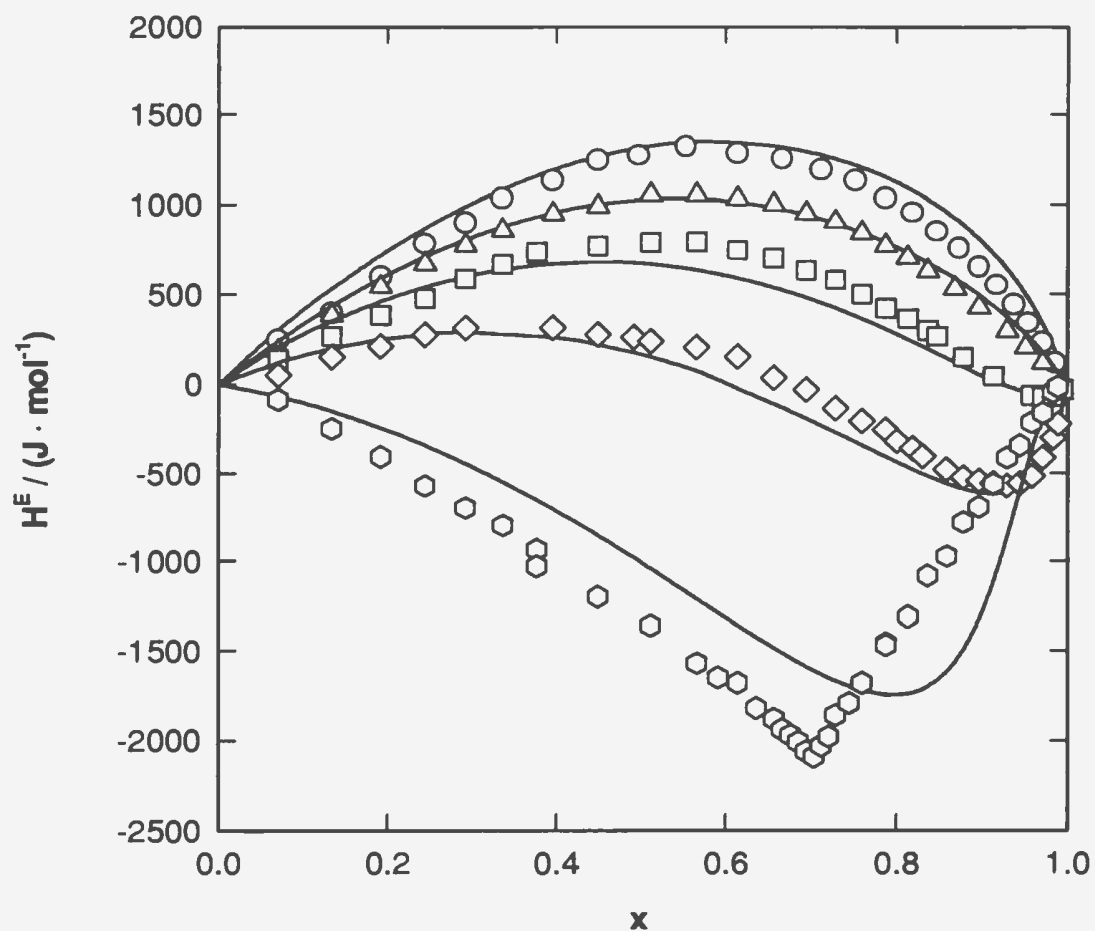
Figure 25. **Comparison of predicted and experimental results for {x CO$_2$ + (1-x) n-decane} at 12.5 MPa.** ○ , 273.15 K; △ , 303.15 K; □ , 313.15 K; ◇ , 323.15 K and ⬡ , 363.15 K.
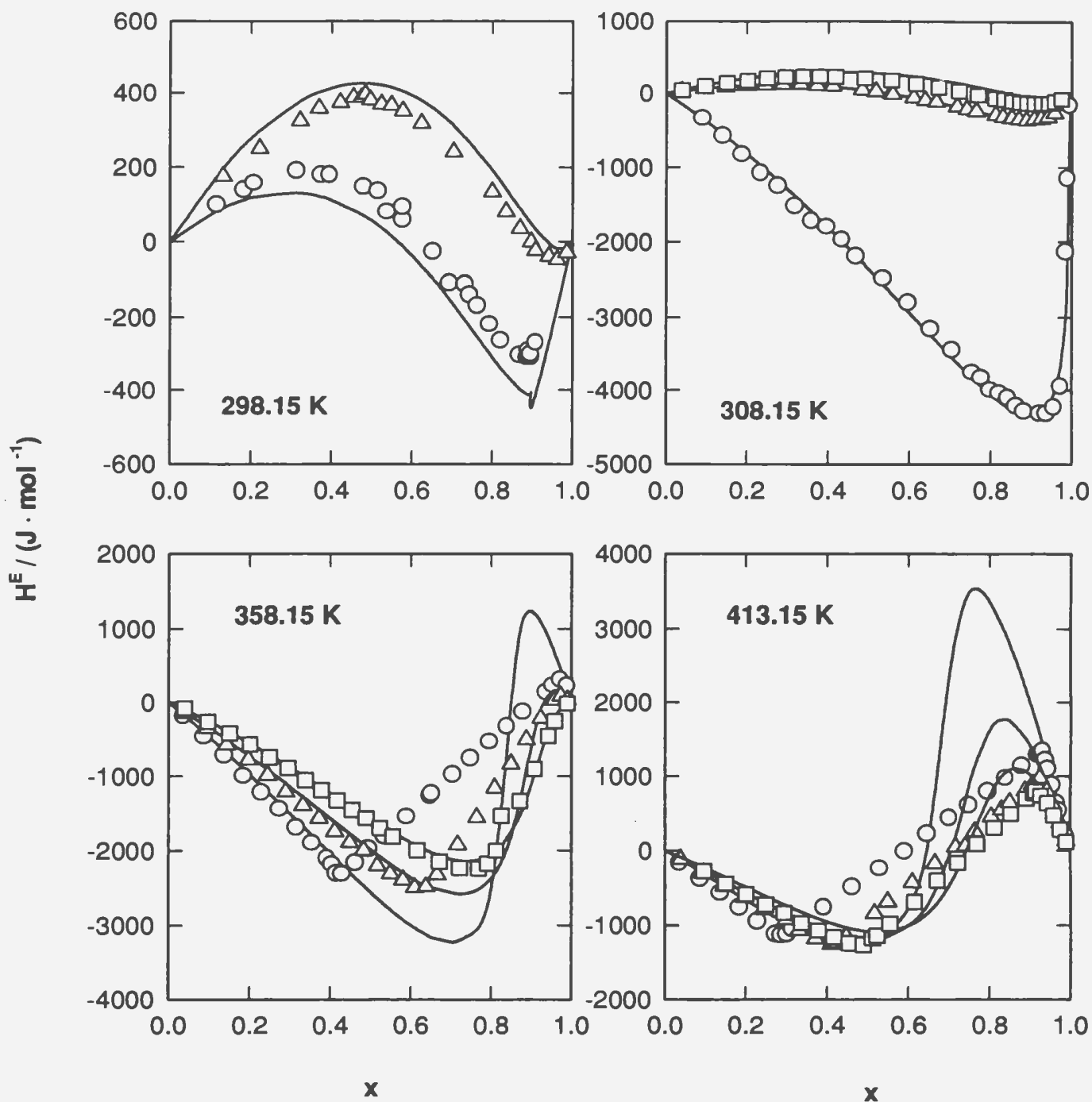
Figure 26. Comparison of predicted and experimental results for {xCO$_2$ + (1-x) toluene}. o, p = 7.5 MPa; △ ,10.64 MPa; □ ,p = 12.67 MPa. Symbols are experimental data reported by Christensen et al.[18] and Wormald[21].
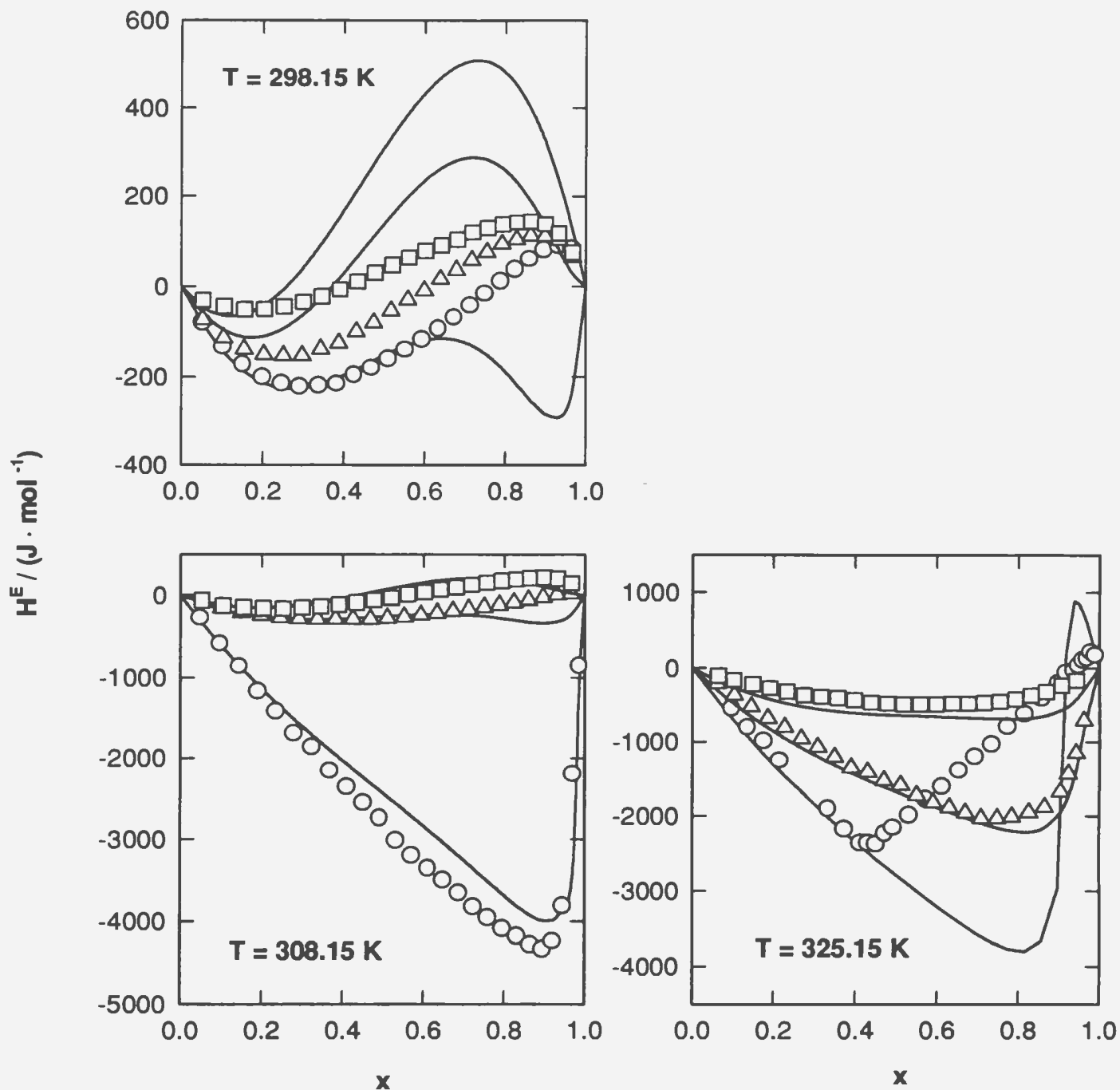
Figure 27. Comparisons of the experimental results with values calculated from the Peng-Robinson equation, with k_{12} and k_{21} given in table A.4.2, for $\{x\ CO_2 + (1-x)\ ethanol\}$. ○ , p = 7.5 Mpa; △ , p = 10.0 Mpa; □ , p = 12.5 Mpa.

mixtures over a wide range of temperature and pressure. The results indicate that the model yields a fairly satisfactory description of excess molar enthalpy as a function of composition, temperature and pressure. Although the predicted H^Es deviate significantly from the experimental results in the vapour-liquid equilibrium region, the results were in good agreement with the experimental data at low and high mole fractions and elevated temperatures.

6.6.2   Model Results for Polar and Hydrogen-Bonded Solvents

The excess molar enthalpies for the mixtures of $\{xCO_2 + (1-x)N$-methyl-ϵ-caprolactam$\}$, $\{xCO_2 + (1-x)1$-formyl piperidine), $\{xCO_2 + (1-x)$propylene carbonate$\}$, $\{xCO_2 + (1-x)[x_2$ sulfolane $+ (1-x_2)$ water$]\}$, $\{xCO_2 + (1-x)$ethanol), $\{xCO_2 + (1-x)$ethylene glycol dimethyl ether$\}$ and $\{xCO_2 + (1-x)2$-methoxyethyl ether$\}$ at temperatures 298.15 and 308.15 K and pressures 7.5, 10.0 and 12.5 MPa were fitted using the Peng-Robinson equation with a composition-dependent parameter. The critical temperatures, critical pressures and isothermal compressibilities of CO_2 and the solvents are listed in Appendix V (Table A.5.1) together with the parameters a and b used in the equations. The parameters k_{12} and k_{21} for each mixture are given in Table A.5.2. Comparisons of the predicted and experimental results of all mixtures studied are given in figures 28 to 34.

In general, the equations predict the correct shape and magnitudes of H^E for all mixtures over the entire composition range except for CO_2-rich regions at the lowest pressure. In these two-phase regions, the predicted values are always more negative than the experimental results. As can be seen from figures 27 to 33, the model overestimates the miscibility of 1-formyl piperidine and N-methyl-ϵ-caprolactam with CO_2 at 308.15 K and 7.5 MPa, and of propylene carbonate and sulfolane with CO_2 at all the temperatures and pressures studied. It is not clear whether the large deviations between the calculated and experimental H^Es may be improved by optimizing the pseudo-critical properties of the solvent to reproduce the vapour-liquid equilibrium data. We were unable to do so.

Although the interaction coefficients k_{12} and k_{21} determined for the Peng-Robinson equation of state from the experimental H^E show no temperature and pressure effects for any of the systems studied here, the calculated results in the CO_2-rich regions and the solvent-rich regions are very sensitive to the exact values of k_{12} and k_{21}, respectively. The use of the composition-dependent interaction parameters defined in equations (51)-(54) gives a significantly better fit to the H^E data relative to that obtained with a composition-independent interaction parameter. The success of the model in fitting the full set of thermodynamic variables (including V^E and VLE data) has, however, not yet been demonstrated.
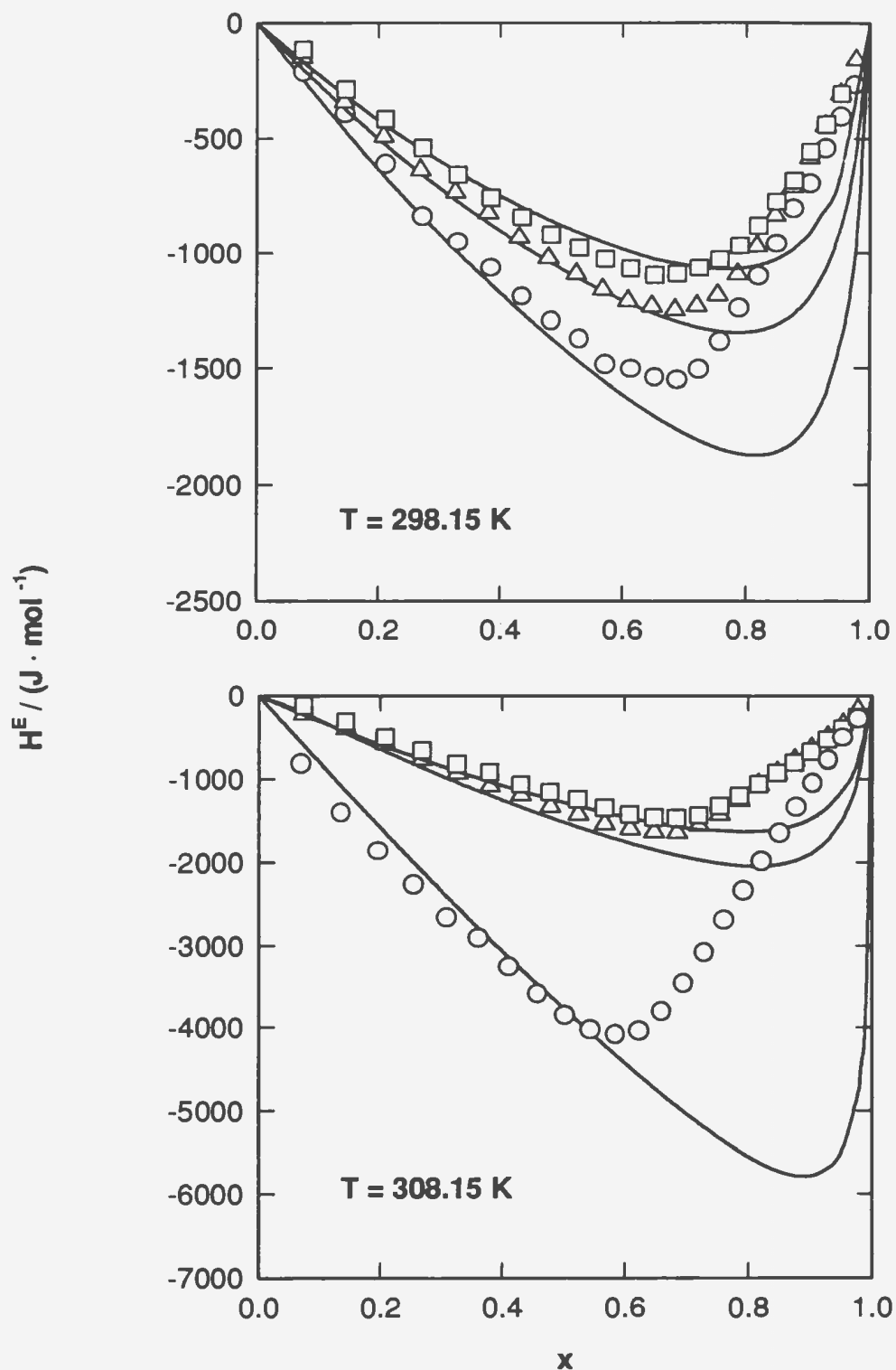
Figure 28. Comparison of the experimental results with values predicted from the Peng-Robinson equation for {xCO$_2$ + (1-x) propylene carbonate}. ○ , p = 7.5 MPa; △ , p = 10.0 MPa; □ , p = 12.5 MPa.
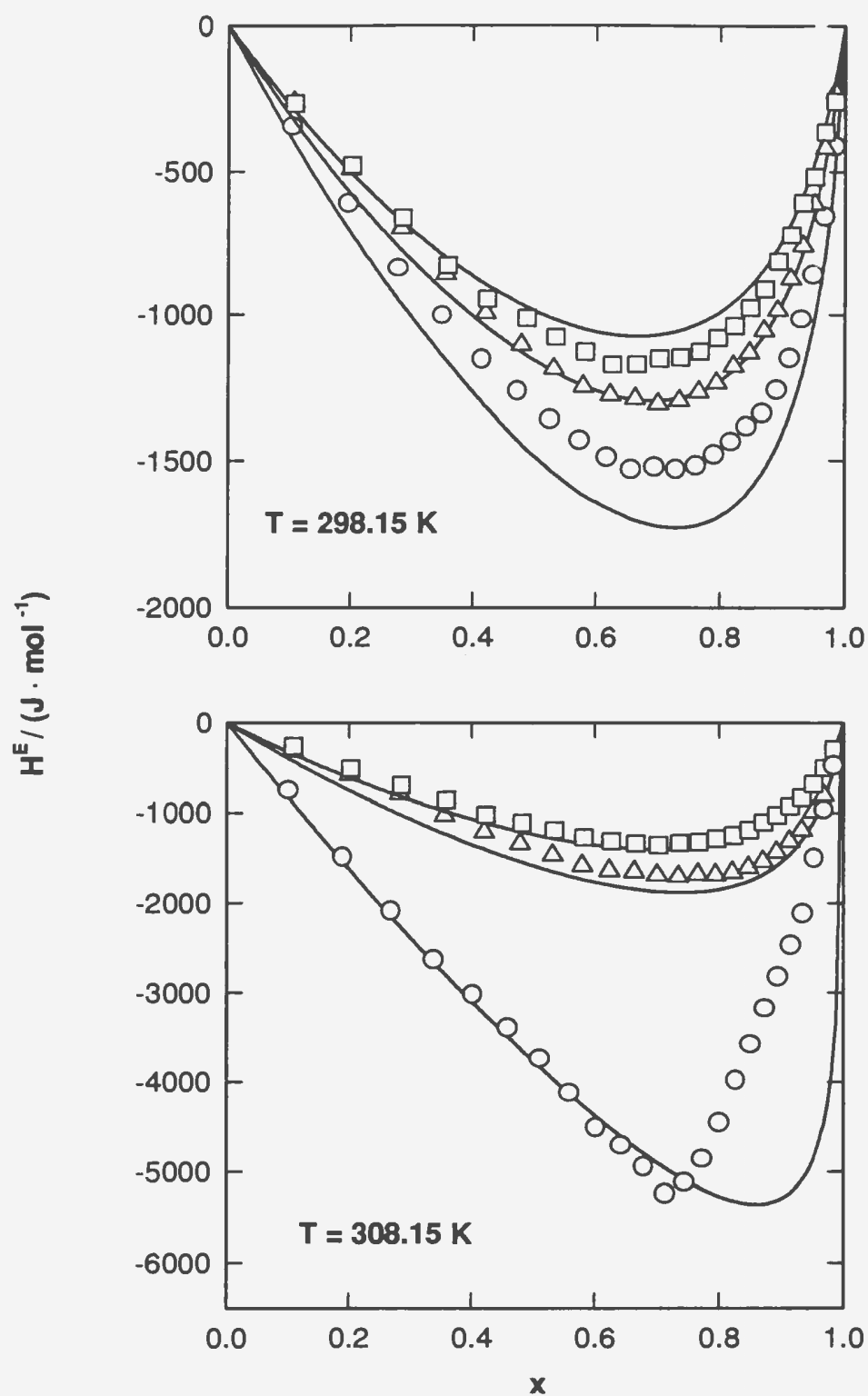
Figure 29. Comparisons of the experimental results with values predicted from the Peng-Robinson equation for {x CO$_2$ + (1-x) N-methyl-e-caprolactam}.
○ , p = 7.5 MPa; △ , p = 10.0 MPa; □ , p = 12.5 MPa.
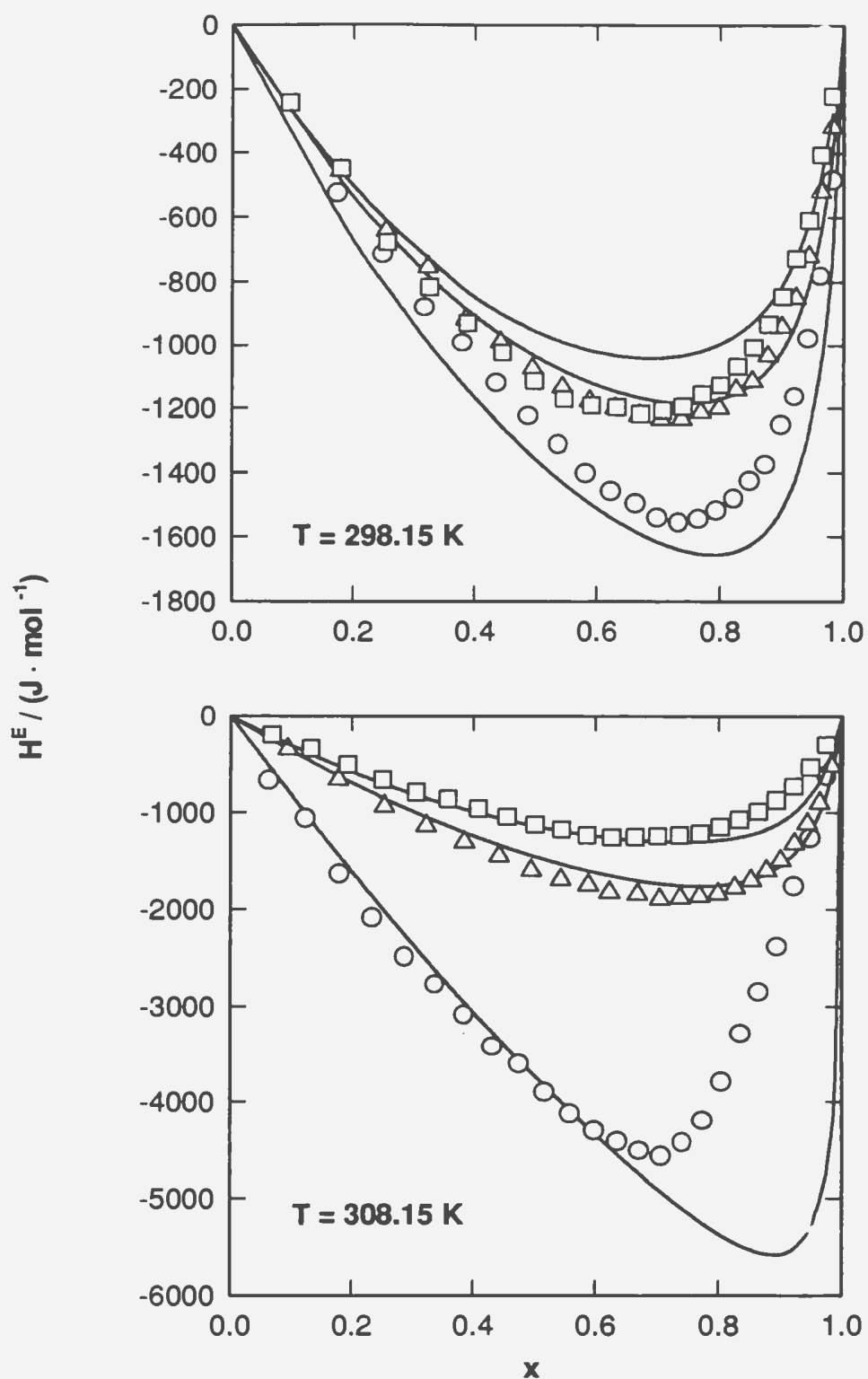
Figure 30. Comparison of the experimental results and values calculated from the Peng-Robinson equation for {x CO_2 + (1-x) 1-formyl piperidine}. ○ , p = 7.5 MPa; △ , p = 10.0 MPa; □ , p = 12.5 MPa.
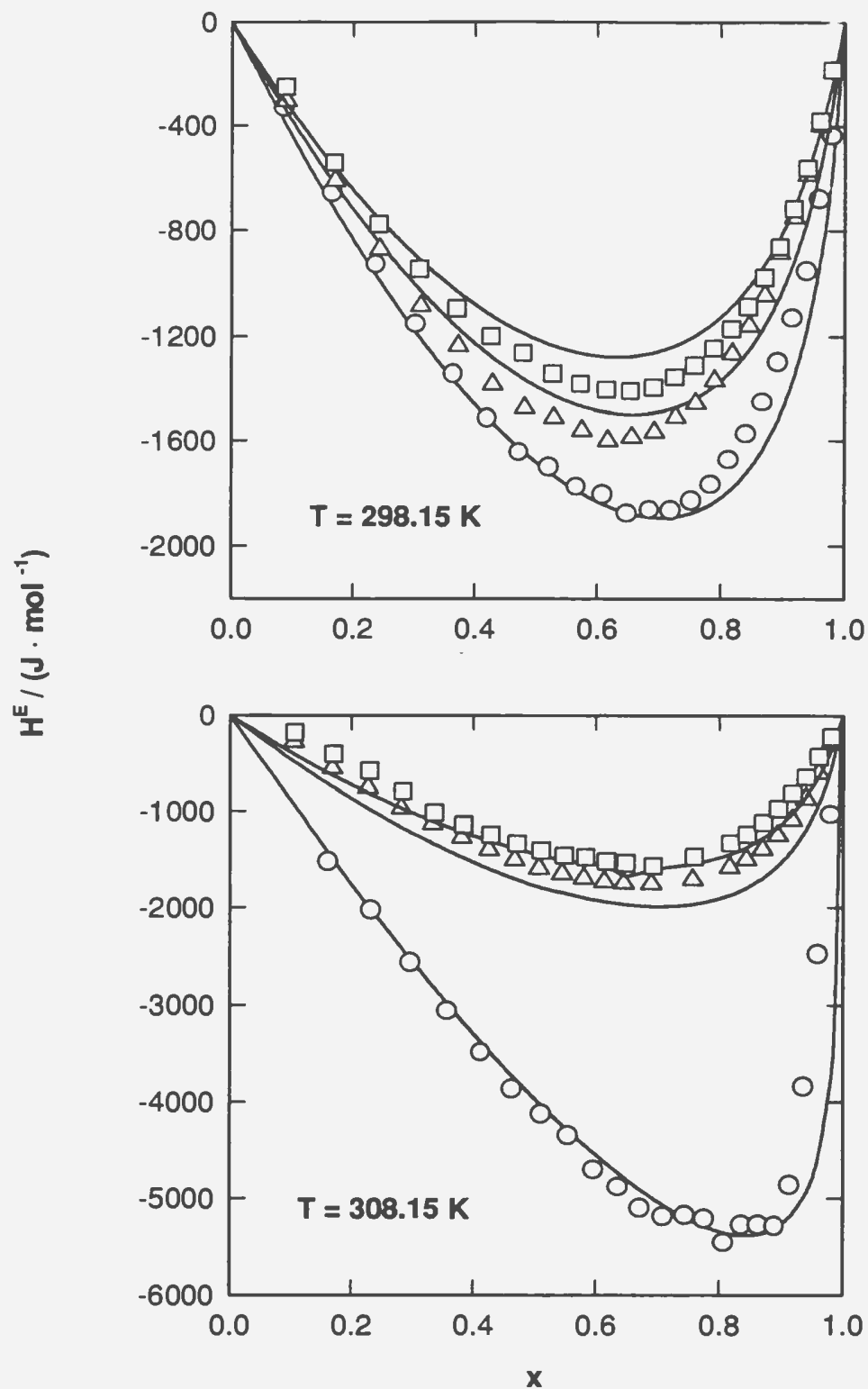
Figure 31. Comparisons of experimental results and values predicted from the Peng-Robinson equation for {x CO_2 + (1-x) ethylene glycol dimethyl ether}. ○, p = 7.5 MPa; △, p = 10.0 MPa; □ , p = 12.5 MPa
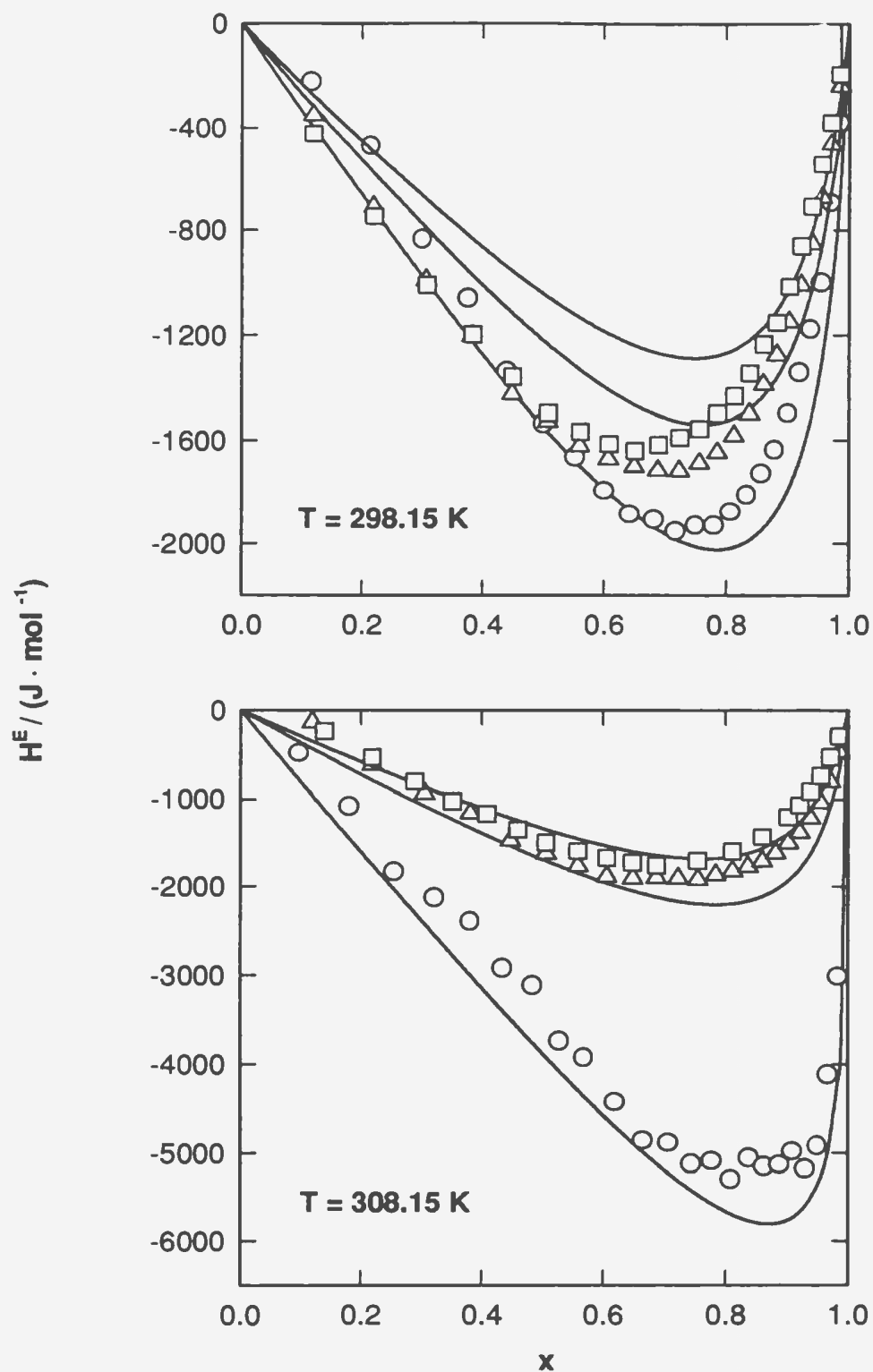
Figure 32.   Comparison of the experimental values with values predicted from the Peng-Robinson equation for {xCO$_2$ + (1-x) 2-methoxyethyl ether}.
○ , p = 7.5 MPa; △ , p = 10.0 MPa; □ , p = 12.5 MPa
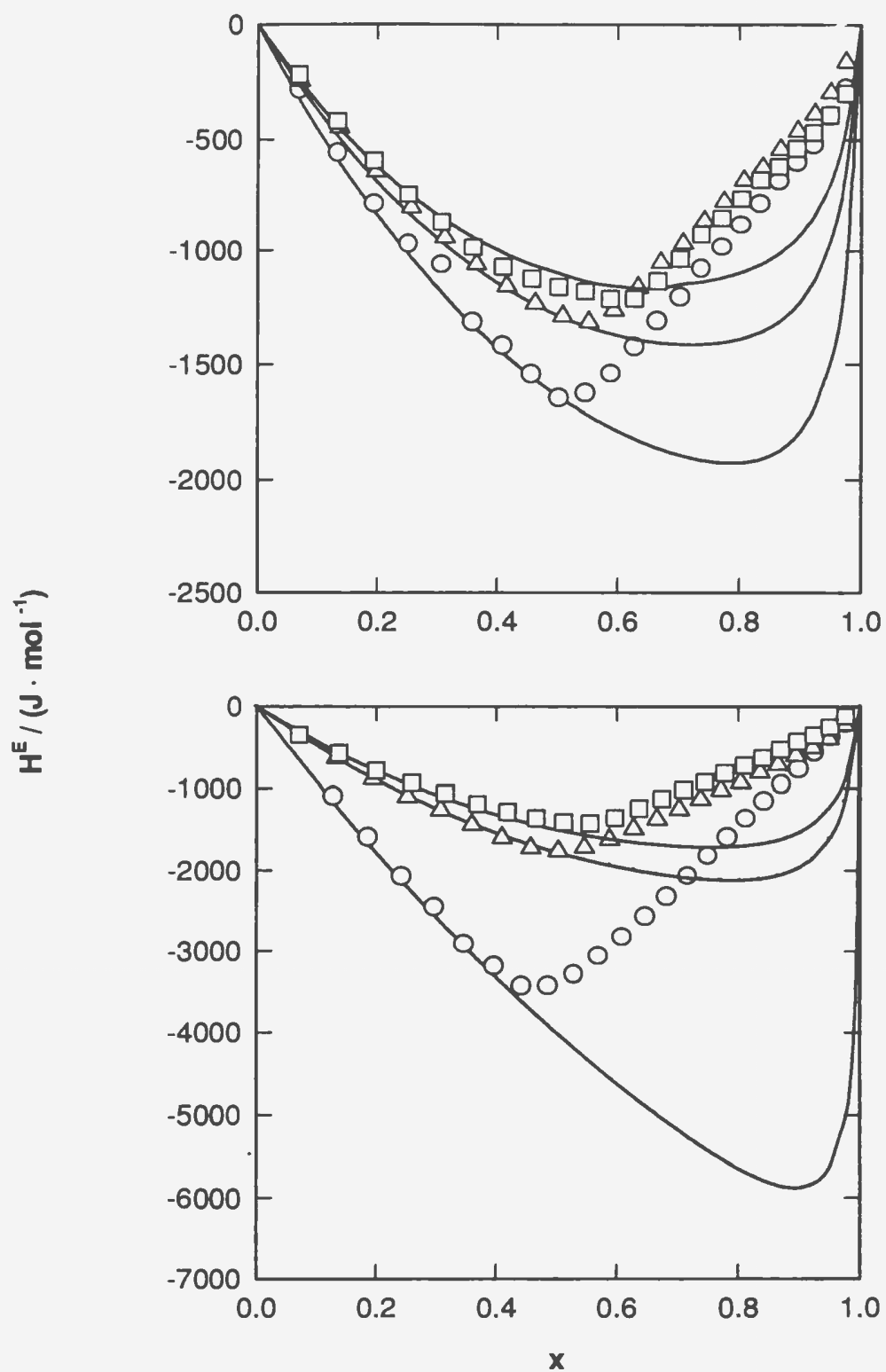
Figure 33. Comparisons of the experimental results and values predicted from the Peng-Robinson equation for {x$_1$CO$_2$ + (1-x$_1$) [x$_2$ sulfolane + (1-x$_2$) water]}. ○ , p = 7.5 MPa; △ , p = 10.0 MPa; □ , p = 12.5 MPa.
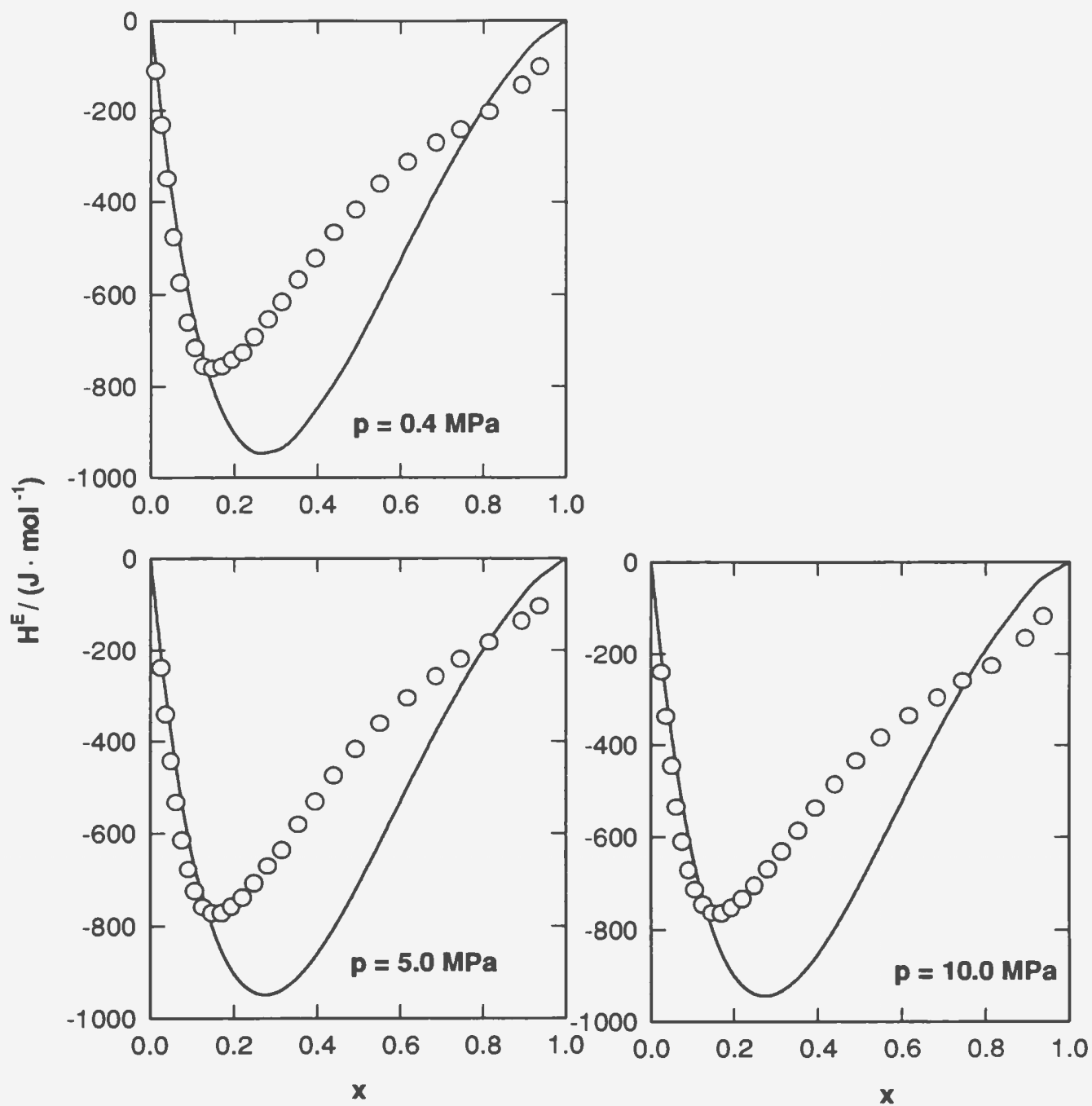
Figure 34. Comparison of the experimental results with values calculated from the Peng-Robinson equation for {x ethanol + (1-x) water} at T = 298.15 K.

6.7   Analysis of the Model

In the past two decades, new experimental techniques have begun to probe many interesting phenomena that occur in the vicinity of the critical region of binary mixtures. A number of theoretical studies in this field have been carried out in recent years for the specific purpose of determining the relative magnitude of classical and non-classical effects. Wormald[75] explored the general behaviour of $H^E(x, p, T)$ and $V^E(x, p, T)$ surfaces for the binary mixtures in the critical region by using the van der Waals equation of state 1-fluid model. He examined hypothetical binary mixtures with critical parameters chosen to represent three classes of system: $(T_{c1} = T_{c2}, p_{c1} > p_{c2})$, $(T_{c1} < T_{c2}, p_{c1} = p_{c2})$, and $(T_{c1} < T_{c2}, p_{c1} > p_{c1})$ and found that the shapes of the $H^E(x, p, T)$ and $V^E(x, p, T)$ surfaces in the region of the critical locus are strongly affected by the properties of the pure components.

As can been seen from Table A.5.1, all mixtures studied here have a common characteristic: the critical temperature of solvent is larger than that of CO_2 and the critical pressure of solvent is smaller than that of CO_2 ($i.e.$ $T_{c1} < T_{c2}, p_{c1} > p_{c2}$). As an example, the $H^E (x, p, T)$ surface for $\{xCO_2 + (1-x)N\text{-methyl-}\epsilon\text{-caprolactam}\}$ at 308.15 K was modelled by the Peng-Robinson equation of state using the parameters presented above. The results are shown in figure 35. The pressure dependence of the $H^E (x = 0.9)$ curve is an S-shaped curve with a maximum of about 3.40 kJ·mol^{-1}
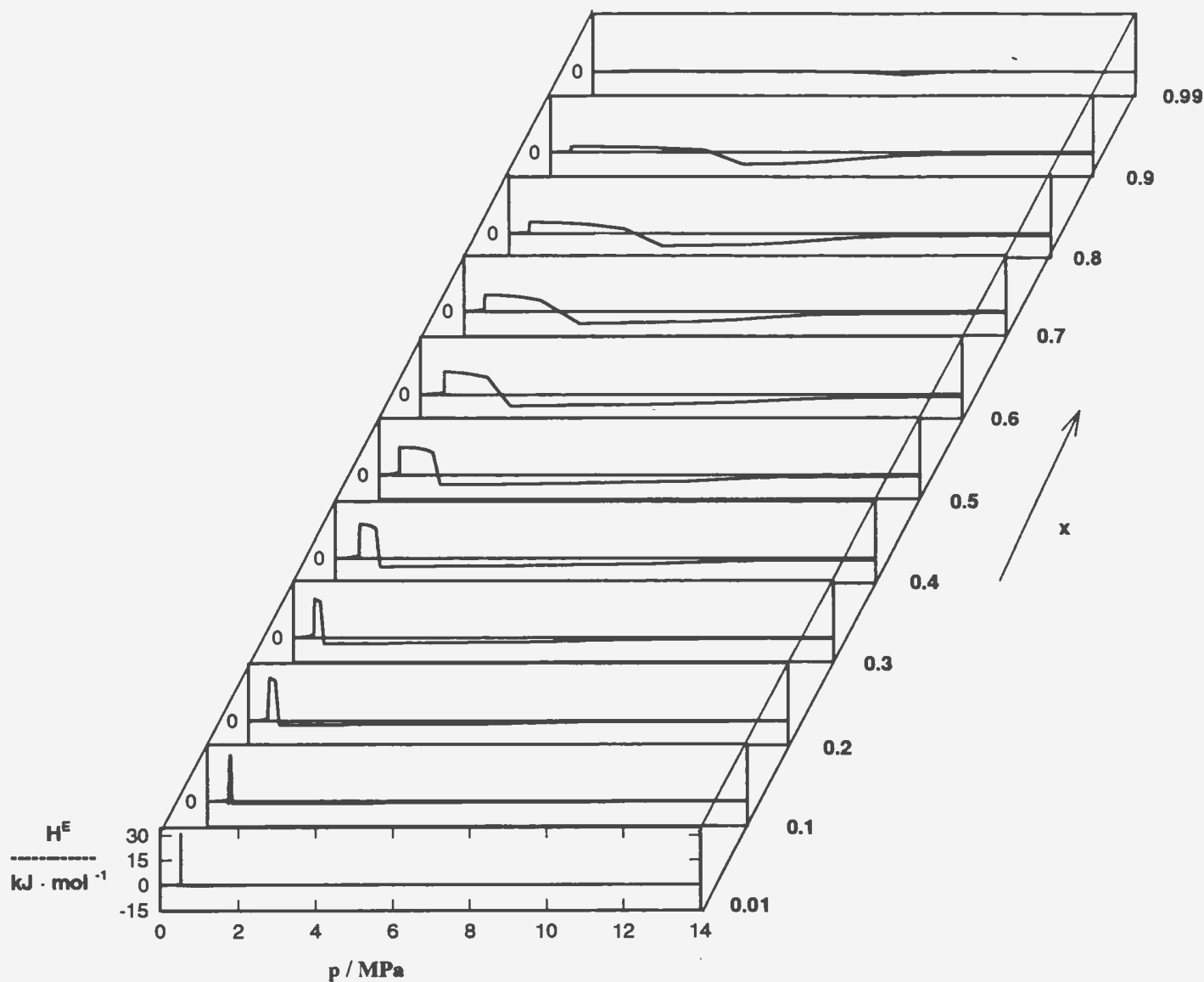
Figure 35.   Excess molar enthalpy surface for $\{x\ CO_2 + (1-x)\ N\text{-methyl-}\epsilon\text{-caprolactam}\}$ at 308.15 K. $T_{c1} = 304.2$ K, $p_{c1} = 7.38$ MPa, $T_{c2} = 570.4$ K and $p_{c2} = 3.38$ MPa with $k_{12} = -0.005$ and $k_{21} = -0.050$.

at 0.54 MPa and a minimum of about -7.38 kJ·mol^{-1}. Decreasing x increases the magnitude of the positive region of the curve and broadens the negative region but diminishes its magnitude. At x = 0.01, a sharp positive peak of 30.9 kJ·mol^{-1} is observed at 0.54 MPa, and the magnitude of the negative H^E values becomes very small over the whole pressure range.

To illustrate the behaviour of H^E (x, p, T), the molar enthalpies of the mixture and its pure components relative to the ideal gas reference state are plotted in figure 36 as a function of pressure. The plot shows the "residual enthalpies"[75] or "departure functions"[76] (H$_1$ - H$_1^o$) for CO$_2$, (H$_2$ - H$_2^o$) for N-methyl-ϵ-caprolactam, and (H$_m$ - H$_m^o$) for the mixture at x = 0.5, where H$_m^o$ = x H$_1^o$ + (1-x) H$_2^o$. Each plot displays a step which corresponds to the saturation pressure. After the step, the enthalpy becomes more negative and is essentially independent of pressure as the result of the transition from a gaseous to a liquid or liquid-like state. The shaded area between these curves corresponds to the H^E at mole fraction x = 0.5. according to the expression:

$$H^E = H_m - x_1 H_1 - x_2 H_2$$

The critical pressure of CO$_2$, p$_{c1}$, is 7.38 MPa. The three arrows indicate the experimental pressures used in the study. At 298.15 K (T$_R$ = 0.98) and pressures above 7.0 MPa, both the pure components and their mixture are liquids, and the departure function are relatively independent of pressure. It is for this reason that
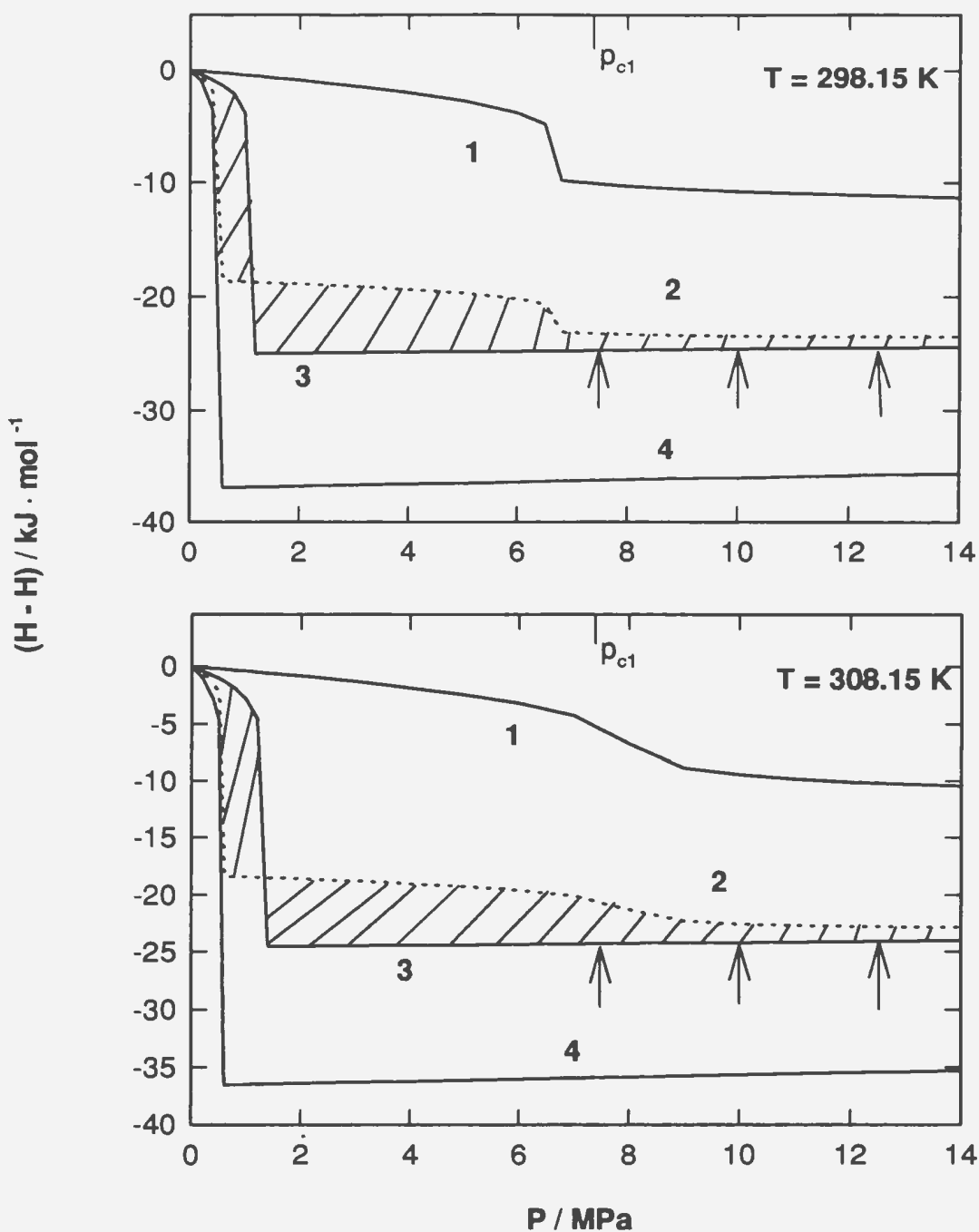
Figure 36. The relationship of H^E curve for {x CO_2 + (1-x) N-methyl-ε-caprolactam} to the residual enthalpies 1. (H_1 - H_1^o) and 4. (H_2 - H_2^o) for the pure solvents and 3. (H_m - H_m^o) for the mixture. The broken curve is [0.5 (H_1- H_1^o) + 0.5 (H_2- H_2^o)] at the same pressure. The shaded area between the (H_m- H_m^o) and the broken curve is the excess enthalpy H^E (x = 0.5).

$H^E(x,p,T)$ is small and relatively independent of pressure(figure 29). At 308.15 K, the lowest experimental pressure, 7.5 MPa, is within the critical region of CO_2 ($T_R = 1.01$, $p_R = 1.02$), while N-methyl-ϵ-caprolactam and the mixture are still liquids. The enthalpy of CO_2 at $T_R = 1.01$, $p_R = 1.02$ is much smaller (more positive) than values of $(H_1 - H_1^\circ)$ at higher pressures. This is the reason why the H^E values at this temperature and pressure have large negative values. As the figure illustrates, the phenomenon is a consequence of the change in the departure function of the pure component, CO_2, rather than that of the mixture.

Although the Peng-Robinson equation can be fitted to the $H^E(T, p, x)$ surface and gives interesting insights into the large influence of near-critical effects, it has major shortcomings which limit its use for accurate work:

(i)　The term $\{x_1(H_1 - H_1^\circ) + x_2(H_2 - H_2^\circ)\}$ is very sensitive to the relative enthalpy of the pure solvent as predicted by the equation of state. There is a very large contribution from $(H_1 - H_1^\circ)$ in the near-critical region studied here. Moreover, the properties of CO_2 in the critical region are not well described by the Peng-Robinson equation because the compressibility factor at the critical point is constrained to be a single value common to all liquids, $Z_c = 0.304$. This causes significant errors in calculating the pure component enthalpy and volume functions in this region. The problem may be a factor in the poor success of the cubic

equation of state in reproducing H^E data for the CO_2 -rich region.

(ii)   The vapour-liquid equilibria for the polar solvents were not correctly calculated by the procedure used here. An evident mistake can be observed in figure 36.   The plot for $(H_2 - H_2^o)$ indicates that at 308.15 K, N-methyl-ϵ-caprolactam is a gas at pressures below 0.54 MPa when, in fact, it is a liquid at 0.1 MPa. This may be due to errors in estimating the critical parameters T_c, p_c and the acentric factor ω of the pure solvent. Clearly, the parameters in any equation of state treatment must be optimized to reproduce these pure component properties if improvements are to be achieved.

7.   CONCLUSIONS

This work reports new measurements of the excess molar enthalpies, H^E, for binary mixtures of CO_2 with several physical solvents used in acidic gas removal processes: {xCO_2 + (1-x)N-methyl-ϵ-caprolactam}, {xCO_2 + (1-x)propylene carbonate}, {xCO_2 + (1-x)1-formyl piperidine}, {xCO_2 + (1-x)ethylene glycol dimethyl ether}, {xCO_2 + (1-x)2-methoxyethyl ether}, {xCO_2 + (1-x)ethanol}, and {xCO_2 + (1-x)[x_2 sulfolane + (1-x_2) water]}. The measurements were restricted to the range: T = 298.15 K and T = 308.15 K, and p = 7.5 MPa, p = 10.0 MPa and p = 12.5 MPa. The operating conditions include the critical temperature and pressure of CO_2 (T_C = 304.2 K, p_C = 7.38 MPa). The H^E values, except those for the mixture {xCO_2 + (1-x)ethanol} at the lower temperature and higher pressure, are all negative over the entire composition range. The plots of H^E vs x for the mixture {xCO_2 + (1-x) ethanol} at 298.15 K from 7.5 to 12.5 MPa and 308.15 K from 10.0 MPa to 12.5 MPa show an S-shaped curve. As expected, large changes in H^E values have been observed at T = 308.15 K and p = 7.5 MPa, which reflect the proximity to the critical point of CO_2. The linear sections indicating the existence of a two-phase region

become more pronounced at increased temperature and decreased pressure. The boundaries of the two-phase regions for each mixture studied here have been determined. The measurements suggest that the system (CO_2 + 2-methoxyethyl ether) may display unusual thermodynamic behaviour at low mole fractions of CO_2.

The Peng-Robinson equation has been applied with some success to model the excess enthalpies of CO_2 with nonpolar solvents over wide ranges of temperature and pressure, and its shortcomings are now quite well understood.[62,74,77,78] The results of this work suggest that it is a useful semiquantitative tool for identifying the relative importance of near-critical effects and intermolecular interactions in highly polar systems. However, it was not possible to model the systems quantitatively over the full range of temperature, pressure, and composition.

Wormald[21] has demonstrated that large deviations in H^E and excess molar volume V^E must always arise at pressures and temperatures near the critical point of the pure components. The results observed for the mixtures of CO_2 with the eight polar solvents studied here are entirely consistent with this behaviour. When used with the linear mixing rule, the Peng-Robinson equation is quite effective in fitting the H^E of mixtures for CO_2 with N-methyl-ϵ-caprolactam, 1-formyl piperidine, and ethylene glycol dimethyl ether at p = 10.0 and p = 12.5 MPa. The poor fit for mixtures in the CO_2-rich region at p = 7.5 MPa can be attributed to the inflexibility

of the Peng-Robinson equation, which constrains the critical compressibility factor Z_c to the value 0.307 and thus introduces large errors in the derivative functions under near-critical conditions. The experimental value of Z_c for CO_2 is 0.275. Use of the Patel-Teja equation[65] substantially reduces this problem for non-polar fluids.

The high values estimated for the vapour pressure of the solvents suggest that difficulties in reproducing the two-phase region may be due to errors in estimating the critical parameters in the Peng-Robinson equation.

The large deviations between the model and the experimental values of H^E for propylene carbonate and sulfolane may be due to errors in estimating the critical parameters of the solvent or to the known limitations in the Panagiotopoulos-Reid mixing rule.[74] The latter is believed to be the case. Propylene carbonate and sulfolane are extremely polar molecules, and it is unreasonable to expect that strong directional intermolecular interactions can be modelled quantitatively by a linear mixing rule over the full range of compositions. Similar problems are also observed in applying the model to the results for (ethanol + water) (figure 34) in which no near critical effects are present.

REFERENCES

1. Xu, Y.; Schutte, R. P.; Hepler, L. G. *Can. J. Chem. Eng.* **1992**, 70, 569.

2. Riesenfeld, F. C.; Kohl, A. L. *Gas Purification* 2nd. edition, Houston, **1974**.

3. Astarita, G.; Savage, D. W. and Bisio, A. *Gas Treating with Chemical Solvents*, John Wiley & Sons, **1983**.

4. Richardson, Ian M. J. and O'Connell, J. P. *Ind. Chem., Process Des. Dev.,* **1975**, 14, 467.

5. Jou, F. -Y.; Otto, F. D. and Mather, A. E. *Fluid Phase Equilibria* **1990**, 56, 313.

6. Murrieta-Guevara, F.; Romero-Martinez, A.; Trejo, A. *Fluid Phase Equilibria* **1988,** 44, 105.

7. Christensen, J. J.; Hank, R. W.; Izatt, R. M. *Handbook of Heats of Mixing* Wiley-Interscience: New York, **1982**.

8. Lewis, K. L.; Mosedale, S. E.; Wormald, C. J. *J. Chem. Thermodynamics* **1977**, 9, 221.

9. Mosedale, S. E.; Wormald, C. J. *J. Chem. Thermodynamics* **1977**, 9, 483.

10. McFall, T. A.; Post, M. E.; Christensen, J. J. and Izatt, R. M. *J. Chem. Thermodynamics* **1981**, 13, 441.

11. Christensen J. J.; Izatt, R. M.; Post, M. E.; and McFall, T. A. *Thermochim. Acta,* **1981**, 50, 73.

12. Schneider, G. M.; Stahl, E. and Wilke, G. *Extraction with Supercritical Gases,* Verlag, Chemie, Weinheim, **1980**.

13. Pando, C.; Renuncio, J. A. R.; McFall, T. A.; Izatt, R. M. and Christensen, J. J. *J. Chem. Thermodynamics* **1983**, 15, 173.

14. Pando, C.; Renuncio, J. A. R.; Izatt, R. M.; and Christensen J. J. *J. Chem. Thermodynamics* **1983**, 15, 259.

15. Christensen, J. J.; Zebolsky, D. M.; and Izatt, R. M. *J. Chem. Thermodynamics* **1985**, 17, 183.

16. Pando, C.; Renuncio, J. A. R.; Izatt, R. M. and Christensen, J. J. *J. Chem. Thermodynamics* **1983**, 15, 235.

17. Christensen, J. J.; Walker, T. C. A.; Schofield, R. S.; Faux, P. W.; Harding, P. R. and Izatt, R. M. *J. Chem. Thermodynamics* **1984**, 16, 445.

18. Christensen, J. J.; Cordray, D. and Izatt, R. M. *J. Chem. Thermodynamics* **1986**, 18, 53.

19. Wormald, C. J.; Lancaster, N. M. and Sellars, A. J. *J. Chem. Thermodynamics* **1986**, 18, 135.

20. Yerlett, T. K. and Wormald, C. J. *J. Chem. Thermodynamics* **1986**, 18, 371.

21. Wormald, C. J.; Eyears, J. M. *J. Chem. Soc. Faraday Trans. I.* **1988**, 84, 1437.

22. Hauser, R. A. *M.Sc. Thesis.* University of Alberta, **1988**.

23. Rouquerol, J. and Zielenkiewicz, W. *Thermochim. Acta* **1986**, 109, 121.

24. Hemminger, W. and Höhne, G. *Calorimetry: Fundamentals and Practice*

1984, Weinheim, Florida,

25. Rossini, F. D. *Experimental Thermochemistry. Vol. 1., Interscience.* New York. **1956**.

26. Sturtevant, J. M., *Techniques of Organic Chemistry, Vol. 1. Weissberger, A.,* Interscience, New York, **1959**.

27. Wilhoit, R. C. *J. Chem. Ed.* **1967**, 44, A517, A568, A853.

28. Picker, P.; Golicoeur, C.; Desnoyers, J. E. *Rev. Sci. Instrum.* **1968**, 39, 676.

29. Monk, P.; Wadsö, I. *Acta Chem. Scand.* **1968**, 22, 1842.

30. Stoesser, P.; Gill, S. J. *Rev. Sci. Instrum.* **1967**, 38, 422.

31. Bennett, J. E.; Benson, G. C. *Can. J. Chem.* **1965**, 43, 1912.

32. Watts, H.; Clarke, E. C. W.; Glew, D. N. *Can. J. Chem.* **1968**, 6, 815.

33. Groszek, A. J. *Lubrication Sci. Technol.* **1966**, 9, 67.

34. Picker, P.; Jolicoeur, C. and Desnoyers, J.E. *J. Chem. Thermodynamics* **1969**, 1, 469.

35. Christensen, J. J.; Johnston, H. D. J. and Izatt, R. M. *Rev. Sci. Instrum.* **1968**, 39, 1356.

36. Christensen, J. J.; Gander, J. W.; Eatough, D. J.; Izatt, R. M.; Watt, P. J. and Hart, R. M. *Rev. Sci. Instrum.* **1973**, 44, 481.

37. Eyraud, C. *C. R. Acad. Sci.* **1954**, 238, 1151.

38. Speros, D. and Woodhouse, R. L. *J. Phys. Chem.* **1963**, 67, 2164.

39. Christensen, J. J. and Izatt, R. M. *Thermochim. Acta,* **1984**, 73, 117.

40. Ott, J. B. and Wormald, C. J. in *Solution Calorimetry*, Marsh, K. N. and O'Hare, P. A. G., ed. Blackwell, London, **1991**.

41. Christensen, J. J.; Cordray, D. R.; Oscarson, J. L. and Izatt, R. M. *J. Chem. Thermodynamics,* **1988**, 20, 867.

42. Cordray, D. R.; Christensen, J. J. and Izatt, R. M. *J. Chem. Thermodynamics,* **1988**, 20, 877.

43. Riddick, J. A.; Bunger, W. B. *Techniques of Chemistry, Volume II. Organic Solvents. 3rd. edition*, Wiley, New York.

44. Picker, P.; Leduc, P. A.; Philip, P. R.; Desnoyers, J. E. *J. Chem. Thermodynamics* **1971**, 3, 631.

45. Angus, S.; Armstrong, B.; de Reuck, K. M. *International Thermodynamic Tables of the Fluid State. Vol. 3. Carbon Dioxide*. Pergamon Press: Oxford. **1976**.

46. David, R. L. *CRC Handbook of Chemistry and Physics, 71st Edition*. CRC: Boca Raton, FL. **1990**.

47. *Aldrich Catalog Handbook of Fine Chemicals*. Aldrich Chemical Company Inc. **1990-1991** Edition.

48. *Fluka Chemika-Biochemika,* Fluka Chemie AG, Buchs/Switzerland, **1993/1994**.

49. Ott, J. B.; Stouffer, C. E.; Cornett, G. V.; Woodfield, B. F.; Wirthlin, R. C.; Christensen, J. J. *J. Chem. Thermodynamics* **1986**, 18, 1.

50. Ott, J. B.; Stouffer, C.E.; Cornett, G. V.; Woodfield, C. G. and Christensen,

J. J. *J. Chem. Thermodynamics,* **1987**, 19, 337.

51. Cordray, D. R.; Izatt, R. M.; Christensen, J. J. and Oscarson, J. L. *J. Chem. Thermodynanics* **1988**, 20, 755.

52 Larkin, J. A. *J. Chem. Thermodynamics* **1975**, 7, 137.

53. Franks, F. and Reid, D. S. in *Water: A Comprehensive Treatise,* Vol. 2, Franks, F. ed. Plenum Press, New York, **1973**.

54. Christensen, J. J.; Cordray, D. R.; Zebolsky, D. M. and Izatt, R. M. *J. Chem. Thermodynamics,* **1985**, 17, 335.

55. Ott, J. B.; Brown, P. R. and Sipowska, J. T. *J. Chem. Thermodynamics,* **1995**, 27, in press.

56. Morrison, R. T. and Boyd, R. N. *Organic Chemistry,* Allyn and Bacon, Boston, **1973**.

57. March, J. *Advanced Organic Chemistry,* 2nd edition, McGraw-Hill, New York, **1977**.

58. Van Eldik, R. and Palmer, D. A. *J. Solution Chem.* **1982**, 11, 339.

59. Palmer, D. A. and van Eldik, R. Van *Chem. Rev.* **1983**, 83, 651.

60. Van der Waals, J. D. *Doctoral Dissertation* **1873,** Leiden.

61. Peng, D-Y.; Robinson, D. B. *Ind. Eng. Chem. Fundam.* **1976**, 15, 59.

62. Redlich, O. and Kwong, J. N. S. *Chem. Rev.* **1949**, 44, 233.

63. Sova, G. *Chem. Eng. Sci.* **1972**, 27, 1197.

64. Adachi, Y.; Lu, B. C.-Y.; Sugie, H. *Fluid Phase Equilibria* **1983**, 13, 133.

65. Patel, N. C. and Teja, A. S. *Chem. Eng. Sci.* **1982**, 37, 463.

66. Panagiotopoulos, A. Z.; Kumar, S. K. *Fluid Phase Equilibria* **1985**, 22, 77.

67. Dohrn, R. J. *Supercritical Fluids* **1992**, 5, 81.

68. Li, C. C. *Can. J. Chem. Eng.* **1971**, 19, 709.

69. Kreglewski, A. and Kay, W. B. *J. Phys. Chem.* **1969**, 73, 3359.

70. Spencer, C. F.; Daubert, T. E. and Danner, R. P. *AIChE J.* **1973**, 19, 522.

71. Reid, R. C.; Prausnitz, J. M. and Poling, B. E. *The Properties of Gases and Liquids,* 4th Edition, McGraw-Hill, New York, **1987**.

72. Luedecke, D. and Prausnitz, J. M. *Fluid Phase Equilibria* **1985**, 22, 1.

73. Wong, D. S. H. and Sandler, S. I. *AIChE J.* **1992**, 38, 671.

74. Panagiotopoulos, A. Z.; Reid, R. C. **1986**. in Chao, K. C.; Robinson R. L.: editors, *"Equations of State-Theories and Applications"*, *ACS Symp. Ser. 300:* 571.

75. Wormald, C. J. *Fluid Phase Equilibria* **1986**, 28, 137.

76. Reid, R. C.; Prausnitz, J. M.; Poling, B. E. *The Properties of Gases and Liquids*, McGraw - Hill, New York, 4th ed. **1987**.

77. Casielles, A. G.; Pando, C.; Renuncio, J. A. R.; Christensen, J. J.; Izatt, R. M. *Thermochim. Acta* **1989**, 154, 57.

78. Shibata, S. K.; Sandler, S. I. *Ind. Eng. Chem. Res.* **1989**, 28, 1898.

79. Harr, L.; Gallagher, J. S.; Kell, G. S. *NBS/NRC Steam Tables,* Hemisphere, Washington, DC, **1984**.

APPENDIX   I

CALORIMETER OPERATING PROCEDURES

This section describes operating procedures for the Tronac 1640 calorimeter and high-pressure injection system, as described in Chapter 4, and figures 6 to 10. The valve numbers cited in section A.1.7 refer to figure 10.

A.1.1 Water Bath

The water bath consists of a thermally insulated container with a motor-driven stirrer, a cooled heater assembly, a PTC-41 precision temperature controller, and a bath temperature probe. The bath is constructed of ABS plastic, silicone rubber, and stainless steel and has a volume of 55 litres. Distilled water was used in the bath to reduce the growth of algae. The reaction vessel and accompanying sample inlet lines are fully immersed in the water bath to ensure complete thermal equilibrium. The Model PTC - 41 precision temperature controller provides a temperature stability with a drift of no more than $\pm$ 0.0003 K per week.

A.1.2 The 450 Console

Figure 37 shows the front panel of the 450 electronics console. The console contains the electrical components necessary for temperature sensing, bridge controls, calibration heating, DVM select switch and bridge output. The main functions of the 450 electronics console are to adjust the potential and the reference point of the Wheatstone bridge, to select the voltage and current across the calibration heater, and to provide signal outputs to the digital voltameter (DVM-select) and recorder (R.V. TEMP) which record the bridge imbalance produced by the temperature sensing thermistor.

The bridge voltage adjust is a lock nut with a screw-driver adjustment. The voltage is adjustable from 1.5 to 15 volts. A voltage of 5.0 to 7.0 volts is recommended for optimum results. The coarse, medium, and fine adjustments vary the set point for the readout of the reaction vessel temperature. If the reaction vessel temperature is considered to be the same as the desired temperature of the water bath and only one liquid is flowing through the reaction, the readout is recorded with a suitable span (1- 100mV for general usage or 0.1-1.0 mV for sensitive woɪk).

A.1.3 The 550 Console

The 550 electronics console is used with the 450 electronics console to convert
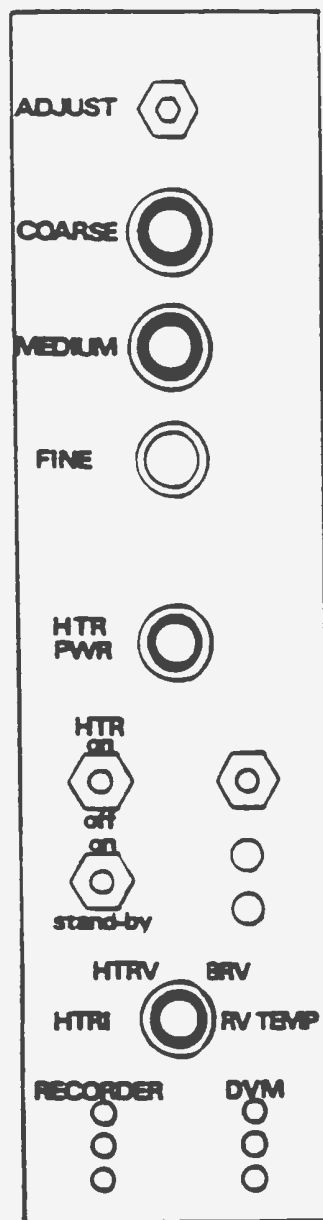
A
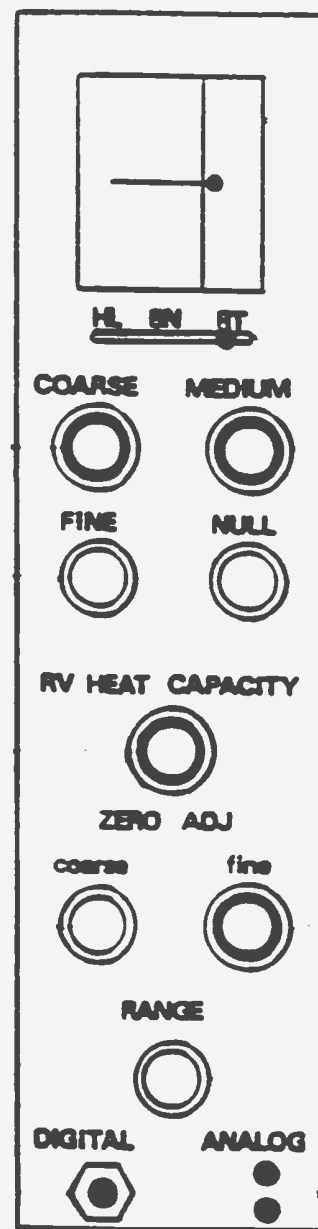
B

Figure 37.   A.   Front panel of the 450 electronics console;   B.   Front panel of the 550 electronic console.

from adiabatic to isothermal operation. Figure 37 also shows the front panel of the 550 console. The console holds the temperature of a reaction vessel constant within $\pm 2 \cdot 10^{-5}$ K relative to the water bath by balancing the heater power against a constant cooling power from the Peltier device, and displays a digital or analog signal of the frequency of heater pulses required to maintain the temperature in the reaction vessel constant during the chemical or electrical equilibration reaction. The difference between the display and initial set point is thus a direct measure of the positive or negative heat produced by the process studied.

The operating temperature range of the control thermistor is from 283.15 K to 373.15 K at the design centre temperature of 298.15 K $\pm$ 10 K. The precision of the reaction vessel temperature control is $\pm 2 \cdot 10^{-5}$ K/hour. Heating and cooling rates are 0.1, 0.2, 0.5, 10, 20 mcal/volt and are continuously variable from 0.2 to 200 mcal/sec, respectively. The 0-2400 Hz range of the heater pulse rate is represented by an analog voltage signal of - 12 to + 12 volts which may be monitored on a DVM.

A.1.4 Equilibration

It is critically important to allow sufficient time for the reaction vessel to come to full thermal equilibrium with the bath. A difference of even a few hundredths of a degree will cause a drifting baseline. First, the water bath must be set to the desired

temperature. After the bath has achieved stable control, the reaction vessel and shields (figure 8) may be lowered into the bath. All electrical connectors from the flow insert to the 450 and 550 consoles should be disconnected until thermal equilibration has taken place. This may take 24 hours or more if the bath temperature differs greatly from ambient. The next step is to select the initial 450 and 550 control setting.

A.1.5 The 450 and 550 Control Settings

(i)   If the values of excess molar enthalpy are estimated in the range of 300 - 500 $J \cdot mol^{-1}$, the 550 controls must be set as follows:

"RANGE" Switch to 5 μcal/volt. "ZERO ADJUST" controls to "D" and "7.0".

"RV HEAT CAPACITY" to 30 cal/°C.

(ii)   If the values of excess molar enthalpy are estimated larger than 4000 $J \cdot mol^{-1}$, the controls should be set as follows:

"RANGE" Switch to 20 μcal/volt.

"ZERO ADJUST" controls to "B" and "7.0".

"RV ADJUST" to 30 cal/°C.

(iii)   The 450 controls are set as follows:

Meter function switch to "RV TEMP".

"HTR PWR" Switch to 50 mcal/sec.

The 550 "DIGITAL" output may be displayed on a multimeter (HP model 3478 A). The 450 "DVM" output may also be displayed on the multimeter through the back connector to determine whether the desired "set point" has been reached. The "set point" is the temperature difference between the reaction vessel and the water bath which should be less than 100 µV.

A.1.6 Loading the Pumps

After the 450 "DVM" output shows a signal of approximately zero mV and the 550 output gives the expected constant value (positive for an exothermic reaction and negative for an endothermic reaction), the HAAKE temperature bath is turned on to maintain the pump containing liquid CO_2 at a constant temperature of 279 ± 0.2 K (figure 10). Before loading the pumps, the pump controllers are set at "constant pressure" mode. Valves 9 and 10 are closed, and valves 5, 7 and 8 are opened. The switch in the pump controller is set to the "REFILL" and "RUN" positions, respectively. The refill rate is determined by pushing the "REFILL RATE" softkey. The refill process is ended by pressing the "STOP" softkey and valves 5, 7 and 8 are then closed.

A.1.7 System Pressurization

Both CO_2 and solvent are collected in a stainless steel vessel with an approximate capacity of 750 cm^3 capable of withstanding operating pressures up to 15 MPa. In case, for any reason, the pressure in the system builds up to undesirable level, the pressure relief valve 25, placed on line, should be set to operate when the pressure in the system exceeds 14.5 MPa.

After the pumps have filled and the thermal equilibration of the reaction vessel has been achieved, the next step is to build up the pressure in the system. At this time, valves 10, 16, 17, 19, and 22 are opened and the pump containing solvent is turned on, allowing the solvent to flow through the system. Valves 5, 7, 9, 20, 23 and 24 remain closed. To pressurize the system, valve 21 is opened and N_2(g) starts flowing through the system. The flow rate of N_2(g) is regulated by valve 21 and the pressure in the system is controlled with the back pressure regulator, 18. The pressure is monitored with the Omega high performance process indicator, 15. The pressure is also indicated in the pump controllers. When the whole system is under the same pressure, the pump containing CO_2 is turned on. The pressure in the pump starts to rise due to valves 5, 7, and 9 still being closed. When the pressure shown in the pump controller display is close to or a little higher than that of the system, valve 9 is opened. A proper adjustment with the back pressure regulator is needed to

maintain the pressure in the system at a desired level. CO_2 is allowed to flow through the system and a few minutes later the pump is turned off. Then, valve 10 is turned on and the solvent pump kept running until the pressure is stable, at which time one can proceed to adjust the settings in the 450 and 550 electronic consoles.

A.1.8 The 450 and 550 Console Connections

To establish the temperature set point of the flow insert, the 15 pin 450 connector is plugged into the back panel of the 450 console, and the bridge controls quickly zeroed to produce about 0.0000V output on the "DVM".

Next, the 12 pin 550 connector and NBC control heater cable are plugged into the back panel of the 550 console. If the reaction vessel temperature differs significantly from the "set point" after the connection is made (more than 100 µV as indicated on the "DVM"), the 15 pin 450 connector and NBC cable must be disconnected from the 550 console and the temperature must be allowed to re-equilibrate for 20 minutes, before the pin is re-connected again. This procedure may be repeated several times until the reaction vessel is controlled at the "set point" as indicated by a near zero reading on the "DVM". When a steady state measurement is achieved, a sample run can be attempted. Then, the 550 controls are quickly adjusted so that the 550 meter on "RV TEMP " is zeroed. Now, only one fluid is

flowing through the reaction vessel, and a baseline may be established by running the calorimeter for 10 to 20 minutes. When a straight baseline is drawn on the computer screen (using the computer program given in Table A.6.1 in Appendix VI.), the mixing process is begun and the raw experimental values are recorded under the same conditions. The values can be either positive or negative depending on whether the mixing process is exothermic or endothermic.

A.1.9   Electrical Calibration

Once a stable baseline is obtained, the HTR ON-OFF switch located in the front panel of the 450 electronics console may be turned on. Within a short period of time (no more than one minute), the value shown on the multimeter starts to decrease (become more negative), an indication that the heater is supplying power to the flow insert. Within 20 minutes, the signal on the multimeter should be stable. Then the analog frequency output from the heater controller (100 to 500 values) can be recorded and displayed on the computer screen at the same time. The ON-OFF switch is turned to the OFF position, and within 30 minutes a stable signal very close to that of the baseline should be obtained. As soon as a flow rate ratio of CO_2 to solvent is selected based on the total flow rate, measurement of excess molar enthalpies may start at the set temperature and pressure.

A.1.10   System Evacuation

Once the run is completed and a signal very close to the initial baseline is obtained, the calorimeter is turned off by setting the "TBY-ON" switch to the standby position. The cables plugged into the 450 and 550 electronic consoles are disconnected. Both pumps must be turned off and the flow of nitrogen is halted by shutting off valve 21. Valve 20 is then opened and the back pressure regulator 18 is opened little by little so that the pressure in the system is reduced gradually. After the indicator and the pump control show a pressure in the system of less than 1 bar, valves 23 and 24 are opened, and the solvent is drained out of the solvent collection vessel. Once all solvent has left the collection vessel, valves 23 and 24 are closed.

APPENDIX II

CALIBRATION OF PUMPS

The two pumps used throughout this work were ISCO Model 260 D Syringe Pumps. Before being used to deliver the reactants, they were calibrated by measuring the mass flow rate of fresh Nanopure water within a range from 0.015 to 0.6 cm^3/min.

Before calibration, the pumps were washed with about 50ml of Nanopure water at least 6 times. Then they were filled with the water, and the water was allowed to come to thermal equilibrium. The water was then pumped for a measured period of time long enough for an accurate determination of its mass, generally 15 to 30 minutes depending on the given flow rate. The water was collected in clean and dry weighing bottles and weighed on a Mettler AE240 dual range balance with the appropriate buoyancy correction.[78]

The procedure was repeated several times until the agreement was within 0.05% or better. Then the values were averaged. The density of the water was taken to be 1.0012 $cm^3 \cdot g^{-1}$ at 298.15 K[79]. An average correction factor of 0 997 was found for both pumps. The weighing results are given in tables A.2.1 and A.2.2. for the two pumps.

Table A.2.1. Calibration of the flow rate in pump A.

nominal flow rate	measured flow rate	relative errors	$F_{meas.} / F_{nom.}$
0.6000	0.5980	0.3333	0.9967
0.5500	0.5483	0.3091	0.9969
0.5250	0.5237	0.2476	0.9975
0.5000	0.4988	0.2400	0.9976
0.4750	0.4739	0.2316	0.9977
0.4500	0.4492	0.1778	0.9982
0.4250	0.4235	0.3529	0.9965
0.4000	0.3993	0.1750	0.9982
0.3520	0.3506	0.3977	0.9960
0.3040	0.3020	0.6579	0.9934
0.2560	0.2553	0.2734	0.9973
0.2080	0.2078	0.0962	0.9990
0.1600	0.1602	-0.1250	1.0012
0.1120	0.1114	0.5357	0.9946
0.0640	0.0640	0.0000	1.0000
0.0160	0.0159	0.6250	0.9938

A.2.2. Calibration of the flow rate in pump B.

nominal flow rate	measured flow rate	Relative error	$F_{meas.}/F_{nom.}$
0.6000	0.5982	0.3000	0.9970
0.5500	0.5487	0.2364	0.9976
0.5250	0.5248	0.0381	0.9996
0.5000	0.4979	0.4200	0.9958
0.4750	0.4741	0.1895	0.9981
0.4500	0.4490	0.2222	0.9978
0.4250	0.4237	0.3059	0.9969
0.4000	0.3990	0.2500	0.9975
0.3520	0.3494	0.7386	0.9926
0.3040	0.3030	0.3289	0.9967
0.2560	0.2558	0.0781	0.9992
0.2080	0.2082	-0.0962	1.0010
0.1600	0.1591	0.5625	0.9944
0.1120	0.1111	0.8036	0.9920
0.0640	0.0637	0.4687	0.9953
0.0160	0.0154	3.7500	0.9625

APPENDIX III
SAMPLE CALCULATION

The raw experimental data were automatically recorded with a computer. The computer programs for recording and reading out from data files are given in tables A.6.1 and A.6.2. of Appendix VI. To monitor the progress of the experiment, the data were displayed as a plot on the computer screen.

The sample calculation shown below corresponds to the experimental run of $\{xCO_2 + (1-x)N\text{-methyl-}\epsilon\text{-caprolactam}\}$ at 308.15 K and 12.5 MPa and to the calculation procedures given in chapter 4. The physical properties of CO_2 and N-methyl-ϵ-caprolactam have been listed in tables 2 and 3. Since the critical point of N-methyl-ϵ-caprolactam (see table A.4.1) was far from the temperatures studied here, the correction for the effect of pressure on the density of the solvent is neglected. For example, the density of propylene carbonate is 1.189 g/cm^3 and the isothermal compressibility is $3.72 \cdot 10^{-10}$ m^2/N at 298.15 K. The corrected density is 1.195 g/cm^3 at 12.5 MPa. The difference is less than 0.5%. The raw experimental data for the mixture of $\{xCO_2 + (1-x)N\text{-methyl-}\epsilon\text{-caprolactam}\}$ at 308.15 K and 12.5 MPa are shown in table A.3.1. The calibration voltage readings during the experimental run

were given as follows:

$$V_{heater} = 4.418V$$

$$V_{std} = 4.415 \ V$$

$$R_{std} = 100.03 \ \Omega$$

The heating power of the calibration heater is given by the equation

$$W = (V_{heater} \cdot V_{std})/R_{std}$$

$$= (4.418 \cdot 4.415) / 100.03 = 0.195 \ J/s \qquad (A.3.1)$$

Next we determine the energy per volt and the relative parameters are given by

$$V_b = 9.7698 \ V; \qquad V_a = 9.8346V; \qquad V_h = -1.4605V$$

where V_b and V_a are the voltage before and after the heater is turned on, and V_h is the voltage while the heater is on. The calibration constant is calculated by the equation

$$E = W \ / \ \{(V_b + V_a) \ / \ 2 - V_h\}$$

$$= 0.195 \ / \ \{(9.7698 + 9.8346) \ / \ 2 - (-1.4605)\} = 0.0173 \ J/s \cdot V \qquad (A.3.2)$$

If we take the values at the experimental point corresponding to 50% CO_2 and 50% N-methyl-ϵ-caprolactam by volumetric flow rate (experimental point 12 in table A.3.1), the molar flow rate F_{CO2} and $F_{solvent}$ are calculated from the equations listed below. The total flow rate is $0.600 cm^3/min$:

$$F_{CO2} = 0.997 \ (f_{co2} \cdot \rho_{co2}) \ / \ (60 \cdot M_{co2})$$

$$= 0.997 \ (0.300 * 0.958) / (60 * 44.01) = 1.085 * 10^{-4} mol/s \qquad (A.3.3)$$

$$F_{solvent} = 0.997 \, (f_{solvent} \cdot \rho_{solvent}) / (60 \cdot M_{solvent})$$

$$= 0.997 \, (0.3 * 0.991) / (60 * 127.19) = 3.884 * 10^{-5} \, mol/s \qquad (A.3.4)$$

where f_{CO2} and $f_{solvent}$ are the volumetric flow rates of $CO_2(l)$ and the solvent. Therefore, the heat effect during the mixing is:

$$Q/dt = \{V_{exp.} - (V_a + V_f) / 2\} \cdot E$$

$$= \{-1.5146 - (9.8346 + 9.8625) / 2\} * 0.0173 = -0.1966 \, J/s \qquad (A.3.5)$$

The mole fraction of CO_2 is given by the equation:

$$x_{co2} = F_{CO2} / (F_{CO2} + F_{solvent})$$

$$= 10.85 * 10^{-5} / (10.85 * 10^{-5} + 3.884 * 10^{-5}) = 0.7364 \qquad (A.3.6)$$

and the mole fraction of N-methyl-ϵ-caprolactam is

$$x_{solvent} = F_{solvent} / (F_{CO2} + F_{solvent})$$

$$= 3.884 * 10^{-5} / (10.85 * 10^{-5} + 3.884 * 10^{-5}) = 0.2636 \qquad (A.3.7)$$

Finally, the excess molar enthalpy at this point is obtained by dividing the heat of reaction by the total molar flow rate

$$H^E = (Q / dt) / (F_{CO2} + F_{solvent})$$

$$= -0.1966 / (10.85 * 10^{-5} + 3.884 * 10^{-5}) = -1334.3 \, J/mol \qquad (A.3.8)$$

The same procedure is followed for determing the excess molar enthalpy of each of the remaining experimental points. The raw experimental data are given in Table A.3.1.

For the ternary mixture $\{x_1 CO_2 + (1-x_1)[x_2$ sulfolane $+ (1-x_2)$ water$\}$, the solvent is a mixture rather than a pure compound. The mass ratio of sulfolane to water is 0.9657 to 0.0343. $\rho_{solvent}$ is the density of the mixture and $F_{solvent}$ is calculated from the equation:

$$F_{solvent} = 0.997 * f_{solvent} / 60 * (0.9657 * \rho_{solvent} / M_{sulfolane} + 0.0343 * \rho_{solvent} / M_{water})$$

$$= F_{sulfolane} + F_{water} \tag{A.3.9}$$

The mole fraction of CO_2 is

$$x_{CO2} = F_{CO2} / (F_{CO2} + F_{sulfolane} + F_{water}) \tag{A.3.10}$$

and the excess molar enthalpy at x_{CO2} is obtained by the equation:

$$H^E = (Q / dt) / (F_{CO2} + F_{sulfolane} + F_{water}) \tag{A.3.11}$$

Table A.3.1   The experimental data for $\{xCO_2 + (1-x)$ N-methyl-ϵ-caprolactam$\}$ at 308.15 K and 12.5 MPa.

Exp. Point	x_{CO2}	H^E / J·mol^{-1}	f / cm^3·min^{-1}*	V_{exp}/ volt
1	0.1083	-259.9	0.0250	8.5950
2	0.2025	-509.2	0.0500	7.2212
3	0.2853	-695.9	0.0750	6.0244
4	0.3585	-862.5	0.1000	4.8197
5	0.4237	-1022.6	0.1250	3.5434
6	0.4822	-1115.0	0.1500	2.5996
7	0.5350	-1193.7	0.1750	1.6871
8	0.5828	-1275.4	0.2000	0.7006
9	0.6263	-1316.2	0.2250	-0.0336
10	0.6662	-1343.6	0.2500	-0.6903
11	0.7027	-1359.1	0.2750	-1.2674
12	0.7364	-1334.6	0.3000	-1.4605
13	0.7675	-1326.4	0.3250	-1.8898
14	0.7964	-1283.8	0.3500	-1.9436
15	0.8232	-1250.5	0.3750	-2.0572
16	0.8482	-1192.4	0.4000	-1.9044
17	0.8715	-1105.1	0.4250	-1.4142
18	0.8934	-1025.7	0.4500	-0.9492
19	0.9139	-929.2	0.4750	-0.2457
20	0.9332	-829.2	0.5000	0.5624
21	0.9514	-681.0	0.5250	1.9943
22	0.9685	-502.7	0.5500	3.8822
23	0.9851	-294.0	0.5750	6.2580

* volumetric flow rate of CO_2 (Liquid) at the pump temperature 279.15 K, cm^3·min^{-1}

APPENDIX IV.   EXPERIMENTAL AND CALCULATED H^E

Table A.4.1.   Experimental and calculated excess molar enthalpies H^E from equations 22 and 24 for {x ethanol + (1-x) water}.

x	$H^E/(J\cdot mol^{-1})$		x	$H^E/(J\cdot mol^{-1})$	
	expt.	calc.		expt.	calc.
T = 298.15 K, p = 0.4 MPa					
0.0126	-113.0	-110.5	0.2810	-654.2	-656.4
0.0260	-233.2	-230.7	0.3153	-616.2	-613.7
0.0402	-350.2	-357.2	0.3531	-572.1	-567.6
0.0553	-478.1	-476.2	0.3949	-523.6	-518.9
0.0713	-575.4	-578.5	0.4412	-469.9	-468.5
0.0884	-660.9	-658.8	0.4930	-416.8	-417.3
0.1067	-715.9	-715.6	0.5512	-361.0	-366.1
0.1263	-756.4	-750.3	0.6172	-313.3	-315.9
0.1473	-765.9	-765.5	0.6825	-270.1	-273.2
0.1699	-762.7	-764.5	0.7452	-242.4	-237.4
0.1944	-746.3	-750.6	0.8154	-202.4	-200.2
0.2208	-724.7	-726.5	0.8944	-150.1	-152.0
0.2496	-691.9	-694.5	0.9452	-103.9	-104.0

Table A.4.1. ------continued.

x	$H^E/(J \cdot mol^{-1})$		x	$H^E/(J \cdot mol^{-1})$	
	expt.	calc.		expt.	calc.
		T = 298.15 K, p = 5.0 MPa			
0.0260	-239.4	-235.8	0.2810	-672.0	-673.0
0.0378	-342.4	-343.7	0.3153	-637.8	-629.9
0.0501	-444.6	-446.2	0.3531	-581.3	-582.2
0.0631	-534.3	-537.9	0.3949	-532.8	-530.8
0.0769	-615.1	-615.1	0.4412	-476.2	-476.6
0.0914	-679.1	-676.5	0.4930	-418.3	-420.6
0.1067	-724.8	-722.0	0.5512	-362.7	-363.7
0.1263	-759.9	-757.2	0.6172	-305.4	-307.4
0.1473	-773.2	-773.8	0.6858	-258.9	-257.5
0.1699	-772.8	-774.9	0.7452	-221.5	-220.6
0.1944	-759.2	-763.2	0.8154	-183.1	-182.3
0.2208	-740.2	-741.1	0.8944	-137.1	-138.3
0.2496	-708.9	-710.5	0.9377	-105.1	-104.7

Table A.4.1. ------continued.

x	$H^E/(J \cdot mol^{-1})$		x	$H^E/(J \cdot mol^{-1})$	
	expt.	calc.		expt.	calc.

<div align="center">T = 298.15 K, p = 10.0 MPa</div>

x	expt.	calc.	x	expt.	calc.
0.0260	-241.3	-236.2	0.2810	-671.0	-671.4
0.0378	-338.6	-344.7	0.3153	-632.1	-630.7
0.0501	-446.5	-446.7	0.3531	-588.1	-585.9
0.0631	-536.5	-536.7	0.3949	-539.1	-537.9
0.0769	-612.2	-611.7	0.4412	-487.4	-487.8
0.0914	-673.6	-670.7	0.4930	-436.3	-436.9
0.1067	-715.0	-714.4	0.5512	-384.9	-386.5
0.1263	-747.9	-748.3	0.6172	-336.1	-337.7
0.1473	-765.0	-764.7	0.6858	-296.7	-294.9
0.1699	-765.2	-766.3	0.7452	-260.3	-262.2
0.1944	-753.8	-755.8	0.8154	-227.1	-223.6
0.2208	-734.4	-735.3	0.8944	-165.1	-166.8
0.2496	-706.9	-706.7	0.9377	-118.8	-118.8

Table A.4.2. Experimental and calculated excess enthalpies H^E from equations 22 and 24 for {x CO_2 + (1-x) ethanol}.

x	$H^E/(J \cdot mol^{-1})$		x	$H^E/(J \cdot mol^{-1})$	
	expt.	calc.		expt.	calc.
		T = 298.15 K, p = 7.5 MPa			
0.0508	-78.8	-79.4	0.5926	-117.3	-118.3
0.1006	-131.9	-135.6	0.6328	-92.4	-93.5
0.1495	-171.7	-174.2	0.6723	-67.9	-67.7
0.1975	-200.0	-199.1	0.7111	-41.7	-41.7
0.2447	-214.2	-213.0	0.7493	-15.4	-14.4
0.2909	-220.6	-218.3	0.7869	11.9	12.2
0.3363	-218.9	-216.6	0.8239	38.1	17.7
0.3810	-215.4	-209.2	0.8602	60.5	61.2
0.4248	-195.5	-197.2	0.8960	80.5	80.6
0.4678	-179.6	-181.5	0.9312	89.0	91.6
0.5102	-159.7	-162.7	0.9659	84.5	82.0
0.5517	-139.0	-141.4			

Table A.4.2. -------continued.

| x | H^E/(J·mol^{-1}) | | x | H^E/(J·mol^{-1}) | |
	expt.	calc.		expt.	calc.
T = 298.15K, p = 10.0 MPa					
0.0520	-72.6	-70.6	0.5985	-9.4	-9.9
0.1029	-112.9	-114.7	0.6385	16.2	13.8
0.1527	-137.6	-139.9	0.6777	36.1	36.6
0.2015	-149.5	-151.6	0.7162	57.3	58.1
0.2492	-152.3	-153.2	0.7539	75.2	77.5
0.2960	-152.1	-147.2	0.7910	93.5	94.0
0.3419	-137.9	-135.7	0.8274	103.8	106.3
0.3868	-125.2	-119.9	0.8632	111.5	113.0
0.4308	-100.2	-101.0	0.8983	111.1	111.4
0.4740	-79.5	-79.9	0.9328	102.4	97.6
0.5163	-52.9	-57.2	0.9667	63.8	64.9
0.5578	-29.8	-33.7			

Table A.4.2. -------continued.

x	H^E/(J·mol^{-1})		x	H^E/(J·mol^{-1})	
	expt.	calc.		expt.	calc.
T = 298.15 K, p = 12.5 MPa					
0.0526	-30.2	-30.6	0.6016	77.9	76.1
0.1041	-43.4	-46.0	0.6414	90.0	91.6
0.1543	-50.3	-51.2	0.6804	103.4	106.1
0.2035	-49.9	-49.4	0.7187	118.9	119.2
0.2516	-44.5	-42.7	0.7562	129.3	130.3
0.2987	-34.7	-32.4	0.7931	137.5	138.7
0.3447	-22.1	-19.7	0.8292	141.6	143.5
0.3898	-7.0	-5.2	0.8646	143.2	143.2
0.4339	10.7	10.4	0.8994	138.2	135.3
0.4771	29.6	26.7	0.9336	117.4	115.7
0.5195	47.1	43.3	0.9671	74.2	76.4
0.5609	62.9	59.9			

Table A.4.2. -------continued.

x	$H^E/(J \cdot mol^{-1})$		x	$H^E/(J \cdot mol^{-1})$	
	expt.	calc.		expt.	calc.
		$T = 308.15$ K, $p = 7.5$ MPa			
0.0488	-268.0	-279.1	0.6104	-3352.1	-3331.4
0.0967	-581.4	-569.3	0.6487	-3500.8	-3495.1
0.1437	-858.1	-857.5	0.6863	-3651.8	-3650.7
0.1899	-1168.1	-1138.3	0.7234	-3825.1	-3800.0
0.2353	-1413.8	-1408.9	0.7599	-3952.9	-3942.7
0.2799	-1693.3	-1668.1	0.7958	-4086.6	-4078.5
0.3237	-1861.2	-1915.2	0.8312	-4177.7	-4204.5
0.3668	-2153.2	-2150.7	0.8660	-4281.6	-4307.3
0.4091	-2358.8	-2374.1	0.8960	-4329.5	-4341.7
0.4507	-2555.6	-2586.1	0.9214	-4235.7	-4242.0
0.4916	-2732.0	-2787.3	0.9465	-3810.0	-3763.8
0.5319	-3009.8	-2978.4	0.9714	-2191.0	-2230.5
0.5717	-3197.6	-3195.1	0.9857	-850.7	-826.7

Table A.4.2. ------continued.

x	H^E/(J·mol^{-1})		x	H^E/(J·mol^{-1})	
	expt.	calc.		expt.	calc.
		T = 308.15 K, p = 10.0 MPa			
0.0508	-72.0	-85.3	0.5926	-237.1	-238.1
0.1006	-150.4	-151.3	0.6328	-213.3	-217.0
0.1495	-206.3	-201.6	0.6723	-192.9	-193.8
0.1975	-244.5	-238.9	0.7111	-169.1	-168.7
0.2447	-267.4	-265.2	0.7493	-142.6	-141.9
0.2909	-282.1	-282.2	0.7869	-115.0	-113.9
0.3363	-290.0	-291.6	0.8239	-86.7	-84.9
0.3810	-289.8	-294.3	0.8602	-59.5	-55.4
0.4248	-289.4	-291.4	0.8960	-23.4	-25.9
0.4678	-284.8	-283.7	0.9312	6.4	2.1
0.5102	-275.0	-271.8	0.9659	22.3	24.4
0.5517	-257.5	-256.5			

Table A.4.2. ------continued.

x	H^E/(J·mol^{-1})		x	H^E/(J·mol^{-1})	
	expt.	calc.		expt.	calc.
T = 308.15 K, p = 12.5 MPa					
0.0526	-63.5	-76.4	0.6016	39.0	33.0
0.1041	-127.5	-123.1	0.6414	69.9	64.3
0.1543	-146.2	-148.7	0.6804	96.4	95.2
0.2035	-158.2	-158.9	0.7187	125.5	124.9
0.2516	-161.6	-157.7	0.7562	151.8	152.7
0.2987	-149.9	-147.9	0.7931	173.3	177.5
0.3447	-136.2	-131.8	0.8292	192.0	197.9
0.3898	-113.3	-110.7	0.8646	206.7	211.3
0.4339	-87.8	-85.9	0.8994	214.7	213.8
0.4771	-57.1	-58.4	0.9336	201.6	197.1
0.5194	-31.5	-29.1	0.9671	144.3	143.2
0.5609	8.7	1.6			

Table A.4. 3.   Experimental and calculated excess molar enthalpies H^E

from equations 22 and 24 for $\{x\ CO_2 + (1-x)\ \text{propylene carbonate}\}$.

x	$H^E/(J \cdot mol^{-1})$		x	$H^E/(J \cdot mol^{-1})$	
	expt.	calc.		expt.	calc.
		$T = 298.15$ K, $p = 7.5$ MPa			
0.0755	-213.8	-215.6	0.6893	-1549.4	-1533.4
0.1458	-392.2	-419.2	0.7244	-1504.2	-1525.7
0.2115	-607.4	-609.0	0.7578	-1384.3	-1379.8
0.2730	-836.6	-783.6	0.7897	-1240.6	-1225.5
0.3307	-950.1	-941.7	0.8201	-1098.4	-1078.2
0.3849	-1064.8	-1082.5	0.8492	-955.9	-937.4
0.4360	-1190.4	-1205.3	0.8771	-802.1	-802.6
0.4842	-1295.0	-1309.4	0.9037	-690.8	-673.6
0.5297	-1373.8	-1394.4	0.9293	-539.5	-549.8
0.5728	-1483.1	-1459.7	0.9538	-403.8	-431.2
0.6137	-1501.5	-1504.9	0.9773	-268.2	-276.8
0.6525	-1538.9	-1529.6			

Table A.4.3. --------continued.

| x | $H^E/(J \cdot mol^{-1})$ | | x | $H^E/(J \cdot mol^{-1})$ | |
	expt.	calc.		expt.	calc.
		T = 298.15 K, p = 10.0 MPa			
0.0740	-147.5	-158.4	0.6847	-1247.3	-1241.7
0.1432	-300.7	-308.5	0.7201	-1230.0	-1225.9
0.2080	-460.8	-450.3	0.7539	-1182.4	-1186.5
0.2688	-585.3	-583.6	0.7861	-1090.0	-1080.6
0.3260	-705.9	-710.0	0.8170	-964.5	-943.3
0.3799	-823.3	-822.6	0.8465	-830.3	-812.1
0.4308	-930.2	-926.7	0.8747	-703.8	-686.7
0.4789	-1021.0	-1018.8	0.9019	-579.1	-565.8
0.5244	-1091.9	-1097.4	0.9279	-443.6	-450.2
0.5676	-1158.3	-1160.9	0.9529	-307.8	-339.0
0.6086	-1208.0	-1207.4	0.9775	-159.8	-159.3
0.6476	-1231.0	-1235.0			

Table A.4. 3.   ------continued.

x	$H^E/(\text{J·mol}^{-1})$		x	$H^E/(\text{J·mol}^{-1})$	
	expt.	calc.		expt.	calc.
		T = 298.15 K, p = 12.5 MPa			
0.0753	-114.7	-133.4	0.6888	-1088.7	-1075.3
0.1455	-286.6	-273.1	0.7239	-1062.5	-1060.4
0.2111	-415.2	-409.7	0.7573	-1024.4	-1030.2
0.2725	-539.9	-537.7	0.7893	-963.7	-984.3
0.3301	-655.0	-654.3	0.8197	-876.3	-873.4
0.3843	-755.1	-758.0	0.8489	-770.6	-757.1
0.4354	-840.6	-847.7	0.8768	-679.4	-646.0
0.4836	-918.1	-922.9	0.9035	-554.0	-539.7
0.5291	-974.4	-983.3	0.9291	-437.8	-437.8
0.5722	-1023.8	-1028.8	0.9537	-306.7	-339.8
0.6131	-1066.3	-1059.4	0.9779	-200.7	-185.0
0.6519	-1094.2	-1074.9			

Table A.4.3.   ------continued.

| x | $H^E/(J \cdot mol^{-1})$ | | x | $H^E/(J \cdot mol^{-1})$ | |
	expt.	calc.		expt.	calc.
		$T = 308.15$ K, $p = 7.5$ MPa			
0.0696	-814.3	-803.4	0.6605	-3805.5	-3834.5
0.1351	-1406.9	-1413.0	0.6957	-3453.1	-3433.5
0.1967	-1858.8	-1882.3	0.7293	-3078.4	-3049.9
0.2549	-2262.2	-2264.1	0.7615	-2684.2	-2682.6
0.3099	-2660.6	-2603.3	0.7924	-2331.4	-2330.3
0.3619	-2900.2	-2933.3	0.8220	-1985.6	-1992.7
0.4113	-3256.2	-3266.6	0.8505	-1654.8	-1667.7
0.4581	-3594.3	-3585.0	0.8778	-1339.8	-1356.3
0.5026	-3848.2	-3851.2	0.9041	-1051.7	-1056.4
0.5449	-4025.4	-4026.0	0.9294	-775.2	-767.9
0.5853	-4085.8	-4088.4	0.9538	-501.2	-489.6
0.6238	-4045.9	-4039.3	0.9773	-322.9	-337.4

Table A.4. 3. ------continued.

x	$H^E/(J \cdot mol^{-1})$		x	$H^E/(J \cdot mol^{-1})$	
	expt.	calc.		expt.	calc.
T = 308.15 K, p = 10.0 MPa					
0.0740	-215.5	-206.0	0.6847	-1638.0	-1644.7
0.1432	-396.2	-400.8	0.7201	-1558.4	-1585.1
0.2080	-576.9	-584.7	0.7539	-1421.5	-1407.1
0.2688	-763.2	-757.6	0.7861	-1253.5	-1237.5
0.3260	-924.3	-919.6	0.8170	-1065.0	-1074.7
0.3799	-1084.0	-1069.9	0.8465	-930.9	-919.4
0.4308	-1190.3	-1207.6	0.8747	-776.5	-770.9
0.4789	-1331.2	-1330.9	0.9019	-632.2	-627.6
0.5244	-1420.0	-1437.8	0.9279	-493.7	-490.7
0.5676	-1539.7	-1526.0	0.9529	-340.1	-359.0
0.6086	-1600.3	-1592.2	0.9775	-169.1	-168.4
0.6476	-1635.4	-1633.0			

Table A.4. 3. ------continued.

x	$H^E/(J \cdot mol^{-1})$		x	$H^E/(J \cdot mol^{-1})$	
	expt.	calc.		expt.	calc.
		T = 308.15 K, p = 12.5 MPa			
0.0738	-120.8	-121.3	0.6842	-1471.8	-1470.0
0.1428	-308.4	-306.0	0.7196	-1438.9	-1457.9
0.2075	-495.9	-497.9	0.7534	-1327.5	-1350.8
0.2682	-662.3	-666.3	0.7857	-1203.7	-1199.9
0.3254	-819.2	-808.2	0.8166	-1062.8	-1055.4
0.3792	-919.4	-933.3	0.8461	-927.3	-917.5
0.4301	-1066.4	-1050.9	0.8744	-803.4	-785.3
0.4782	-1157.9	-1162.1	0.9016	-674.1	-658.1
0.5237	-1246.7	-1263.1	0.9277	-525.5	-536.1
0.5669	-1349.2	-1348.7	0.9527	-398.2	-419.3
0.6080	-1428.5	-1413.9	0.9768	-253.8	-236.1
0.6470	-1466.1	-1455.0			

Table A.4. 4.   Experimental and calculated excess molar enthalpies H^E

from equations 22 and 24 for $\{x\ CO_2 + (1-x)\ N\text{-methyl-}\epsilon\text{-caprolactam}\}$.

x	$H^E/(J \cdot mol^{-1})$		x	$H^E/(J \cdot mol^{-1})$	
	expt.	calc.		expt.	calc.
		T = 298.15 K, p = 7.5 MPa			
0.1048	-343.3	-332.5	0.7608	-1515.4	-1512.9
0.1966	-608.4	-604.9	0.7903	-1479.3	-1486.1
0.2777	-835.9	-827.9	0.8177	-1435.8	-1446.3
0.3500	-1002.1	-1009.5	0.8433	-1383.4	-1393.3
0.4146	-1153.7	-1156.1	0.8673	-1337.2	-1326.3
0.4729	-1263.6	-1272.8	0.8898	-1257.5	-1243.7
0.5257	-1358.1	-1363.7	0.9109	-1148.6	-1142.8
0.5737	-1429.0	-1432.1	0.9308	-1014.1	-1019.1
0.6176	-1488.2	-1480.7	0.9496	-857.2	-864.7
0.6578	-1528.8	-1511.5	0.9673	-653.8	-665.9
0.6949	-1520.8	-1526.4	0.9841	-412.3	-396.5
0.7291	-1528.6	-1526.5			

Table A.4.4.   -------continued.

x	H^E/(J·mol⁻¹) expt.	calc.	x	H^E/(J·mol⁻¹) expt.	calc.
	T = 298.15 K, p = 10.0 MPa				
0.1071	-260.7	-281.5	0.7653	-1264.8	-1275.9
0.2005	-489.6	-513.8	0.7943	-1234.2	-1242.3
0.2827	-695.9	-705.3	0.8214	-1176.8	-1195.0
0.3556	-855.6	-862.3	0.8466	-1131.0	-1134.4
0.4206	-993.9	-989.6	0.8701	-1054.0	-1060.1
0.4791	-1104.5	-1091.4	0.8922	-984.4	-970.9
0.5318	-1186.5	-1170.3	0.9129	-873.5	-866.1
0.5797	-1245.7	-1229.2	0.9324	-755.9	-743.5
0.6234	-1275.3	-1269.9	0.9508	-610.8	-600.6
0.6634	-1287.5	-1293.8	0.9681	-419.2	-434.1
0.7001	-1306.8	-1302.3	0.9845	-226.5	-236.9
0.7340	-1294.8	-1296.1			

Table A.4.4.   ------continued.

x	$H^E/(J \cdot mol^{-1})$		x	$H^E/(J \cdot mol^{-1})$	
	expt.	calc.		expt.	calc.
		T = 298.15 K, p = 12.5 MPa			
0.1083	-266.5	-268.7	0.7675	-1127.4	-1126.1
0.2025	-476.7	-488.0	0.7964	-1080.0	-1085.9
0.2853	-659.6	-666.6	0.8232	-1038.9	-1034.2
0.3585	-826.5	-810.7	0.8482	-975.1	-971.3
0.4237	-945.0	-925.2	0.8715	-909.3	-897.9
0.4882	-1011.8	-1022.7	0.8934	-811.9	-813.6
0.5350	-1077.1	-1081.3	0.9139	-719.0	-719.3
0.5828	-1127.8	-1128.4	0.9332	-606.8	-614.7
0.6263	-1171.0	-1157.7	0.9514	-517.7	-500.4
0.6662	-1171.0	-1171.0	0.9685	-364.2	-378.4
0.7027	-1151.0	-1169.4	0.9847	-260.0	-257.6
0.7364	-1146.3	-1154.2			

Table A.4.4.   ------continued.

x	H^E/(J·mol^{-1})		x	H^E/(J·mol^{-1})	
	expt.	calc.		expt.	calc.
		T = 308.15K, p = 7.5 MPa			
0.1008	-754.8	-806.9	0.7446	-5112.6	-5116.1
0.1897	-1490.1	-1493.0	0.7741	-4856.7	-4896.7
0.2685	-2086.2	-2080.1	0.8015	-4456.2	-4423.7
0.3389	-2628.5	-2586.6	0.8271	-3985.4	-3981.4
0.4022	-3016.4	-3028.5	0.8512	-3584.5	-3566.9
0.4595	-3404.6	-3420.4	0.8738	-3176.9	-3177.7
0.5114	-3747.0	-3776.5	0.8950	-2816.7	-2811.6
0.5588	-4126.0	-4109.6	0.9150	-2470.6	-2466.5
0.6022	-4485.9	-4428.9	0.9339	-2118.3	-2140.7
0.6422	-4706.4	-4733.0	0.9518	-1505.8	-1460.0
0.6790	-4941.2	-4994.9	0.9687	-970.1	-1003.9
0.7130	-5200.4	-5149.8	0.9848	-474.0	-518.8

Table A.4. 4. ------continued

x	$H^E/(J \cdot mol^{-1})$		x	$H^E/(J \cdot mol^{-1})$	
	expt.	calc.		expt.	calc.
		T = 308.15 K, p = 10.0 MPa			
0.1071	-315.1	-286.9	0.7653	-1681.7	-1696.6
0.2005	-577.1	-565.5	0.7943	-1689.9	-1678.1
0.2827	-790.1	-817.3	0.8214	-1658.9	-1645.2
0.3556	-1028.2	-1033.7	0.8466	-1605.6	-1597.1
0.4206	-1211.1	-1212.9	0.8701	-1537.2	-1532.4
0.4791	-1341.6	-1357.7	0.8922	-1436.5	-1447.8
0.5318	-1467.4	-1471.1	0.9129	-1315.3	-1339.3
0.5797	-1584.2	-1557.8	0.9324	-1193.7	-1200.1
0.6234	-1640.4	-1621.4	0.9508	-987.7	-1019.6
0.6634	-1653.0	-1664.9	0.9681	-807.8	-782.4
0.7001	-1691.3	-1690.9	0.9845	-496.8	-459.0
0.7340	-1703.0	-1701.1			

Table A.4.4. ------continued

x	$H^E/(J \cdot mol^{-1})$		x	$H^E/(J \cdot mol^{-1})$	
	expt.	calc.		expt.	calc.

<div align="center">T = 308.15 K, p = 12.5 MPa</div>

x	expt.	calc.	x	expt.	calc.
0.1083	-259.8	-256.0	0.7675	-1326.4	-1318.4
0.2025	-509.2	-494.1	0.7964	-1283.7	-1288.6
0.2853	-695.9	-702.3	0.8232	-1250.4	-1246.8
0.3585	-862.5	-876.1	0.8482	-1192.4	-1192.5
0.4237	-1022.5	-1016.2	0.8715	-1105.0	-1124.8
0.4822	-1115.0	-1125.8	0.8934	-1025.6	-1041.7
0.5350	-1193.7	-1208.9	0.9139	-929.2	-941.5
0.5828	-1275.4	-1269.0	0.9332	-829.2	-820.4
0.6263	-1316.2	-1309.3	0.9514	-680.9	-673.8
0.6662	-1343.6	-1332.8	0.9685	-502.7	-495.8
0.7027	-1359.0	-1341.2	0.9847	-294.0	-275.7
0.7364	-1334.6	-1336.1			

Table A.4.5.   Experimental and calculated excess molar enthalpies H^E

from equations 22 and 24 for {x CO_2 + (1-x) 1-formyl piperidine}.

x	$H^E/(J \cdot mol^{-1})$		x	$H^E/(J \cdot mol^{-1})$	
	expt.	calc.		expt.	calc.
T = 298.15 K, p = 7.5 MPa					
0.0918	-304.8	-265.5	0.7332	-1555.9	-1536.5
0.1745	-526.2	-495.6	0.7650	-1545.6	-1533.7
0.2494	-715.0	-694.5	0.7949	-1518.3	-1516.3
0.3175	-879.7	-866.2	0.8230	-1481.0	-1483.3
0.3797	-991.4	-1013.6	0.8496	-1425.5	-1433.5
0.4367	-1120.8	-1139.2	0.8746	-1374.5	-1364.5
0.4892	-1224.3	-1245.0	0.8983	-1253.2	-1272.8
0.5376	-1313.1	-1332.8	0.9208	-1164.5	-1152.4
0.5825	-1401.6	-1403.8	0.9421	-977.5	-993.6
0.6242	-1459.2	-1459.0	0.9624	-781.6	-778.8
0.6630	-1495.5	-1499.2	0.9816	-483.2	-473.6
0.6993	-1540.1	-1525.0			

Table A.4.5. ------continued

x	H^E/(J·mol^{-1})		x	H^E/(J·mol^{-1})	
	expt.	calc.		expt.	calc.
T = 298.15 K, p = 10.0 MPa					
0.0939	-231.3	-241.0	0.7380	-1274.3	-1268.3
0.1781	-455.6	-447.1	0.7694	-1252.2	-1250.3
0.2540	-641.1	-622.7	0.7989	-1227.0	-1219.0
0.3228	-753.1	-771.8	0.8266	-1161.5	-1174.3
0.3855	-915.8	-897.5	0.8527	-1115.1	-1115.4
0.4427	-989.7	-1001.7	0.8773	-1033.7	-1041.5
0.4953	-1084.2	-1087.0	0.9006	-941.3	-950.4
0.5438	-1144.2	-1154.9	0.9226	-849.4	-839.7
0.5885	-1207.8	-1206.4	0.9435	-720.8	-703.9
0.6300	-1233.5	-1242.8	0.9633	-518.6	-534.7
0.6685	-1273.4	-1264.9	0.9821	-317.7	-314.2
0.7045	-1282.3	-1273.3			

Table A.4.5.   ------continued

x	$H^E/(J \cdot mol^{-1})$		x	$H^E/(J \cdot mol^{-1})$	
	expt.	calc.		expt.	calc.

T = 298.15 K, p = 12.5 MPa

x	expt.	calc.	x	expt.	calc.
0.0950	-242.6	-263.7	0.7404	-1195.2	-1197.8
0.1799	-448.5	-481.9	0.7717	-1155.8	-1168.3
0.2564	-677.0	-662.1	0.8009	-1126.8	-1127.0
0.3256	-816.3	-809.7	0.8284	-1068.3	-1073.6
0.3885	-928.6	-929.1	0.8543	-1006.8	-1007.4
0.4459	-1024.1	-1024.1	0.8787	-932.7	-927.7
0.4985	-1114.4	-1097.6	0.9017	-845.9	-833.0
0.5469	-1171.9	-1152.2	0.9235	-727.5	-720.7
0.5916	-1191.2	-1189.8	0.9441	-609.7	-587.8
0.6329	-1196.7	-1212.0	0.9637	-405.0	-428.8
0.6713	-1218.3	-1220.2	0.9823	-219.9	-236.7
0.7071	-1207.2	-1215.2			

Table A.4. 5. ------continued

x	$H^E/(J \cdot mol^{-1})$		x	$H^E/(J \cdot mol^{-1})$	
	expt.	calc.		expt.	calc.
T = 308.15 K, p = 7.5 MPa					
0.0630	-676.1	-642.7	0.6362	-4410.3	-4428.5
0.1231	-1161.5	-1187.2	0.6726	-4507.0	-4521.3
0.1804	-1636.9	-1658.9	0.7077	-4563.3	-4551.8
0.2352	-2089.3	-2075.8	0.7416	-4494.0	-4668.0
0.2876	-2485.0	-2450.3	0.7743	-4195.8	-4165.6
0.3377	-2770.6	-2790.7	0.8059	-3789.1	-3682.7
0.3857	-3090.5	-3102.7	0.8364	-3281.9	-3214.8
0.4317	-3419.2	-3389.8	0.8659	-2845.7	-2762.3
0.4759	-3604.9	-3653.3	0.8945	-2384.6	-2324.5
0.5184	-3904.5	-3892.7	0.9221	-1828.0	-1900.7
0.5592	-4126.9	-4105.4	0.9489	-1390.9	-1490.1
0.5984	-4301.2	-4286.5	0.9748	-624.6	-640.8

Table A.4.5.   ------continued

x	$H^E/(J \cdot mol^{-1})$		x	$H^E/(J \cdot mol^{-1})$	
	expt.	calc.		expt.	calc.
		T = 308.15 K, p = 10.0 MPa			
0.0939	-351.2	-356.6	0.7380	-1884.8	-1879.8
0.1781	-664.2	-659.8	0.7694	-1863.3	-1862.7
0.2540	-940.9	-917.0	0.7989	-1840.1	-1827.9
0.3228	-1139.3	-1134.5	0.8266	-1778.6	-1774.8
0.3855	-1309.4	-1317.1	0.8527	-1703.3	-1702.0
0.4427	-1452.6	-1468.7	0.8773	-1600.7	-1607.0
0.4953	-1600.4	-1592.9	0.9006	-1495.9	-1485.8
0.5437	-1693.6	-1692.3	0.9229	-1317.4	-1332.1
0.5885	-1749.5	-1769.0	0.9435	-1111.5	-1135.2
0.6230	-1828.1	-1824.9	0.9633	-902.8	-876.8
0.6685	-1846.6	-1861.4	0.9821	-521.0	-522.3
0.7045	-1892.8	-1879.5			

Table A.4. 5. ------continued

x	$H^E/(J \cdot mol^{-1})$		x	$H^E/(J \cdot mol^{-1})$	
	expt.	calc.		expt.	calc.
		T = 308.15 K, p = 12.5 MPa			
0.0679	-198.3	-190.2	0.6645	-1255.8	-1256.8
0.1322	-340.5	-361.3	0.7011	-1245.4	-1256.4
0.1931	-510.0	-514.5	0.7363	-1235.8	-1240.8
0.2510	-664.6	-651.6	0.7702	-1218.9	-1208.5
0.3060	-791.1	-773.2	0.8027	-1146.1	-1158.3
0.3584	-864.0	-880.5	0.8341	-1074.0	-1087.4
0.4083	-960.7	-973.8	0.8643	-988.6	-993.5
0.4559	-1044.6	-1053.7	0.8934	-871.8	-872.9
0.5013	-1125.3	-1120.4	0.9214	-732.2	-721.2
0.5448	-1177.0	-1174.4	0.9485	-538.0	-531.3
0.5864	-1237.2	-1215.2	0.9747	-301.4	-294.7
0.6263	-1257.0	-1242.9			

Table A.4.6.   Experimental and calculated excess molar enthalpies H^E from equation 22 for {x CO_2 + (1-x) ethylene glycol dimethyl ether}.

x	$H^E/(J \cdot mol^{-1})$		x	$H^E/(J \cdot mol^{-1})$	
	expt.	calc.		expt.	calc.
T = 298.15 K, p = 7.5 MPa					
0.0866	-332.6	-332.5	0.7204	-1865.9	-1855.4
0.1654	-655.8	-663.7	0.7532	-1829.2	-1816.4
0.2375	-927.5	-924.6	0.7842	-1767.4	-1756.3
0.3062	-1152.9	-1147.8	0.8134	-1672.7	-1675.2
0.3646	-1342.4	-1336.2	0.8411	-1572.8	-1572.8
0.4209	-1514.0	-1492.6	0.8674	-1451.3	-1448.7
0.4730	-1643.8	-1619.6	0.8923	-1296.0	-1302.1
0.5215	-1699.9	-1719.2	0.9160	-1130.2	-1131.5
0.5667	-1775.8	-1793.1	0.9385	-953.7	-934.4
0.6089	-1804.3	-1842.7	0.9600	-679.1	-705.4
0.6485	-1876.3	-1869.1	0.9805	-437.8	-428.3
0.6855	-1863.8	-1873.1			

Table A. 4. 6. ------continued

x	$H^E/(J \cdot mol^{-1})$		x	$H^E/(J \cdot mol^{-1})$	
	expt.	calc.		expt.	calc.
		T = 298.15 K, p = 10.0 MPa			
0.0894	-305.7	-304.8	0.7274	-1507.7	-1511.2
0.1703	-610.2	-612.8	0.7597	-1454.7	-1448.3
0.2440	-871.5	-871.2	0.7901	-1367.1	-1368.7
0.3111	-1084.9	-1079.1	0.8187	-1265.8	-1273.2
0.3727	-1235.4	-1243.8	0.8458	-1159.1	-1162.3
0.4294	-1382.3	-1371.3	0.8713	-1044.8	-1036.9
0.4818	-1473.9	-1466.2	0.8956	-885.4	-897.3
0.5303	-1510.7	-1532.2	0.9186	-748.2	-744.0
0.5753	-1560.6	-1572.1	0.9405	-586.9	-577.4
0.6173	-1599.6	-1588.2	0.9613	-398.0	-397.7
0.6564	-1586.7	-1582.3	0.9811	-192.2	-205.2
0.6931	-1564.5	-1556.2			

Table A.4.6.   ------continued.

| x | $H^E/(J \cdot mol^{-1})$ | | x | $H^E/(J \cdot mol^{-1})$ | |
	expt.	calc.		expt.	calc.
		T = 298.15 K, p = 12.5 MPa			
0.0885	-250.3	-249.9	0.7253	-1354.5	-1359.3
0.1688	-540.9	-542.9	0.7576	-1309.6	-1312.9
0.2420	-775.3	-772.7	0.7883	-1244.3	-1251.1
0.3089	-946.0	-948.7	0.8171	-1170.9	-1173.9
0.3703	-1094.0	-1087.0	0.8444	-1086.9	-1081.7
0.4269	-1198.6	-1195.5	0.8702	-977.5	-974.4
0.4792	-1263.2	-1278.8	0.8946	-861.4	-851.8
0.5277	-1341.2	-1339.5	0.9178	-716.3	-713.7
0.5728	-1380.2	-1379.6	0.9399	-561.4	-560.0
0.6148	-1402.9	-1400.7	0.9609	-381.1	-390.2
0.6541	-1408.7	-1403.7	0.9809	-184.4	-203.7
0.6908	-1395.2	-1389.7			

Table A.4. 6. ------continued

x	H^E/(J·mol^{-1})		x	H^E/(J·mol^{-1})	
	expt.	calc.		expt.	calc.
		T = 308.15K, p = 7.5 MPa			
0.0848	-878.0	-749.5	0.7093	-5192.9	-5113.7
0.1620	-1528.6	-1439.2	0.7440	-5176.0	-5221.3
0.2326	-2029.0	-2060.5	0.7766	-5210.8	-5306.2
0.2974	-2562.7	-2611.4	0.8073	-5456.3	-5367.2
0.3572	-3057.0	-3093.7	0.8362	-5274.8	-5394.7
0.4124	-3482.3	-3511.5	0.8635	-5278.7	-5361.0
0.4636	-3860.9	-3870.2	0.8892	-5290.9	-5200.5
0.5112	-4130.9	-4175.5	0.9138	-4860.6	-4780.8
0.5556	-4349.6	-4433.5	0.9370	-3841.3	-3904.9
0.5970	-4707.1	-4649.9	0.9591	-2480.7	-2501.9
0.6359	-4882.7	-4830.5	0.9803	-1031.6	-989.0
0.6723	-5104.1	-4980.4			

Table A.4.6. ------continued

x	H^E/(J·mol^{-1})		x	H^E/(J·mol^{-1})	
	expt.	calc.		expt.	calc.

x	expt.	calc.	x	expt.	calc.
		T = 308.15 K, p = 10.0 MPa			
0.1047	-273.6	-274.0	0.6452	-1748.0	-1757.7
0.1681	-553.7	-545.7	0.6897	-1754.6	-1767.4
0.2269	-758.3	-773.8	0.7568	-1711.2	-1720.4
0.2817	-970.9	-968.7	0.8163	-1582.5	-1593.6
0.3329	-1134.0	-1135.4	0.8437	-1499.5	-1498.4
0.3807	-1275.6	-1277.6	0.8696	-1392.7	-1380.1
0.4256	-1400.6	-1397.9	0.8941	-1251.9	-1236.5
0.4677	-1508.5	-1498.5	0.9174	-1090.1	-1064.7
0.5074	-1595.7	-1581.2	0.9396	-871.6	-860.9
0.5448	-1651.5	-1647.4	0.9607	-600.2	-620.3
0.5801	-1693.6	-1698.3	0.9808	-280.1	-336.1
0.6135	-1734.5	-1734.8			

Table A.4. 6. ------continued

| x | $H^E/(J \cdot mol^{-1})$ | | x | $H^E/(J \cdot mol^{-1})$ | |
	expt.	calc.		expt.	calc.
		T = 308.15 K, p = 12.5 MPa			
0.1060	-176.7	-178.7	0.6483	-1543.3	-1549.4
0.1701	-401.5	-383.3	0.6926	-1569.4	-1543.5
0.2293	-579.3	-607.9	0.7593	-1475.5	-1472.1
0.2845	-794.0	-811.6	0.8184	-1333.4	-1327.4
0.3359	-1017.3	-984.1	0.8455	-1241.6	-1228.1
0.3839	-1142.9	-1126.7	0.8711	-1121.5	-1110.8
0.4289	-1247.0	-1243.5	0.8954	-972.4	-975.0
0.4711	-1339.3	-1337.9	0.9185	-814.1	-820.5
0.5108	-1408.9	-1412.6	0.9404	-645.4	-646.6
0.5482	-1463.7	-1469.7	0.9612	-426.8	-452.5
0.5834	-1480.8	-1510.8	0.9811	-221.7	-237.4
0.6168	-1523.5	-1537.0			

Table A.4.7. Experimental and calculated excess molar enthalpies H^E

from equation 22 for {x CO_2 + (1-x) 2-methoxyethyl ether}.

x	$H^E/(J \cdot mol^{-1})$		x	$H^E/(J \cdot mol^{-1})$	
	expt.	calc.		expt.	calc.
T = 298.15 K, p = 7.5 MPa					
0.1155	-219.1	-203.6	0.7802	-1930.9	-1917.8
0.2145	-470.6	-493.7	0.8079	-1876.4	-1876.6
0.3002	-835.1	-803.1	0.8335	-1810.0	-1815.9
0.3753	-1059.7	-1089.2	0.8573	-1729.1	-1735.3
0.4415	-1337.4	-1332.6	0.8794	-1637.1	-1633.7
0.5003	-1536.6	-1528.7	0.9001	-1496.8	-1509.2
0.5529	-1663.7	-1680.1	0.9194	-1342.2	-1358.8
0.6003	-1794.8	-1791.8	0.9376	-1177.6	-1178.5
0.6431	-1885.9	-1869.3	0.9546	-1000.6	-962.2
0.6821	-1907.7	-1917.3	0.9706	-694.6	-702.1
0.7176	-1953.0	-1939.7	0.9858	-380.5	-386.8
0.7502	-1931.0	-1939.2			

Table A.4. 7. ------continued

x	H^E/(J·mol^{-1})		x	H^E/(J·mol^{-1})	
	expt.	calc.		expt.	calc.
		T = 298.15 K, p = 10.0 MPa			
0.1185	-350.9	-351.1	0.7852	-1646.2	-1637.3
0.2194	-710.3	-706.5	0.8124	-1581.0	-1573.0
0.3064	-990.5	-995.1	0.8375	-1498.0	-1492.2
0.3821	-1202.9	-1221.1	0.8608	-1387.1	-1395.5
0.4487	-1422.4	-1394.4	0.8824	-1276.0	-1282.7
0.5076	-1525.8	-1523.9	0.9027	-1149.4	-1153.8
0.5601	-1620.3	-1616.7	0.9216	-1007.3	-1008.2
0.6073	-1670.8	-1678.4	0.9393	-850.4	-845.5
0.6498	-1700.5	-1713.1	0.9558	-672.9	-664.6
0.6884	-1715.3	-1724.2	0.9714	-466.1	-464.4
0.7235	-1716.8	-1714.1	0.9861	-237.1	-243.4
0.7556	-1687.8	-1684.7			

Table A.4.7.   ------continued.

| x | $H^E/(J \cdot mol^{-1})$ | | x | $H^E/(J \cdot mol^{-1})$ | |
	expt.	calc.		expt.	calc.
		T = 298.15 K, p = 12.5 MPa			
0.1191	-423.6	-414.9	0.7862	-1497.9	-1504.3
0.2205	-747.1	-746.9	0.8133	-1430.8	-1431.3
0.3077	-1009.1	-1009.1	0.8383	-1345.5	-1343.9
0.3835	-1197.6	-1212.8	0.8615	-1236.0	-1243.1
0.4501	-1357.0	-1558.5	0.8831	-1152.6	-1129.5
0.5091	-1496.0	-1480.6	0.9032	-1015.8	-1003.5
0.5616	-1566.6	-1558.5	0.9220	-860.6	-865.5
0.6087	-1613.6	-1606.0	0.9396	-710.0	-715.8
0.6511	-1639.7	-1627.2	0.9561	-545.5	-554.4
0.6896	-1616.2	-1625.3	0.9716	-382.0	-381.4
0.7247	-1589.1	-1602.8	0.9862	-192.4	-196.6
0.7567	-1555.8	-1561.9			

Table A.4. 7. ------continued

x	H^E/(J·mol^{-1})		x	H^E/(J·mol^{-1})	
	expt.	calc.		expt.	calc.
			T = 308.15K, p = 7.5 MPa		
0.0960	-480.3	-607.3	0.7448	-5122.1	-5090.6
0.1802	-1088.2	-1146.7	0.7787	-5087.0	-5166.5
0.2549	-1827.7	-1632.9	0.8096	-5296.4	-5210.7
0.3214	-2126.2	-2078.1	0.8378	-5256.4	-5231.4
0.3811	-2394.8	-2493.1	0.8639	-5144.4	-5227.1
0.4349	-2927.1	-2887.0	0.8878	-5127.1	-5190.2
0.4837	-3112.6	-3266.3	0.9100	-4978.6	-5106.0
0.5282	-3738.5	-3632.9	0.9306	-5177.0	-4948.3
0.5688	-3925.7	-3981.5	0.9497	-4715.9	-4666.3
0.6203	-4423.3	-4413.9	0.9676	-4118.6	-4145.7
0.6662	-4854.3	-4744.3	0.9844	-3015.3	-3063.1
0.7075	-4882.9	-4961.3			

Table A.4.7. ------continued

| x | $H^E/(J \cdot mol^{-1})$ | | x | $H^E/(J \cdot mol^{-1})$ | |
	expt.	calc.		expt.	calc.
		T = 308.15 K, p = 10.0 MPa			
0.1180	-136.5	-147.5	0.7844	-1862.2	-1879.2
0.2187	-608.3	-572.0	0.8117	-1823.7	-1832.5
0.3054	-938.1	-937.2	0.8369	-1766.3	-1771.1
0.3811	-1163.2	-1228.2	0.8603	-1707.2	-1695.3
0.4475	-1467.8	-1453.5	0.8820	-1610.4	-1604.6
0.5064	-1618.0	-1623.6	0.9023	-1499.8	-1497.4
0.5590	-1759.6	-1748.1	0.9212	-1376.8	-1370.7
0.6062	-1883.2	-1834.7	0.9390	-1215.5	-1219.1
0.6487	-1905.0	-1889.8	0.9557	-1035.1	-1033.5
0.6874	-1899.4	-1918.2	0.9713	-799.0	-796.8
0.7226	-1902.1	-1924.0	0.9861	-468.7	-476.5
0.7548	-1914.4	-1910.2			

Table A.4. 7. ------continued

x	$H^E/(J \cdot mol^{-1})$		x	$H^E/(J \cdot mol^{-1})$	
	expt.	calc.		expt.	calc.
		T = 308.15 K, p = 12.5 MPa			
0.1394	-237.2	-240.1	0.6874	-1758.2	-1740.1
0.2187	-528.9	-528.5	0.7548	-1703.3	-1710.4
0.2890	-800.5	-790.5	0.8117	-1594.2	-1604.1
0.3520	-1030.1	-1015.1	0.8603	-1431.0	-1433.4
0.4086	-1168.3	-1202.5	0.9022	-1202.3	-1203.6
0.4599	-1350.2	-1355.8	0.9212	-1070.5	-1065.6
0.5064	-1492.2	-1478.5	0.9390	-914.8	-910.2
0.5590	-1591.7	-1594.0	0.9557	-737.0	-734.2
0.6062	-1670.4	-1673.0	0.9713	-528.0	-532.0
0.6487	-1724.3	-1720.3	0.9861	-290.0	-293.5

Table A.4.8.   Experimental and calculated excess enthalpies H^E from

equations 22 and 24 for $\{x_1 \ CO_2 + (1-x_1)[x_2 \ \text{sulfolane} + (1-x_2) \ \text{water}]^*\}$.

x	$H^E/(J \cdot mol^{-1})$		x	$H^E/(J \cdot mol^{-1})$	
	expt.	calc.		expt.	calc.
		T = 298.15 K, p = 7.5 MPa			
0.0683	-281.5	-289.1	0.6659	-1307.1	-1304.7
0.1329	-557.0	-547.7	0.7025	-1202.3	-1192.1
0.1941	-787.2	-777.4	0.7376	-1079.0	-1084.0
0.2522	-970.6	-979.7	0.7713	-982.5	-980.1
0.3074	1159.7	-1155.9	0.8037	-883.1	-880.2
0.3598	-1311.6	-1307.2	0.8350	-785.3	-784.1
0.4098	-1418.5	-1434.9	0.8650	-683.2	-691.6
0.4575	-1543.1	-1541.7	0.8940	-598.8	-602.5
0.5029	-1646.8	-1642.7	0.9219	-520.9	-516.5
0.5464	-1625.4	-1623.5	0.9488	-395.5	-395.5
0.5879	-1538.0	-1544.6	0.9749	-275.3	-275.2
0.6277	-1422.1	-1422.1			

* $x_2 = 0.8085$, which is the mole fraction of sulfolane in the sulfolane/water
mixture.

Table A.4.8. ------continued

x	$H^E/(J \cdot mol^{-1})$		x	$H^E/(J \cdot mol^{-1})$	
	expt.	calc.		expt.	calc.
		T = 298.15 K, P = 10.0 MPa			
0.0699	-243.1	-243.1	0.6713	-1052.1	-1055.9
0.1358	-446.5	-446.6	0.7076	-965.8	-959.7
0.1980	-639.9	-636.3	0.7423	-864.8	-867.8
0.2569	-805.1	-803.9	0.7756	-776.5	-779.7
0.3126	-941.0	-947.4	0.8076	-680.5	-694.9
0.3655	-1059.1	-1066.1	0.8383	-620.9	-613.6
0.4158	-1155.8	-1159.6	0.8679	-542.2	-535.2
0.4636	-1231.0	-1227.8	0.8963	-459.4	-460.0
0.5091	-1286.4	-1271.3	0.9237	-388.6	-409.3
0.5525	-1311.5	-1291.0	0.9500	-295.1	-275.4
0.5939	-1261.1	-1288.3	0.9755	-162.3	-138.2
0.6335	-1160.6	-1156.0			

Table A.4.8.　　-------continued.

x	$H^E/(J \cdot mol^{-1})$		x	$H^E/(J \cdot mol^{-1})$	
	expt.	calc.		expt.	calc.
		T = 298.15 K, p = 12.5 MPa			
0.0683	-218.1	-222.5	0.6659	-1034.8	-1030.3
0.1329	-419.5	-420.5	0.7025	-925.8	-939.3
0.1941	-591.9	-594.4	0.7376	-852.8	-852.1
0.2522	-745.0	-744.8	0.7713	-763.8	-768.4
0.3074	-870.9	-872.3	0.8037	-678.1	-687.9
0.3598	-984.8	-977.4	0.8350	-619.3	-610.1
0.4098	-1071.1	-1061.4	0.8650	-538.6	-535.6
0.4575	-1123.2	-1124.8	0.8940	-468.4	-463.5
0.5029	-1159.6	-1168.4	0.9219	-391.6	-394.2
0.5464	-1179.6	-1193.3	0.9489	-298.5	-310.5
0.5880	-1212.6	-1200.2	0.9749	-183.2	-159.8
0.6277	-1133.4	-1125.2			

Table A.4.8. ------continued

x	$H^E/(J \cdot mol^{-1})$		x	$H^E/(J \cdot mol^{-1})$	
	expt.	calc.		expt.	calc.
		T = 308.15 K, p = 7.5 MPa			
0.0657	-614.6	-589.5	0.6462	-2565.6	-2564.7
0.1279	-1097.4	-1116.0	0.6822	-2316.0	-2306.6
0.1870	-1586.6	-1597.5	0.7167	-2063.7	-2058.4
0.2431	-2069.3	-2049.4	0.7499	-1819.3	-1819.7
0.2966	-2453.4	-2479.6	0.7818	-1589.0	-1589.9
0.3475	-2913.1	-2879.0	0.8126	-1365.0	-1368.6
0.3961	-3181.3	-3210.2	0.8423	-1154.3	-1155.2
0.4424	-3430.1	-3411.5	0.8709	-951.1	-949.5
0.4868	-3432.4	-3435.6	0.8985	-758.9	-750.9
0.5292	-3285.4	-3294.2	0.9252	-553.8	-559.6
0.5699	-3056.1	-3050.7	0.9510	-370.0	-373.7
0.6089	-2822.8	-2833.6	0.9759	-207.0	-194.8

Table A.4.8. ------continued

x	$H^E/(J \cdot mol^{-1})$		x	$H^E/(J \cdot mol^{-1})$	
	expt.	calc.		expt.	calc.
		T = 308.15 K, p = 10.0 MPa			
0.0683	-329.9	-328.6	0.6659	-1374.9	-1381.4
0.1329	-630.2	-618.0	0.7025	-1255.2	-1256.3
0.1941	-881.3	-871.8	0.7376	-1135.7	-1136.4
0.2522	-1103.9	-1093.5	0.7713	-1024.0	-1021.3
0.3074	-1261.0	-1286.0	0.8037	-924.1	-910.6
0.3598	-1441.5	-1451.8	0.8350	-802.2	-803.7
0.4098	-1594.5	-1592.8	0.8650	-706.0	-701.2
0.4575	-1720.5	-1703.8	0.8940	-598.9	-602.2
0.5029	-1757.6	-1761.9	0.9219	-499.1	-506.9
0.5464	-1717.9	-1725.8	0.9488	-392.6	-399.4
0.5879	-1618.3	-1607.7	0.9748	-228.5	-207.1
0.6277	-1492.6	-1498.7			

Table A.4.8. ------continued

| x | $H^E/(J \cdot mol^{-1})$ | | x | $H^E/(J \cdot mol^{-1})$ | |
	expt.	calc.		expt.	calc.
	T = 308.15 K, p = 12.5 MPa				
0.0707	-350.4	-313.8	0.6741	-1127.6	-1135.0
0.1373	-574.8	-571.2	0.7102	-1020.6	-1022.6
0.2000	-784.7	-779.8	0.7447	-919.2	-915.2
0.2593	-933.1	-947.4	0.7778	-814.8	-812.2
0.3153	-1060.9	-1080.9	0.8095	-718.5	-713.5
0.3685	-1189.8	-1188.3	0.8400	-628.9	-618.6
0.4188	-1291.4	-1277.6	0.8693	-526.8	-527.4
0.4667	-1360.8	-1357.4	0.8974	-431.8	-439.9
0.5122	-1414.4	-1421.5	0.9245	-351.9	-355.6
0.5556	-1426.3	-1426.2	0.9506	-256.8	-242.3
0.5969	-1359.4	-1351.4	0.9758	-123.4	-122.1
0.6364	-1243.4	-1251.7			

APPENDIX V.   THE PENG-ROBINSON PARAMETERS

Table A.5.1. The Peng-Robinson parameters a, b, T_c and p_c.

solvents	$\dfrac{T}{K}$	$\dfrac{a}{Pa \cdot m^6 \cdot mol^{-2}}$	$\dfrac{10^5 \cdot b}{m^3 \cdot mol^{-1}}$	$\dfrac{p_c}{kPa}$	$\dfrac{T_c}{K}$	ω
$C_4H_6O_3$ [a]	298.15	7.4093	9.9786	4920.7	759.1	0.526
	308.15	7.2884	9.9786			
$C_7H_{13}NO$ [a]	298.15	4.5832	10.926	3376.8	570.4	0.304
	308.15	4.5099	10.926			
$C_6H_{11}NO$ [a]	298.15	6.7608	12.059	3864.2	720.4	0.490
	308.15	8.0833	12.059			
$C_4H_{10}O_2$ [a]	298.15	3.5203	8.9141	3915.6	539.6	0.343
	308.15	3.4584	8.9141			
$C_6H_{14}O_3$ [a]	298.15	7.1609	13.494	2971.1	619.8	0.483
	308.15	7.0296	13.494			
$C_4H_8SO_2$ [a]	298.15	10.396	11.993	4261.5	790.1	0.675
	308.15	10.214	11.993			
CO_2	298.15	0.4016	2.6637	7387.0	304.2	0.225
	308.15	0.3923	2.6637			
C_2H_5OH	298.15	2.2267	5.2313	6383.8	516.3	0.635
	308.15	2.1731	5.2313			
H_2O	298.15	0.9848	1.8931	22120.4	647.4	0.348
$[x_2C_4H_8SO_2 + (1-x_2)H_2O]$						
	298.15	5.7691	6.8077	7470.0	782.6	0.650
	308.15	5.6691	6.8077			

[a] Parameters for these solvents were calculated by Dohrn's method [67].

Table A.5.2. The parameters k_{12} and k_{21} used in the Peng-Robinson equation of state.

Mixtures	k_{12}	k_{21}
$\{xCO_2 + (1-x)C_4H_6O_3\}$	0.040	0.010
$\{xCO_2 + (1-x)C_7H_{13}NO\}$	-0.005	-0.050
$\{xCO_2 + (1-x)C_6H_{11}NO\}$	0.060	0.000
$\{xCO_2 + (1-x)C_4H_{10}O_2\}$	-0.010	-0.070
$\{xCO_2 + (1-x)C_6H_{14}O_3\}$	-0.020	-0.020
$\{xCO_2 + (1-x)C_2H_5OH\}$	0.150	0.030
$\{C_2H_5OH + (1-x)H_2O\}$	-0.150	-0.200
$\{xCO_2 + (1-x)[x_2C_4H_8SO_2 + (1-x_2)H_2O]\}$	-0.020	-0.080

APPENDIX VI

COMPUTER PROGRAMS

Table A.6.1.   Computer program for obtaining the raw experimental data.

```
10    CLEAR SCREEN

20    GCLEAR

30    INPUT "Do you want to keep the model?(y/n)",Response$

40    IF Response$="Y" OR Response$="y" THEN

50    ! Jianping zhao, Jun 4th,1993

60    PRINT "A(C:): tron-2.prg",Prg

70    PRINT "The time of the test:           "

80    PRINT "The system of the test: (xCO_2 + (1-x)C_2H_5OH"

90    PRINT "The temperature:   35C  "

100   PRINT "the pressure:     12.5 MPa "

110   INPUT " The name of the file:",A$

120   PRINT "The name of the file:",A$
```

Table A.6.1.   ---------continued.

```
130  ! Create a new file

140  CREATE A$,1

150  ! Using white color160   PEN 1

170  ! Using solid line

180  LINE TYPE 1

190  ! draw a full grid pattern for axes

200  INPUT "Ratio:",C

210  ! Calculate the number of grid

220  INPUT "The number of experimental points:",E

230  ! ratio*100/e

240  A=C*100/E

250  ! The span is b=a/ratio

260  B=A/C

270  AXES RATIO*B,8.33333333333

280  GRID RATIO*B,8.33333333333

290  ! define x, y axes
```

Table A.6.1.   ----------continued.

```
300   ! The start point of x axis is ratio*100/e

310   AXES A,0

320   ! define x axis

330   FOR I=1 TO E340   MOVE I*A-8.5,95

350   LABEL I

360   NEXT I

370   ! define y axis

380   FOR I=1 TO 12

390   MOVE 0,I*8.33333333333-2

400   LABEL -12+I

410   NEXT I

420   MOVE 0,100

430   LINE TYPE 1

440   PEN 2

450   ! Write H data to a$ file

460   OUTPUT 711;"F1R1Z1N5"
```

Table A.6.1.   ----------continued.

```
470   Data=15000

480   DIM H(15001),T(15001)

490   FOR N=500 TO 15000 STEP 500

500   FOR I=N-500 TO N

510   ! Calculate values of T(I)

520   T(I)=I*C*100/Data

530   ! Read H data from A$ file

540   ENTER 711;H(I)

550   PRINT H(I)

560   DRAW T(I),H(I)*8.33333333333+100

570   NEXT I

580   BEEP

590   PAUSE

600   NEXT N

610   ASSIGN @File TO A$

620   OUTPUT @File;H(*)
```

Table A.6.1.   ----------continued.

---

630   PRINT "Finished"

640   ELSE

650   END IF

660   END

A.6.2. Computer program for reading out the raw experimental data

from the computer.

```
10   CLEAR SCREEN

20   GCLEAR

30   ! Jianping zhao, Jun 4th,1993

40   PRINT "A(C:): ZHAO-3-2.prg",Prg

50   PRINT "the system is ethanol+water",Sys

60   PRINT "the temperature = 25C",Tem

70   PRINT "the pressure = 58 p.s.i.",Pre

80   INPUT "do you remeber the Ratio?(y/n)",Response$

90   IF Response$="Y" OR Response$="y" THEN

100  INPUT "do you want to keep the data?(y/n)",Response$

110  IF Response$="Y" OR Response$="y" THEN

120  DIM H(2700)

130  INPUT "file name of experiment:",A$

140  ASSIGN @File TO A$

150  ENTER @File;H(*)
```

Table A.6.2.   ----------continued.

```
160  ! using white color

170  PEN 1

180  ! using solid line

190  LINE TYPE 1

200  ! draw a full grid pattern for axes

210  INPUT "Ratio:",C

220  ! Calculate the number of grid

230  INPUT "The number of experimental points:",E

240  ! ratio*100/e

250  A=C*100/E

260  ! The span is b=a/ratio

270  B=A/C

280  AXES RATIO*B,8.33333333333

290  GRID RATIO*B,8.33333333333

300  ! define x, y axes

310  ! The start point of x axis is ratio*100/e
```

Table A.6.2.   ----------continued.

```
320   AXES A,0

330   ! define x axis

340   FOR I=1 TO E

350   MOVE I*A-8.5,95

360   LABEL I

370   NEXT I

380   ! define y axis

390   FOR I=1 TO 24

400   MOVE 0,I*4.16666666667*2-2

410   LABEL (-6+I)*2

420   NEXT I

430   MOVE 0,50

440   LINE TYPE 1

450   PEN 2

460   ! Read H data from a$ file

470   Data=2700
```

Table A.6.2. ----------- continued.

```
480   FOR N=100 TO 2700 STEP 100

490   FOR I=N-100 TO N

491   ! since I*RATIO/X = A

492   ! So x=I*RATIO/A

493   X=100*E/100

500   DRAW I*RATIO/X,H(I)*4.166666667+50

510   NEXT I

520   NEXT N

521   N=0

523   FOR D=1 TO E-3

880   INPUT "The initial value of the experimental point:",Ii

890   INPUT "The finial value of the experimental point:",Ff

900   Ex=0

910   FOR I=Ii TO Ff

920   Ex=Ex+H(I)

930   NEXT I
```

Table A.6.2.   ----------continued.

---

940   Exp=Ex/(Ff-Ii+1)

950   PRINT USING "DDDD.DDDD";No,Exp

960   N=N+100

961   No=D+1

980   PRINT "No,N:",No,N

990   NEXT D

991   INPUT "The initial value of the baseline 3:",Ii

992   INPUT "The final value of the baseline 3:",F

993   Be=0

994   FOR I=Ii TO F

995   Be=Be+H(I)

996   NEXT I

997   Bad=Be/(F-Ii+1)

998   PRINT " The average value of the Bad:",Bad

999   N=N+100

1000   No=No+1

Table A.6.2.   ---------continued.

```
1002  PRINT "No:",No

1003  INPUT "The initial value of the calibration:",Ii

1004  INPUT "The finial value of the calibration:",F

1005  Cali=0

1006  FOR I=Ii TO F

1007  Cali=Cali+H(I)

1008  NEXT I

1009  Cali=Cali/(F-Ii+1)

1010  PRINT "The average value of the calibration:",Call

1011   N=N+100

1012   No=No+1

1014   PRINT "No:",No

1015   INPUT "The initial value of baseline 4:",Ii

1016   INPUT "The finial value of baseline 4:",F

1017   Ba4=0

1018   FOR I=Ii TO F
```